DEVELOPMENT OF PSMA-TARGETED RADIOPHARMACUTICALS FOR ROUTINE CLINICAL APPLICATIONS

A Dissertation

by

MOHAMMED SALEH M ABUSALEM

Submitted to the Graduate and Professional School of
Texas A&M University
in partial fulfillment of the requirements for the degree of

DOCTOR OF PHILOSOPHY

Chair of Committee,	John R. Ford
Committee Members,	Pavel V. Tsvetkov
	Shaheen Azim Dewji
	Michael Deveau
Head of Department,	Michael Nastasi

May 2022

Major Subject: Nuclear Engineering

ABSTRACT

Prostate cancer (PCa) is regarded one of the most prevalent cancer diagnoses amongst men in the United States and worldwide. Moreover, PCa is the second leading cause of cancer deaths in America. Prostate specific membrane antigen (PSMA) has been recognized as a promising molecular target in the detection of PCa, which has led to the development of specific radiolabeled tracers for PCa imaging and radioligand therapy. Consequently, PSMA-targeted radiopharmaceuticals applications in molecular imaging have significantly grown in recent years, evidenced by the number of clinical studies published, and the recent U.S. Food and Drug Administration (FDA) approval of Gallium-68 labeled PSMA-11 (^{68}Ga-PSMA-11), a positron emission tomography imaging agent for PSMA positive lesions in men with prostate cancer. In this study, the aim is to preclinically evaluate Copper-64 labeled PSMA-I&T (^{64}Cu-PSMA-I&T), as a potential PSMA-targeted imaging agent for routine clinical applications. *In vitro* and *in vivo* biological evaluation studies will be conducted to assess the specificity and binding affinity of the radiotracer to target, as well as estimating the absorbed dose delivered to target organs via internal radiation dosimetry measurements. PSMA-I&T (for Imaging & Therapy) offers high potential as a PSMA-binding-inhibitor, and is considered one of the first theranostic tracers, as it can be radiolabeled with various radiometals for imaging or therapy of PCa. While ^{64}Cu is a well-established clinically available PET isotope that can be produced in large batches by a cyclotron and has a relatively long half-life (12.7 hrs.), which is important to facilitate the accessibility to and overcome logistical burdens associated with the production and commercial distribution of medical radioisotopes.

DEDICATION

To my family, I love you all thank you for your support throughout these years.

ACKNOWLEDGEMENTS

I would like to thank my committee chair, Dr. John Ford, for his mentorship and his unlimited continuous support throughout the course of my studies. It has been such a blessing, and I am ever so grateful for his help over the years. Next, I would like to thank Professor Osama Mawlawi, for his guidance and for hosting me in his lab at the Imaging Physics Department, MD Anderson Cancer Center. Special thanks also extend to Dr. Gregory Ravizzini at the Nuclear Medicine Department, MD Anderson Cancer Center for his valuable input and for facilitating this research work. I would also like to thank Dr. Dao Le former director of the Cyclotron and Radiochemistry Facility (CRF), MD Anderson Cancer Center. Many thanks also go to Dr. Mai Lin, senior radiochemist at CRF, for his endless assistance, and the rest of the staff at CRF. I would like to thank Professor Waldemar Priebe, Dr. Rafal J. Zielinski, Dr. Lucia Martini, and Dr. Roberto Cardenas of the Department of Experimental Therapeutics, MD Anderson Cancer Center. I would also like to thank the staff at the Small Animal Imaging Facility (SAIF), MD Anderson Cancer Center.

Finally, my sincere thanks to my parents, my wife and son for their unconditional love, support, and encouragement to complete this work to the best of my ability.

CONTRIBUTORS AND FUNDING SOURCES

Contributors

This work was directed by a dissertation committee consisting of Professor John Ford, Chair, and Professors Shaheen Dewji and Pavel Tsvetkov of the Department of Nuclear Engineering, and Professor Michael Deveau of the Department of Veterinary Medicine. All work for the dissertation was completed by the student, under the advisement of Dr. John Ford of the Department of Nuclear Engineering.

Funding Sources

Graduate study was funded by a fellowship from King Faisal Specialist Hospital & Research Center, Riyadh, Saudi Arabia through the Saudi Arabian Cultural Mission to the US.

This research was also made possible by the Nuclear Medicine Chair Fund of the Department of Nuclear Medicine, the University of Texas MD Anderson Cancer Center. All work for the dissertation was completed independently by the student. The content of this research is the sole responsibility of the authors and do not necessarily reflect the official views of King Faisal Specialist Hospital & Research Center nor the Saudi Arabian Cultural Mission to the US or the University of Texas MD Anderson Cancer Center.

TABLE OF CONTENTS

Page

LIST OF FIGURES

Page

LIST OF TABLES

Page

1. INTRODUCTION

The use of radiation in medicine over the past century has revolutionized how medical conditions, specifically, cancerous diseases are diagnosed, monitored, and treated. This has paved the way for nuclear medicine to be officially recognized as a medical specialty by the American Medical Association in 1971 [1]. Presently, major hospitals around the world have nuclear medicine departments where radiopharmaceuticals are safely, and effectively administered into patients for imaging and treatment. Moreover, it is estimated that 20 million nuclear medicine procedures are conducted annually in the United States alone [2].

One of the most prevalent cancer diagnoses amongst men is prostate cancer (PCa) in the United States [3], and worldwide [4]. It is expected that around 250,000 new cases will be diagnosed in 2021 [3]. Prostate cancer is thus the second leading cause of cancer deaths in America [3], and the fifth leading cause of death worldwide [5]. Additionally, in a recent study of global cancer statistics (GLOBOCAN) of the incidence and mortality of different cancer types in 185 countries, the prevalence of prostate cancer cases worldwide is estimated to be around 5 million cases [4].

1.1 Prostate Cancer Biomarkers

Two of the most significant prostate cancer biomarkers are prostate specific antigen (PSA) and prostate specific membrane antigen (PSMA). An overview of each antigen and its functions with respect to prostate cancer is discussed in the following sections.

1.1.1 Prostate-Specific Antigen (PSA)

A crucial prostate cancer serum biomarker is the prostate specific antigen (PSA). PSA is an androgen-regulated serine protease made by prostate cancer and the epithelial cells of the prostate. In addition, as an important protein in semen coagulum, PSA is used to fragment semenogelins. PSA is released into the ducts of the prostate in the form of inactive 244–amino acid proenzyme (proPSA), and it becomes activated once the seven N-terminal amino acids are fragmented [6]. Moreover, the protease inhibitors bind to the activated PSA that is admitted into the circulation, and the inactivated portion travels as free PSA. More importantly, this process is found to be disrupted along with structural damage of the basement membrane and the layer of the basal cell as schematically shown in Figure 1 during the onset of prostate cancer, hence leading to elevated levels of PSA in the peripheral circulation and ultimately in the bloodstream [6-7].

As a result, the widely used serum PSA test is based on the principle of measuring the level of PSA in the bloodstream. Furthermore, the amount of PSA tends to have a positive correlation with tumor size and cancer stage [7]. However, even though PSA testing is a recommended diagnostic tool in the clinic for prostate cancer, the test is limited, lacks specificity to diagnose PCa, and additional examinations are to be performed such as immunohistology or prostate biopsy to confirm tumor stages for individual patients.

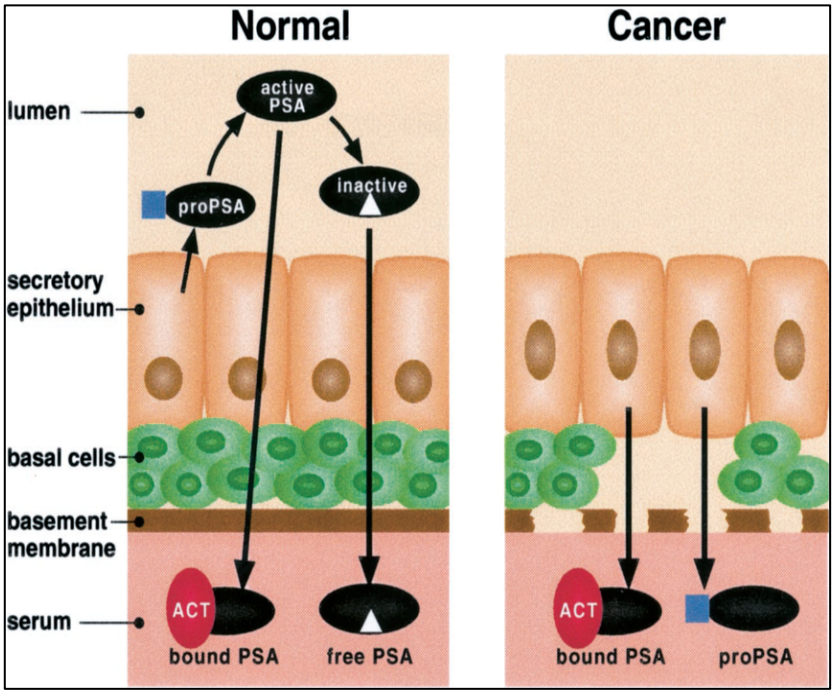

Figure 1 Schematic representation of PSA production in normal cells vs. cancerous tissues. Reprinted with permission from [6].

1.1.2 Prostate-Specific Membrane Antigen (PSMA)

PSMA is a type II transmembrane glycoprotein containing 750 amino acids with folate hydrolase activity made by prostatic epithelium and is expressed in prostate cancer cells and in tumor neovasculature [8]. A typical PSMA protein consists of three parts: an external segment of 707-amino acids, a transmembrane domain of 24-amino acids, and an internal region of 19-amino-acids. A schematic structure of PSMA is shown in Figure 2.

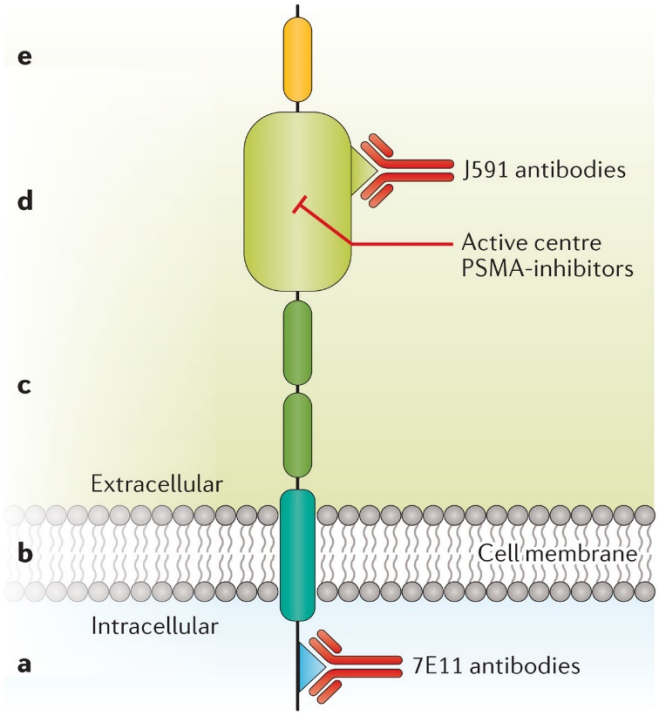

Figure 2 (a) The binding site of the intracellular region that can be targeted with 7E11 antibodies; (b) the hydrophobic transmembrane region; (c) the extracellular part of PSMA; (d) the active site targeted by PSMA inhibitors, in addition to the binding site for the J591; and (e) the final domain of unknown function. Reprinted with permission from [9].

Some of the vital enzymatic functions played by PSMA as a glutamate - carboxypeptidase are folate hydrolase (catalyzing the hydrolysis of N-acetylaspartylglutamate (NAAG) and NAALADase (N-Acetylated alpha-linked acidic dipeptidase, a neuropeptidase regulating glutamatergic neurotransmission) activities, in addition to being recycled by endocytic vesicles [10]. These enzymatic processes are significant as they could potentially indicate the presence of PCa, as it was shown that at increased levels of prostatic carcinomas one type of NAALADase was expressed [11].

Additionally, high folate hydrolase activity was observed in human prostate cancer cells producing PSMA [12].

Furthermore, PSMA is reported to have an internalization signal, which enables it to enter an endosomal cycle once internalized on the cell surface [13]. The five N-terminal amino acids (MWNLL) located at the cytoplasmic tail of PSMA facilitate its internalization, which occurs through a clathrin-dependent endocytic mechanism as demonstrated by Rajasekaran et al. [14]. This important feature is advantageous when considering PSMA as a promising antigenic biomarker for imaging or therapy of prostate cancer [13].

More importantly, PSMA is overexpressed at different stages of prostatic cancer [10], and its expression is in proportion to the grade of the tumor [7]. Additionally, PSMA is regulated negatively by androgen and its expression tends to be in inverse proportion with androgen amounts [15], and PSMA levels are also increased when cancer cells are androgen independent. Consequently, PSMA is considered a promising and effective diagnostic and prognostic biomarker of prostate cancer [16].

1.2 Diagnostic Procedures for Prostate Cancer

Over the years different detection methods have been developed to effectively diagnose patients with PCa. Some of the most common diagnostics used for PCa are highlighted in the following sections.

1.2.1 Conventional Detection Methods

One of the initial and common clinical tests used to screen for prostate cancer in patients is the prostate specific antigen (PSA) blood test. The test is principally based on measuring PSA levels in the blood, as PSA is a protein produced only by the prostate and high PSA levels are indicative of the presence of prostate cancer. However, as previously mentioned, even though, the test can be useful in detecting early signs of prostate cancer, it lacks specificity and sensitivity in diagnosing PCa, as high levels of PSA could also be due to inflammation of the prostate, as well as giving very minimum information of the cancer stage or severity [17].

Another routine test to initially detect PCa is the digital rectal examination (DRE). During this exam the healthcare provider physically examines the patient's prostate. The DRE exam is typically done along with a PSA test, and it helps to examine for any issues i.e., abnormal enlargement of the prostate, which could be a sign of PCa. Even though, the PSA and the DRE tests are clinically used, they do not provide enough information to conclude a definitive PCa diagnosis. Nonetheless, the outcomes of the PSA and DRE exams would help to determine if an ultrasound-guided biopsy of the prostate is needed or not, where small pieces of the prostrate tissue is removed and examined for cancer cells which can then be graded using the Gleason score if cancer is identified [18].

1.2.2 Imaging Based Detection Methods

A clinical imaging procedure and one of the first scans that was approved by the Food and Drug Administration (FDA) for prostate cancer is the ProstaScint™. The scan involves radiolabeling of monoclonal antibody (7E11C5.3) with indium-111, and once injected into the patient, it is followed by planar and cross-sectional single photon emission computed tomography (SPECT) imaging. The radiolabeled antibody binds and can recognize the intracellular portion of PSMA, a membrane glycoprotein that is overexpressed in prostate cancer. However, the scan lacks sensitivity, and the results interpretation can be technically challenging, and depends highly on the reader's experience [17].

Additionally, some of the traditional conventional scanning methods for prostate cancer included pelvic magnetic resonance (MR) imaging, contrast material–enhanced computed tomography (CT), and bone scintigraphy. But with limited sensitivity and low rates of detection in biochemical relapse, especially, at low levels of PSA expressions these methods were not clinically viable [19]. Alternatively, some promising positron emission tomography (PET)/CT based radiotracers, which offer superior sensitivity, have been investigated and evaluated for their clinical applications. These radiotracers include ^{18}F-Fluorodeoxyglucose (FDG), ^{18}F-Choline, ^{18}F-Sodium Fluoride (NaF), ^{18}F-Fluciclovine (FACBC), and ^{11}C-Choline. However, their detection capabilities are limited, as identifying sites of active disease remains challenging when the tumor burden is low. A summary of their potential advantages and limitations are illustrated in Table 1 [19].

Table 1 Clinically Used PET Radiotracers for Prostate Cancer Imaging. Adopted with permission from [19].

PET Tracer	Target	Benefit for PCa	Role in PCa Imaging
FDG	Glucose metabolism	None/ Limited	Response assessment of osseous disease in metastatic castration resistant PCa
^{11}C- & ^{18}F-labled Choline	Cell membrane metabolism	Yes, in large studies	High-risk staging; biochemical relapse at high PSA levels
^{18}F-NaF	Osteoblastic activity	Bone metastases	Bone metastases only
^{18}F-FACBC	Amino acids	Yes, in initial results	Undergoing evaluation but appears superior to choline in the setting of biochemical relapse

1.3 Prostate Specific Membrane Antigen Targeted Imaging

Molecular imaging specifically, PSMA-based PET/CT imaging is increasingly playing a valuable role in managing patients with prostate cancer. As PSMA is overexpressed at different stages of prostatic cancer by 100-1000-fold in 95% of PCa cells [10,20], and its expression is in proportion to the grade of the tumor [7]. Particularly, PSMA possesses an internalization signal, which allows it to enter an endosomal cycle once internalized on the cell surface. Hence, PSMA is highly considered as a promising antigenic biomarker for imaging or therapy of prostate cancer [13].

With such desirable characteristics, research and development of PSMA-targeted radiopharmaceuticals has gained immense interests in the scientific community, and drug manufacturing companies alike. Generally, PSMA-based imaging agents are classified into three groups: A) antibodies; B) aptamers; and C) PSMA inhibitors of low molecular weight [21]. Although, advances have been made in all categories, it is the latter one that has offered the most promise. This has resulted in producing ^{68}Ga-PSMA-11, which was developed and preclinically tested by investigators from the German Cancer Research Center and Heidelberg University [22-24]. Subsequently, with highly promising results, the German group initiated the first proof-of-concept studies in men [25-26].

Today, ^{68}Ga-PSMA-11 is considered the gold standard for prostate cancer imaging, due to its sensitivity and superiority compared to other PET radiotracers, as verified by various clinical trials [27-32].

Even though, ^{68}Ga-PSMA-11 was clinically being used in many countries, until recently, it was only under investigational use in the US. However, a unique partnership between the University of California Los Angeles (UCLA) and University of California San Francisco (UCSF) initiated a pivotal phase 3 clinical trial of ^{68}Ga-PSMA-11 as part of their New Drug Applications (NDAs) submitted to the FDA. On December 1, 2020, both institutions UCLA and UCSF had received FDA approval for their NDAs for the first PET imaging drug of PSMA-positive lesions in men with prostate cancer in the US [33].

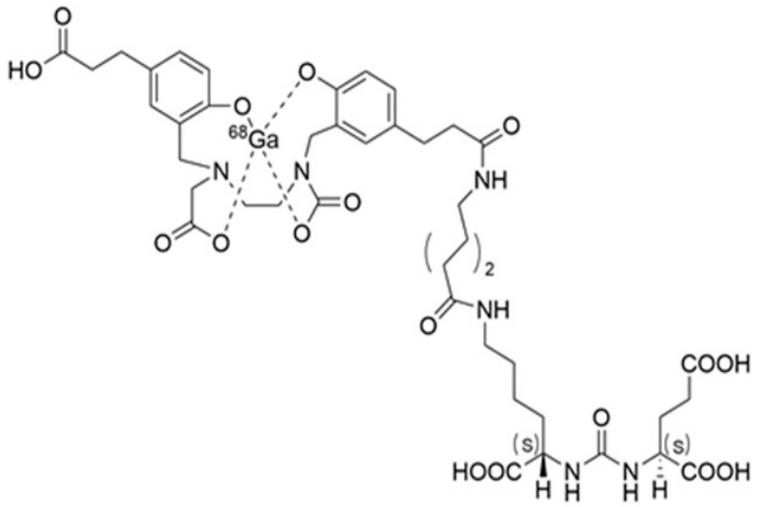

Figure 3 Chemical structure of ^{68}Ga-PSMA-11.

The excellent molecular imaging performance that the PSMA-11 ligand achieved in detecting PCa when radiolabeled with Gallium-68, has triggered great interest in evaluating other potential analogues based on its scaffold for imaging or therapy of PCa. A highly potential PSMA-binding-inhibitor that has been clinically evaluated is PSMA-I&T (for Imaging and Therapy) [34]. PSMA-I&T is considered one of the first theranostic tracers, as it can be radiolabeled with various radiometals such as ^{64}Cu, ^{68}Ga,^{111}In and ^{44}Sc for imaging or ^{225}Ac, ^{213}Bi, and ^{212}Pb for α-therapy or ^{177}Lu and ^{67}Cu for β-therapy [35]. In fact, several clinical trials evaluated the safety and efficacy of ^{177}Lu-PSMA-I&T in PCa patients [36-38]. The investigators were able to demonstrate the efficacy of the treatment of ^{177}Lu-PSMA-I&T, with a patient receiving 4 cycles of radioligand therapy (RTL) of 7.4 GBq ^{177}Lu-PSMA-I&T as illustrated in Figure 5 [38-39]. This is in contrast with PSMA-11 that can only be radiolabeled with ^{68}Ga, due to its Ga-specific acyclic chelator (HBED-CC), limiting its use for diagnostic applications only.

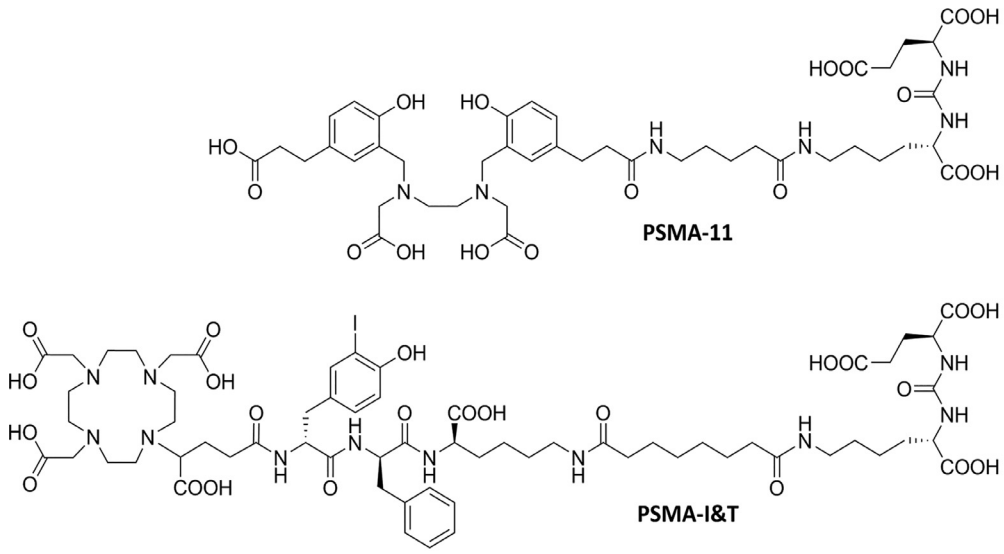

Figure 4 Chemical structures of PSMA-11 and PSMA I&T. Reprinted with permission from [34].

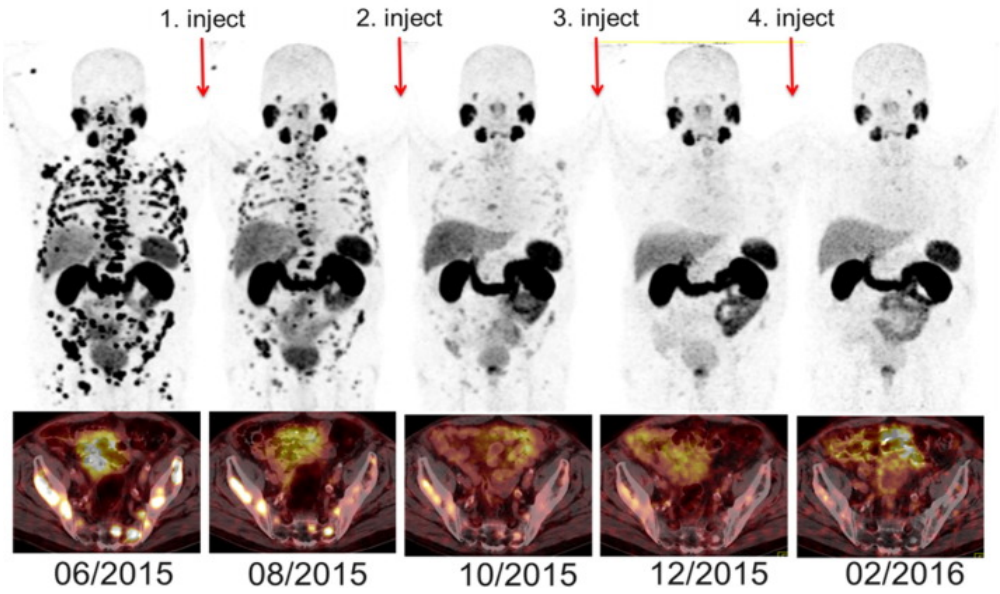

Figure 5 ^{68}Ga-PSMA-11 PET/CT imaging during and after treatment with ^{177}Lu-PSMA-I&T, showing decline in PSA level from 1200 ng/mL to 13ng/ml. Reprinted with permission from [39].

1.4 Research Motivation

The continuous interest in investigating and advancing the applications of PSMA-based radiotracers is largely attributed to the success demonstrated by ^{68}Ga-PSMA-11 in detecting PCa, along with the commercial availability of the Germanium-68 (^{68}Ge)/^{68}Ga-generator. However, ^{68}Ga-PSMA-11 has no true matched therapeutic pair,^{177}Lu-PSMA-617 or ^{177}Lu-PSMA-I&T remain the only viable options for radioligand therapy. ^{68}Ga decays by (β+: 89% [1.92 MeV]), and has a positron range of (4mm), which combined lead to lower resolution and suboptimal PET images. ^{68}Ga is mostly available via the ^{68}Ge/^{68}Ga generator, with limited activity per day and a short half-life (68 min) this makes it inadequate to be shipped to long distances. As a result, this research was designed to investigate an alternative radiometal-based PSMA-targeted radiopharmaceutical. A highly promising radioisotope of choice was ^{64}Cu that can be radiolabeled with PSMA-I&T for PSMA-based PET imaging. ^{64}Cu has desirable physical characteristics in terms of its decay properties, positron range and half-life that makes it an ideal imaging agent. It decays by (β+: 17.9% [0.653 MeV]) with a positron range of 1mm, and a half-life of ($t_{1/2}$: 12.7 h). The relatively long half-life of ^{64}Cu is optimal for centralized radioisotope production at regional or national cyclotron facilities to be distributed to local or remote nuclear medicine departments. This is advantageous when compared to the short half-life of ^{68}Ga (68 min). Moreover, ^{64}Cu can have a therapeutic surrogate radiometal (^{67}Cu) for β-therapy (β–: 100%, t1/2: 2.58 d), which its therapeutic efficacy has been reported to be preclinically comparable to that of ^{177}Lu [40]. This could potentially be developed to become what is referred to as a matched theranostic pair (^{64}Cu for imaging and ^{67}Cu for therapy). In fact, there is growing interests to use ^{67}Cu

for radioligand therapy [41-44], as ^{177}Lu is still the only radioisotope of choice for RTL [39]. Lastly, ^{64}Cu-based radiopharmaceuticals have been extensively used in numerous nuclear medicine applications, with some receiving FDA approval for routine PET imaging procedures [39, 45-47].

1.5 Study Objective

This report describes the preclinical evaluation of ^{64}Cu-PSMA-I&T in xenograft tumor models at MD Anderson Cancer Center, as part of the research efforts into potential radiopharmaceuticals for nuclear medicine procedures. ^{64}Cu-PSMA-I&T was synthesized and tested for its stability at room temperature up to 24 hrs. post synthesis. *In vitro* cell uptake assays were conducted by incubation of LNCaP (positive human prostate carcinoma cells) and PC-3 (negative human prostate carcinoma cells) with ^{64}Cu-PSMA-I&T for 1 h, followed by determination of specific target binding to PCa cells. *In vivo* biological evaluations: PET/CT imaging and biodistribution studies were performed on mice bearing LNCaP or PC-3 xenografts at 2, 24 and 48 hrs. post injection of ^{64}Cu-PSMA-I&T (± 5.5 MBq). In addition, the dosimetry of ^{64}Cu-PSMA-I&T was estimated in tumor bearing mice. This work is the first to estimate and report the radiation dosimetry of ^{64}Cu-PSMA-I&T as well as performing a comprehensive head-to-head comparison of ^{64}Cu-PSMA-I&T biodistribution, and dosimetry to that of ^{68}Ga-PSMA-I&T and ^{68}Ga-PSMA-11 in xenografts animal models. The flow chart in Figure 6 is a summary of the methods used in this study. A full detailed description of the materials and methods, data processing and analysis is found in the following sections.

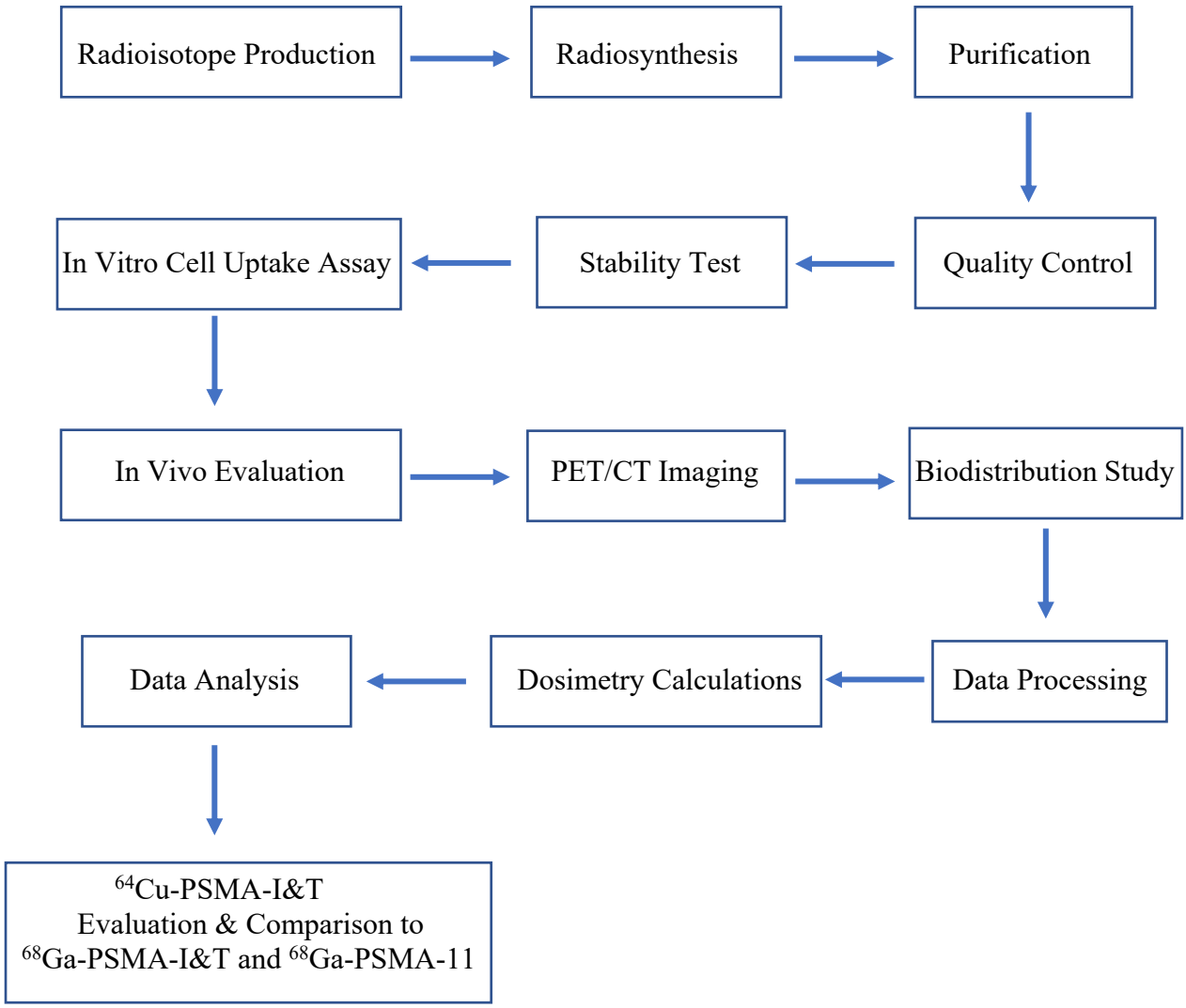

Figure 6 Summary of the methodology executed in this research work.

2. MATERIALS AND METHODS

2.1 Radiopharmaceuticals Production

Diagnostic and therapeutic applications of radiometal-based radiopharmaceuticals in nuclear medicine procedures have considerably increased over the past decades, with the continuous advancement of radionuclides production and radiolabeling methods. Most of the common radiometals (e.g., ^{64}Cu, ^{68}Ga and ^{89}Zr) used in the clinic, can be produced by on-site particle accelerators known as cyclotrons. While, cyclotron design and operation, all cyclotrons share the same basic characteristics: an ion source to produce ions, a vacuum chamber to accelerate them by a high frequency alternating voltage applied between two D-shaped electrodes (dees), and a magnet to keep the ions on a circular path schematically shown in Figure 7.

Once the radiometal of interest is produced and purified, it is conjugated to a targeting biomolecule via a bifunctional chelating agent (BFCA), which establishes a stable covalent bond between the label and the targeting ligand (Figure 8). In addition, BFCA also assures that the compound structure of the metal is stable in vivo. A typical chelator consists of several functional groups for coordination to the radiometal of choice, which leads to high thermodynamic and kinetic stability of the complex, as well as in its rapid and quantitative formation [50].

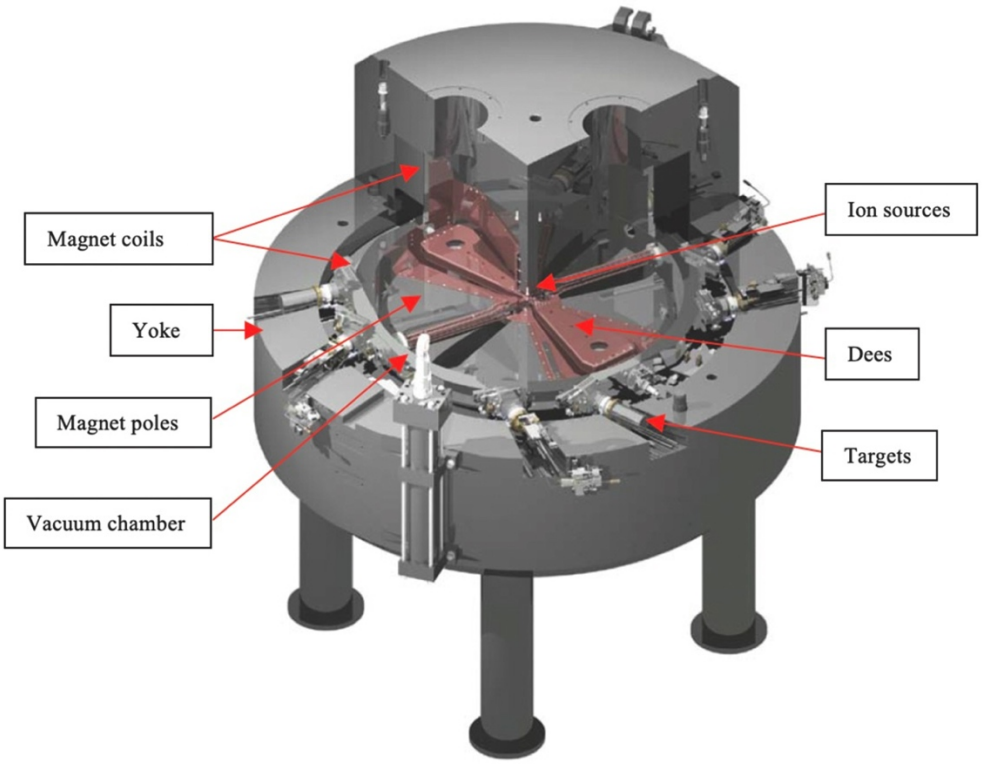

Figure 7 Schematic of internal parts of a typical cyclotron. Reprinted with permission from [48].

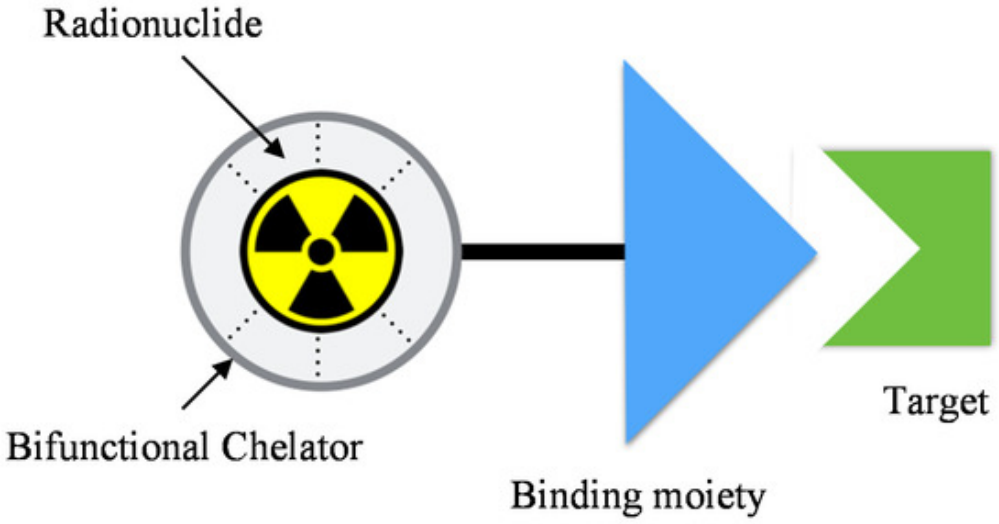

Figure 8 A radiopharmaceutical structure contains a radionuclide conjugated to a bifunctional chelator, which is linked to a binding moiety that drives the radiopharmaceutical to attach to the target of interest. Reprinted with permission from [49]

2.1.1 Copper-64 (^{64}Cu) Production

^{64}Cu has become an important radiometal in clinical applications, and its radiochemistry has been well-developed over the years, as it can be incorporated into different chelator complexes to form links with biomolecules such as proteins, antibodies, and peptides [47]. It has a unique decay profile decaying by positron emission (17%), β^- emission (39%) and electron capture (44%). ^{64}Cu is produced by a cyclotron via several nuclear reactions: ^{64}Ni (p, n)^{64}Cu, ^{66}Zn (d, a)^{64}Cu and ^{68}Zn (p, an)^{64}Cu, however, the most common method used is the ^{64}Ni (p, n)^{64}Cu.

Table 2 ^{64}Cu Decay Properties

Emission	Fraction	$Energy_{max}$ (MeV)	$Energy_{Average}$ (MeV)
Positron (β^+)	0.174	0.653	0.2782
Electron Capture	0.390	0.578	0.1902
Photon	0.348	0.511	0.511

The production of ^{64}Cu was done through a series of steps from preparing the target for irradiation to the purification of the final product. The production was performed at the Cyclotron and Radiochemistry Facility (CRF) at the University of Texas MD Anderson Cancer Center, which was done under current good manufacturing practice (cGMP). In this work, a highly enriched ^{64}Ni solid target (enrichment: 99+%, 80-100 mg) that had been electroplated on a platinum plate (see Appendix A for details) was irradiated with protons at 11.4 MeV energy, and beam current of 45 μA via the ^{64}Ni (p, n) ^{64}Cu nuclear reaction.

Briefly, ^{64}Cu was processed by first dissolving the irritated ^{64}Ni target as follows: 10 mL of Milli-Q H_2O was added to Vial (A), and a concentration of 6.0 M hydrochloric acid (HCl) was added to Vial (B) on the PRF module. In addition, 5 mL of 6 M HCl was added to vial (R3) and another 10 mL of 6 M HCl to vial (R4). Lastly, 2 mL of 0.1 M HCl and 5 mL of 0.1 M HCl were added to vials (R5&R6) respectively.

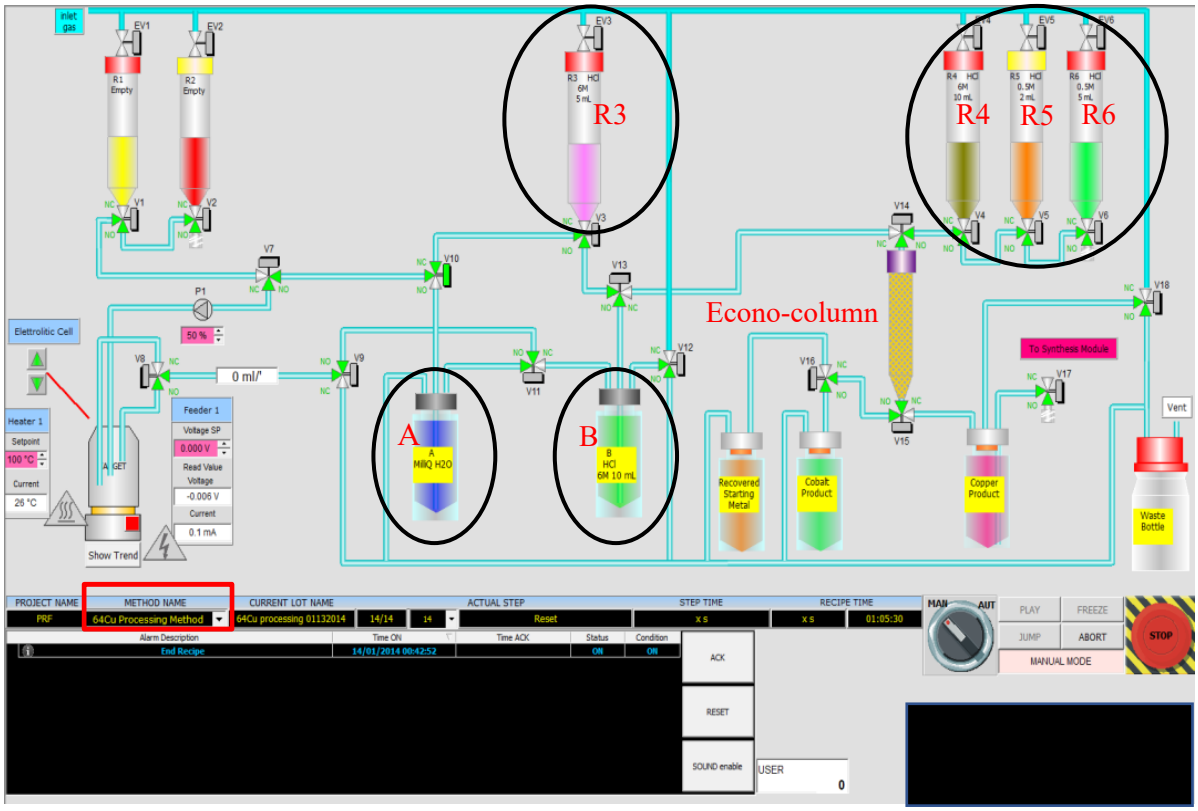

Figure 9 The software interface of the PRF module and vials positions.

Next, the ^{64}Ni irritated target was dissolved in 10 mL of 6 M HCl and heated at 90˚ C for 40 minutes until the solution evaporated to dryness. The residue (the crude ^{64}Cu/^{64}Ni solution) was then dissolved in 3 ml of 6 M HCl, and then transferred to a pre-conditioned econo-column (an anion exchange column) loaded with AG 1-X8 resin (Bio-Rad, Hercules,

CA) for purification. The ^{64}Ni fraction was first eluted with 15 mL of 6 M HCI and collected for recycle. The column was then washed with 10 mL Milli-Q H_2O, then the purified ^{64}Cu product was eluted with 8-10 mL 0.5-0.1 M HCI and collected. Lastly, the activity of the collected ^{64}Cu fraction was measured in the dose calibrator and recorded. A detailed description of the preparation protocols is found in Appendix A.

2.1.2 ^{64}Cu-PSMA-I&T Radiosynthesis

Once the radiometal (^{64}Cu) was produced and purified, the radiolabeling of ^{64}Cu-PSMA-I&T was performed according as follows: the activity of ^{64}Cu (5-10 mCi) was transferred to a reactor containing the precursor PSMA-I&T (50 μg) (ABX, Radeberg, Germany) in 0.1 M NaOAc sodium acetate solution (200 μL) with pH at 5.0. Radiolabeling was then performed by heating the mixture for 20 min at 95° C. Once completed, the reaction mixture was purified on a C-18 cartridge (Waters, Milford, MA) by eluting impurities with 10 mL H_2O and the final product was then eluted with 1 mL ethanol (EtOH). The overall radiochemical procedure was around 30 min with the radiochemical yield of > 70%.

2.1.3 Gallium-68 (^{68}Ga) Production

^{68}Ga-based radiopharmaceuticals applications in molecular imaging have grown considerably over the past decades. ^{68}Ga is a positron emitter (89%), which makes it an ideal PET imaging agent. It can be radiolabeled with various biomolecules from nanoparticles to low molecular weight peptides or macromolecules, showing highly promising imaging

capabilities [51-56]. ^{68}Ga can be produced by a cyclotron that is an active area of research or obtained via the elution of a ^{68}Ge/^{68}Ga-generator, as $^{68}GaCl_3$ solution for direct radiolabeling. The ^{68}Ge/^{68}Ga-generator is based on the principle of having a long-lived parent (^{68}Ge, $t_{1/2}$= 207 days) radionuclide that spontaneously decays to the daughter nuclide, ^{68}Ga ($t_{1/2}$= 68 mins) and are in equilibrium. ^{68}Ge is typically produced by a high energy cyclotron with energies around (60-66 MeV) via the ^{69}Ga (p,2n) ^{68}Ge nuclear reaction, it is then loaded onto a matrix column made of titanium dioxide (TiO_2). The column is placed inside a shielded container with an inlet and outlet ports for eluting (^{68}Ga) as gallium chloride solution. The decay process between the mother nuclide (^{68}Ge) and the daughter nuclide is described to be in secular equilibrium, as ^{68}Ge half-life ($t_{1/2}$= 207 days) is more than a hundredfold longer than that of ^{68}Ga ($t_{1/2}$= 68 mins). As a result, based on the buildup kinetics the maximum activity of ^{68}Ga can be obtained at 14 hrs. post initial elution that is both radionuclides reach equilibrium, and 25% or 50% activity is achieved after 28 and 68 minutes respectively.

In this work, a ^{68}Ge/^{68}Ga-generator was eluted to acquire ^{68}Ga to perform the radiolabeling for the ^{68}GaPSMA-11 and ^{68}Ga-PSMA-I&T. In brief, the generator was eluted with 5 mL sterile ultrapure 0.1 M hydrochloric acid filled in a syringe and attached to a port on the stopcock manifold, and a collection vial was connected to the outlet line using the appropriate (nonmetallic) connector. Next, the valve of the stopcock manifold was turned where the syringe is connected to the inlet port of the generator at a rate not greater than 2 mL/minute. The eluate was then collected in a shielded collection vial and the solution was measured with a calibrated dose calibrator to determine the yield.

2.1.4 ^{68}Ga-PSMA-I&T Radiosynthesis

The activity of ^{68}Ga (15-20 mCi) was transferred to a reactor containing the precursor PSMA-I&T (50 µg) (ABX, Radeberg, Germany) in 0.5 M sodium acetate solution (1.1 mL) with pH of 3.0-4.0. Radiolabeling was performed at 95° C for 10 min, product was then purified on a C-18 cartridge for final collection. The overall radiochemical procedure was around 25 min with the radiochemical yield of > 70 %.

Figure 10 Inside of the hot cell where the radiolabeling was performed, a) heat block, and b) final product collected.

2.1.5 ^{68}Ga-PSMA-11 Radiosynthesis

The activity of ^{68}Ga (15-20 mCi) was transferred to a reactor containing the precursor PSMA-11 (25 μg) (ABX, Radeberg, Germany) in 0.5 M sodium acetate solution (1.1 mL) with pH of 3.0-4.0. Radiolabeling was performed at 95° C for 10 min, product was then purified on a C-18 cartridge for final collection. The overall radiochemical procedure was around 25 min with the radiochemical yield of > 70 %.

2.1.6 Radiotracers Quality Control

The final product of each radiotracer was determined to be sterile, colorless, and tested to verify that the radiosynthesis was successfully done. First, their radiochemical purities were determined by radio-HPLC (High Performance Liquid Chromatography) using an Agilent 1260 infinity system (Agilent Technologies, Diegem, Belgium) and the Luna C18 reversed-phase column (4.6 × 250 mm, 5 μm, Torrance, CA) at 40 °C and a mobile phase using a gradient system (Solvent A: water (0.1% TFA); Solvent B: acetonitrile; 0-8 min: 0% B, 8-12 min: from 0 to 75% B, 13-15 min: from 75 to 0% B) at a flow rate of 1 mL/min. At which the Ultraviolet (UV) absorption was detected with an Agilent 1260 variable wavelength detector at a wavelength of 220 nm in series with a Scan-RAM detector (LabLogic Systems, Tampa, FL) for radioactivity detection. The pH of the final products was also checked using pH-FX 0.0–14.0 strips (MACHEREY-NAGEL, Bethlehem, PA). Additionally, the stability of each radiotracer was determined as a function of time at room

temperature by injecting (10 µL) into the HPLC at set time points as follows: ^{64}Cu-PSMA-I&T at 2, 4, 8 and 24 hrs., ^{68}Ga-PSMA-I&T and ^{68}Ga-PSMA-11 at 0, 2, and 4 hrs. The percentage of the radiolabeling yield of each radiotracer was also determined by the instant thin layer chromatography (ITLC). Briefly, 10 µL of the radiotracer was spotted at the origin of a microfiber chromatography paper impregnated with silica gel (ITLC-SG), which was then placed into a chromatography chamber (mobile phase: methanol:1M ammonium acetate). Once, the solvent front reached the desired distance, the strip was removed from the chamber and allowed to dry. The strip was then placed on the scanning bed of the radio-TLC (Scan-Ram, LabLogic, Tampa, FL), and scanned by the radioactivity detector.

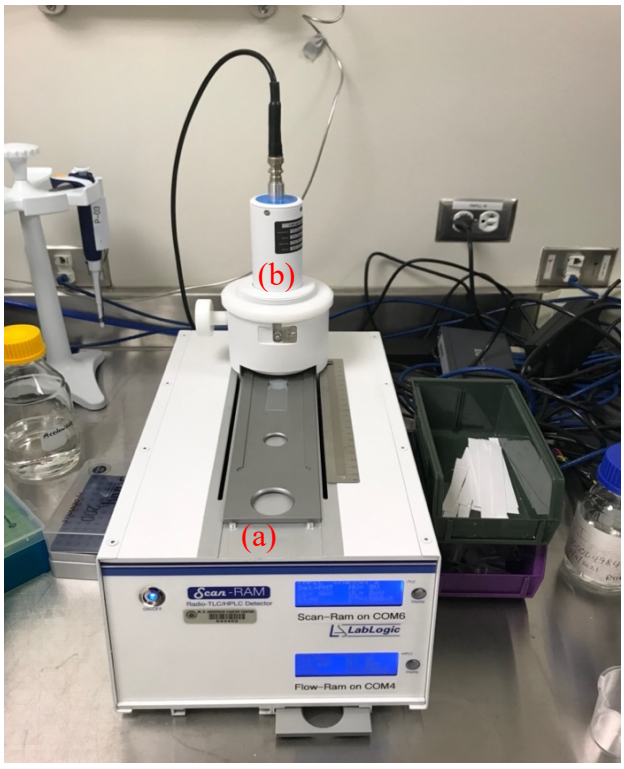

Figure 11 The Scan-Ram radio-TLC system used to determine the radiolabeling yield. The scanning bed (a); and the radioactivity detector (b).

2.2 In Vitro Cell Uptake Evaluation

The human prostate carcinoma cell lines LNCaP ($PSMA^+$) and PC-3 ($PSMA^-$) were selected to evaluate the uptake of ^{64}Cu-PSMA-I&T, ^{68}Ga-PSMA-I&T and ^{68}Ga-PSMA-11 in vitro. The cells were acquired from the American Type Culture Collection (ATCC, Manassas, VA) and were cultured in RPMI 1640 medium (Cytiva, Marlborough, MA) supplemented with 10% fetal bovine serum, and 1% antibiotics (penicillin 100 U/mL, streptomycin 10 ug/mL). The cells were incubated at 37 °C in a humidified incubator at 5% CO_2. Additionally, the expression analysis of PSMA in the selected cell lines was validated on the protein level by western blot (see Appendix C for details).

2.2.1 PSMA Specific Binding Assay

LNCaP ($PSMA^+$) and PC-3 (PSMA-) cells were plated into 6-well plates each (5 x10^5 cells per well) and incubated for 24 hr. prior to the experiment. At experiment day, the media in the wells was discarded and cells were washed with 1mL PBS. Next, the cells were exposed to ^{64}Cu-PSMA-I&T at (0.5-1.0 μCi) and incubated for 1 hr., followed by wash with 1mL PBS and cell lysis with 2mL 1 N NaOH. The lysates were then collected and transferred to scintillation vials and radioactivity was measured using an automatic gamma counter (2480 WIZARD2, Perkin Elmer, USA). The uptake was expressed as %ID and normalized to the cell number. The same protocol was applied to evaluate the cell uptake of each ^{68}Ga-PSMA-I&T and ^{68}Ga-PSMA-11 separately.

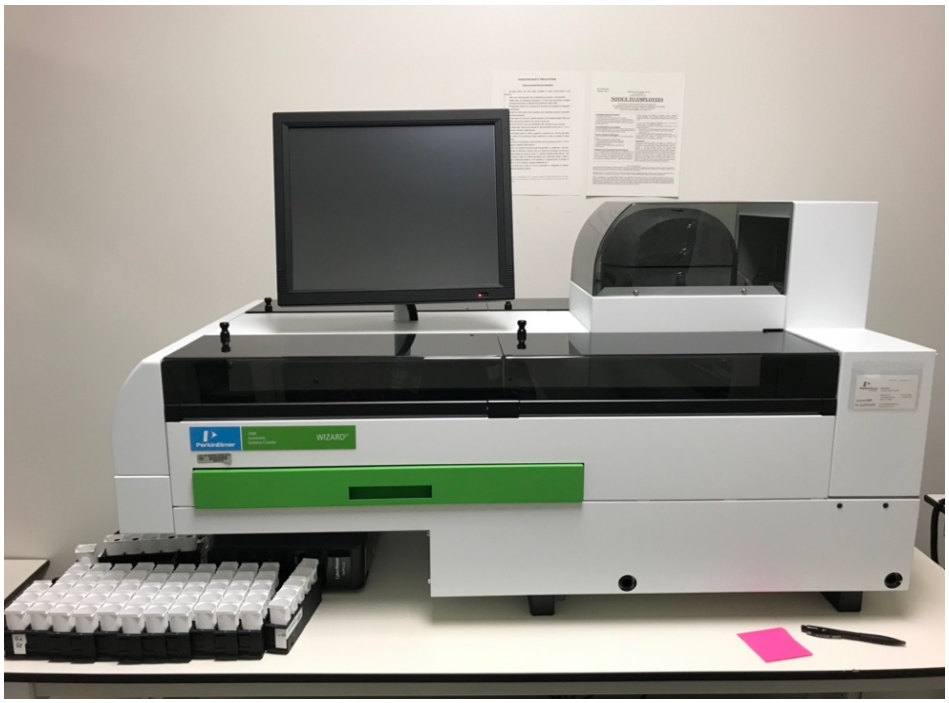

Figure 12 The Perkin Elmer gamma counter used to measure the radioactivity in the tubes.

2.3 In Vivo Biological Evaluation

^{64}Cu-PSMA-I&T was evaluated as a potential PSMA imaging agent in tumor xenograft mouse models by Positron Emission Tomography and Computed Tomography (PET)/(CT) imaging. Its performance was then compared to that of ^{68}Ga-PSMA-I&T and ^{68}Ga-PSMA-11 that were also included in the study. Additionally, biodistribution studies were performed to evaluate and measure the uptake and organ accumulation of each radiotracer in tumor-bearing mice at selected time points as detailed in the following sections.

2.3.1 Mouse Models of Prostate Cancer

Athymic nude immunodeficient mice (male, 6-8 weeks old, n= 60) obtained from (Envigo, Indianapolis, IN) were subcutaneously injected with (PSMA+) LNCaP and (PSMA−) PC-3 cells, for comparison between positive and negative based on radiotracers targeting. Prior to injection, the LNCaP and PC-3 cells were washed twice with FBS-free RPMI 1640 medium and two cell suspensions of (5×10^6 cells /100 μL) were prepared and kept on ice until inoculation. The mice were then injected at shoulder height with 100 μL 1:1 cell: Matrigel suspension. Tumor growth was monitored weekly, and once tumor reached 5-10 mm in diameter (2-4 weeks after injection) mice were ready for imaging. All animal work and handling were in compliance with and approved by the Institutional Animal Care and Use Committee (IACUC), and the Institutional Radiation Safety Committee at the University of Texas MD Anderson Cancer Center.

2.3.2 Small-Animal PET/CT Imaging

Dynamic PET/CT images of tumor-bearing mice were acquired by the (PET/SPECT/CT Bruker Alibra scanner). At 2, 24, and 48 hr. after intravenous injection (i.v.) of (150–200 uCi) of ^{64}Cu-PSMA I&T per mouse of LNCaP xenograft model (n=3) and PC-3 model (n=3), images were obtained for 60 min under inhalation anesthesia (isoflurane, 1.5%). In addition, images of both ^{68}Ga-PSMA I&T and ^{68}Ga-PSMA-11 in LNCaP xenograft mice models (n=3) and PC-3 models (n=3) for each radiotracer, were acquired after i.v. injection of (100-150 uCi) for 60 min, then again for 45 min. The dynamic PET

images were then reconstructed as follows: (6 frames x 10 seconds, 4 frames x 60 seconds, 5 frames x 120 seconds, 3 frames x 300 seconds, 6 frames x 600 seconds, and 3 frames x 900 seconds) using the filtered back-projection (FBP) method, as well as applying attenuation correction to the scatter and decay by CT. Next, volumes of interests (VOIs) (also known as regions of interests (ROIs)) of selected organs (e.g., salivary glands, heart, muscle, tumor, liver, and kidney) were drawn on the CT images. These VOIs were then applied to the corresponding organs on the time-integrated reconstructed PET images, to estimate the accumulation of ^{64}Cu-PSMA-I&T in each organ. Time activity curves (TACs) of the organs were then generated based on the PET image biodistribution data.

The radiotracer activity in tissue was calculated as ((tracer tissue concentration / (tracer injected dose / body weight)). The measured activity in (kBq/cc) was normalized to the total injected activity, as percent injected dose per gram (%ID/g), which was dependent on the recorded weight of the imaged mice, dose values, injection times, the radionuclide half-life, and decay corrections of the injected activity. The same method was used to process the ^{68}Ga-PSMA-I&T and ^{68}Ga-PSMA-11 data. All imaging data analysis was performed using the PMOD software (version 3.3, PMOD Technologies Ltd, Zurich, Switzerland).

Figure 13 PET/CT Albira scanner (left), and the scanner bed (right) with mice bearing LNCaP (left) and PC-3 (right) tumor models ready for imaging.

2.3.3 Biodistribution Studies

The biodistribution studies of ^{64}Cu-PSMA-I&T, ^{68}Ga-PSMA-I&T and ^{68}Ga-PSMA-11 were performed when the tumors growth reached a diameter of 0.7-0.8 cm. The athymic nude mice bearing subcutaneous LNCaP and PC-3 xenografts were anesthetized by isoflurane inhalation and injected with 10-15 µCi of each tracer in 100-150 µL of saline via tail vein. The mice were sacrificed for biodistribution analysis of ^{64}Cu-PSMA-I&T post 2, 24, and 48 hr. injection for (n = 4 per group), while post 1 and 2 hr. injection for ^{68}Ga-PSMA-I&T and ^{68}Ga-PSMA-11 for (n = 4 per group). The organs of interest (ex. blood, lung, liver, intestines, kidney, muscle) and tumor, were removed, weighted, and counted by

the gamma counter. The percent injected dose per gram (%ID/g) and percent injected dose per organ (%ID/organ) were calculated by comparison to a weighted and counted standard.

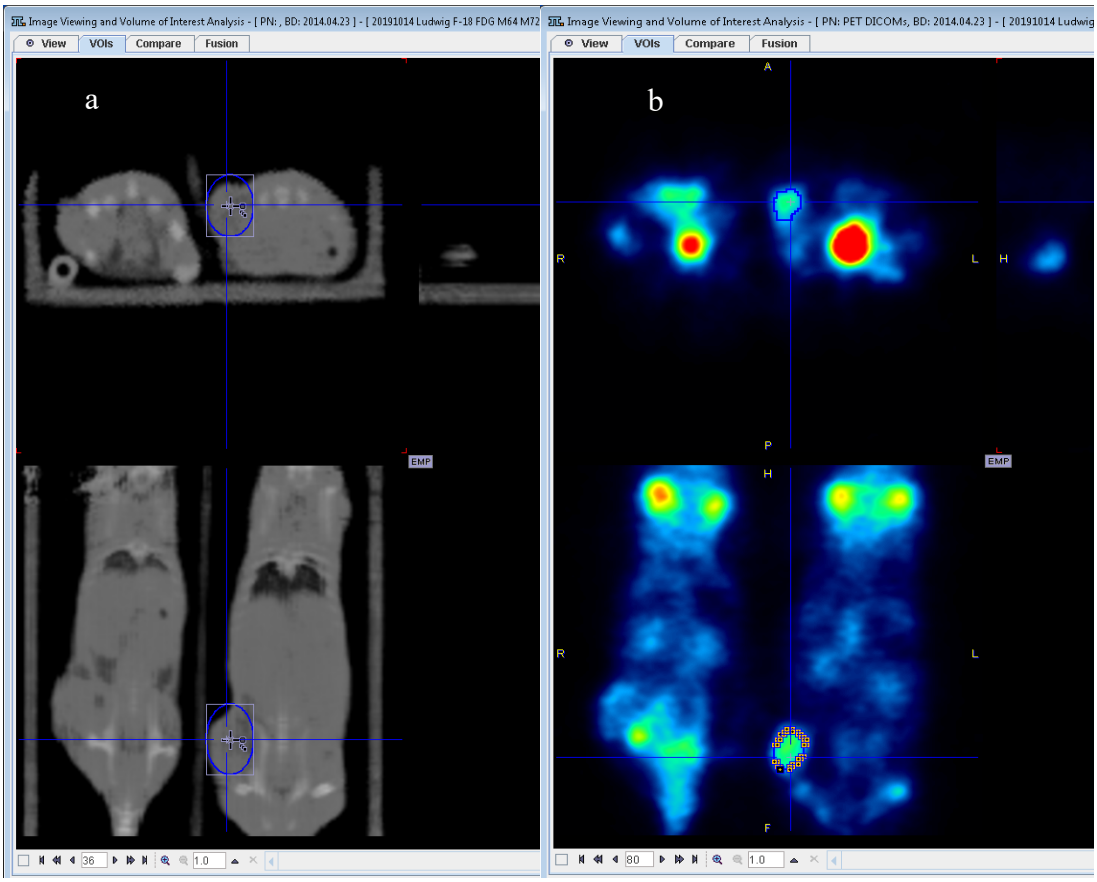

Figure 14 Illustration of drawing the volumes of interest (VOI's) on selected organs in the reconstructed CT (a) and PET (b) images in PMOD.

2.4 Radiation Dosimetry Measurements

The time-activity curves (TACs) generated from the PET/CT imaging data, were used to estimate the target organ mean absorbed dose D (r_T) of ^{64}Cu-PSMA-I&T. The dosimetry was calculated in accordance with the Medical Internal Radiation Dose committee of the Society of Nuclear Medicine (MIRD) schema [57]. The MIRD method is commonly used in nuclear medicine applications to assess the dosimetry of radiopharmaceuticals, where the mean absorbed dose D (r_T, t) delivered to a target organ (r_T) from a source organ (r_S) at time (t) after injection of a radiotracer is given as:

$$D\ (r_T, t) = \sum_{rS} \tilde{A}\ (r_S, t).S\ (r_T \leftarrow\ r_S, t) \qquad \text{(Eq. 1)}$$

where:

$\tilde{A}\ (r_S, t)$ = is the time-integrated activity of the administered radiopharmaceutical in the source organ (r_S):

$$\tilde{A} = \int_0^\infty A\ (A\ \ t)\ dt = \tilde{a}\ (r_S)\ .A_0 \qquad \text{(Eq. 2)}$$

which gives, the time integrated activity coefficient (also known as residence time) as:

$$\tilde{a}\ (r_S) = \frac{\tilde{A}\ (r_S)}{A_0} \qquad \text{(Eq. 3)}$$

and:

$S\ (r_T \leftarrow\ r_S, t)$= the radionuclide-specific quantity reflecting the mean absorbed dose rate to target tissue (r_T) at time (t) after injection per unit activity present in source tissue (r_S):

$$S\ (r_T, \leftarrow\ r_S, t) = \frac{1}{M(r_T, t)} \sum_i \Delta_i\ \emptyset\ (r_T, \leftarrow\ r_S, E_i, t) \qquad \text{(Eq. 4)}$$

where:

Δ_i = mean energy of the (i^{th}) transition per nuclear transformation

$\emptyset\ (r_T, \leftarrow\ r_S, E_i, t)$ = the absorbed fraction of radiation energy E_i emitted within the source tissue (r_S) at time (t) that is absorbed in the target tissue (r_T)

$M(r_T, t)$ = the time-dependent mass of the target tissue (r_T) in the reference individual

The time-integrated activity (Ã) in the source organs (r_S), was calculated for each organ as the area under the curve (AUC) of the corresponding organ TAC from the PET imaging biodistribution data, by fitting the TAC to exponential equations using GraphPad Prism software (version 8.0, GraphPad Software, La Jolla, CA). The residence times (time integrated activity coefficients (ã)) of the source organs were then determined and used as inputs in the Organ Level Internal Dose Assessment (OLINDA 2.0) software (Vanderbilt University, Nashville, TN) to calculate the organ doses. The same statical analysis methods were applied to determine the dosimetry for both ^{68}Ga-PSMA-I&T and ^{68}Ga-PSMA-11.

3. RESULTS

3.1 Radiosynthesis Quality Control

One of the crucial aspects of preparing compounded radiopharmaceuticals is ensuring that the product passes acceptable quality control criteria for it to be effective and safe to administer into humans or for preclinical research studies. As such the U.S. Pharmacopeia (USP) Chapter <823> details the required quality control tests that PET radiopharmaceuticals must meet in terms of purity and quality to be released for final use [58]. In this study the radiochemical purity (RCP), which is defined as the percent of the radioactivity present in the desired chemical form in a radiopharmaceutical was analyzed by HPLC. The RCP for all the three radiopharmaceuticals produced ^{64}Cu-PSMA-I&T, ^{68}Ga-PSAM-I&T and ^{68}Ga-PSMA-11 was ≥ 95%. This result was satisfactory and an indication of high radiolabeling efficiency. More importantly, meeting acceptable RCP standards ensures that the quality of the PET imaging is not comprised by any unwanted impurities, or producing unacceptable high radiation absorbed doses. Additionally, the stability of the radiotracers was tested by HPLC at selected time points ^{64}Cu-PSMA-I&T (Figures 15-19), ^{68}Ga-PSMA-I&T (Figures 20-22), and ^{68}Ga-PSMA-11 (Figures 23-25). All the three radiotracers proved to be stable at room temperature with RCP of ≥ 95%.

3.1.1 ^{64}Cu-PSMA-I&T Quality Control & Stability Test

As it can be seen from the radiochromatograms in Figures 15-19, ^{64}Cu-PSMA-I&T exhibited constant stability up to 24 hrs. at room temperature. In addition, this results also shows that the radiotracer did not undergo any radiolysis, which is the dissociation of molecules by ionizing radiation. This is critical as the premature decomposition of a radiopharmaceutical can be detrimental to the imaging study leading to false results and unwanted radiation exposure.

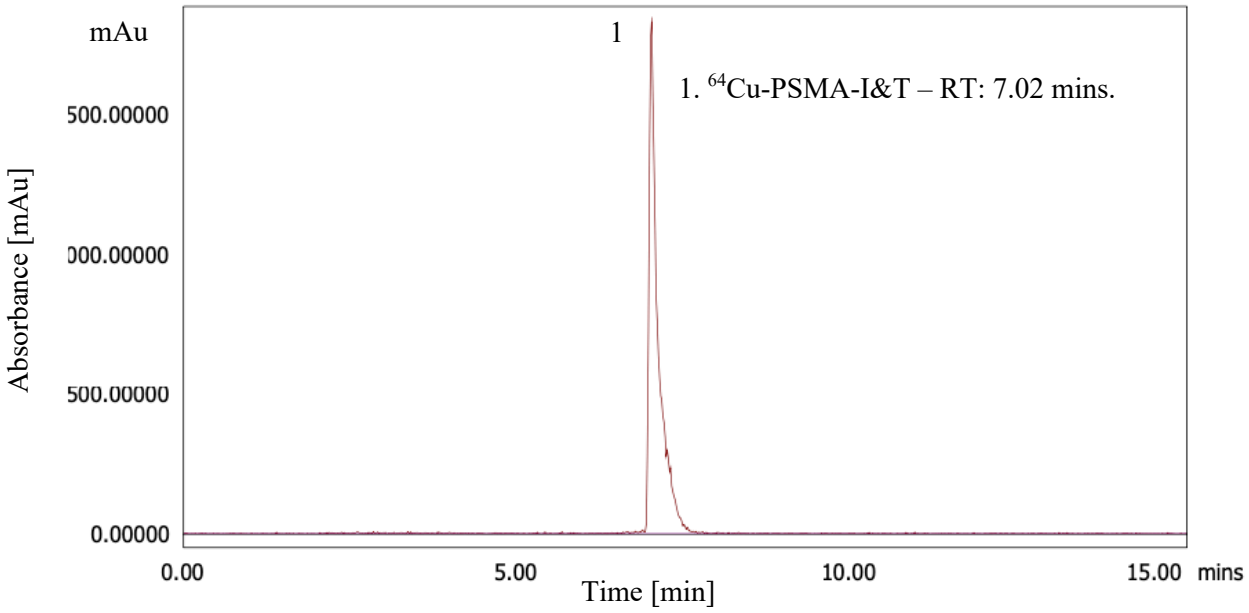

Figure 15 Chromatogram for the RCP and stability test of ^{64}Cu-PSMA-I&T at end of synthesis (EOS). Peak 1: Retention time: 7.02 min. and RCP ≥ 95%.

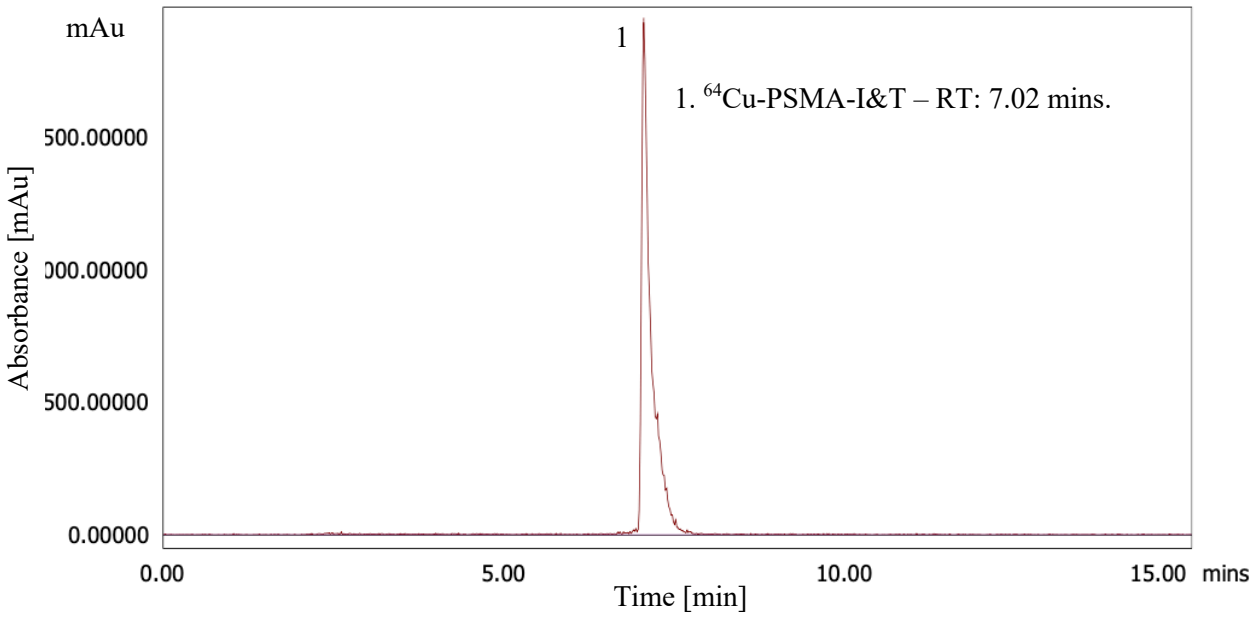

Figure 16 Chromatogram for the RCP and stability test of ^{64}Cu-PSMA-I&T at 2 hrs. Peak 1: Retention time: 7.02 min. and RCP ≥ 95%.

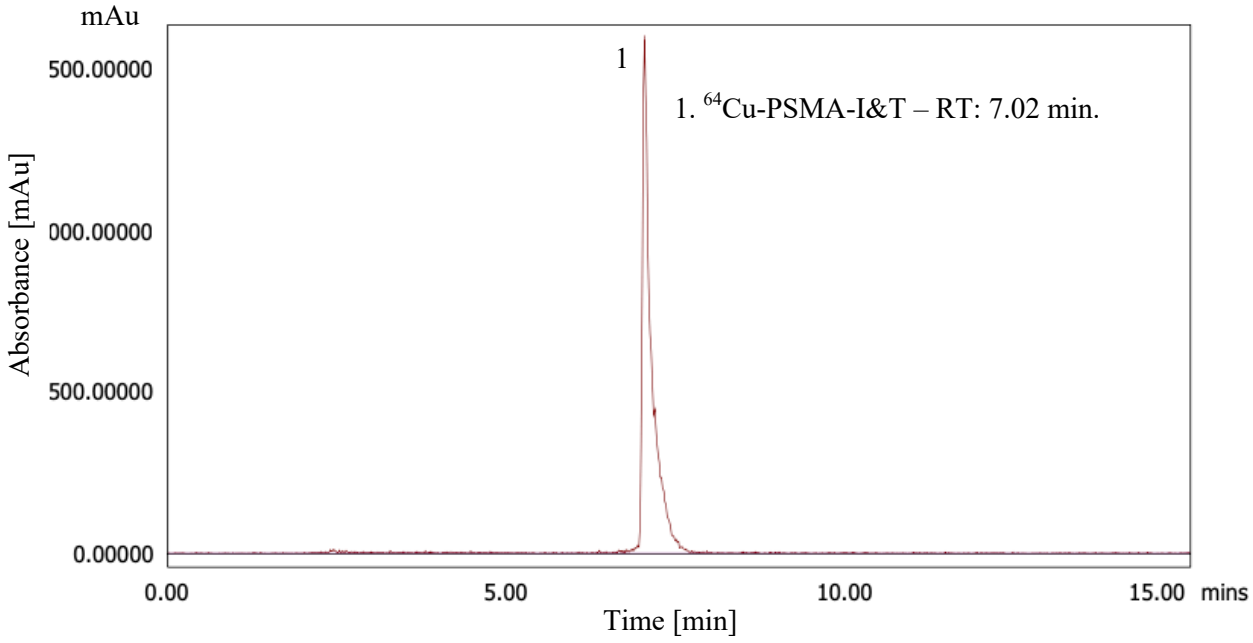

Figure 17 Chromatogram for the RCP and stability test of ^{64}Cu-PSMA-I&T at 4 hrs. Peak 1: Retention time: 7.02 min. and RCP ≥ 95%.

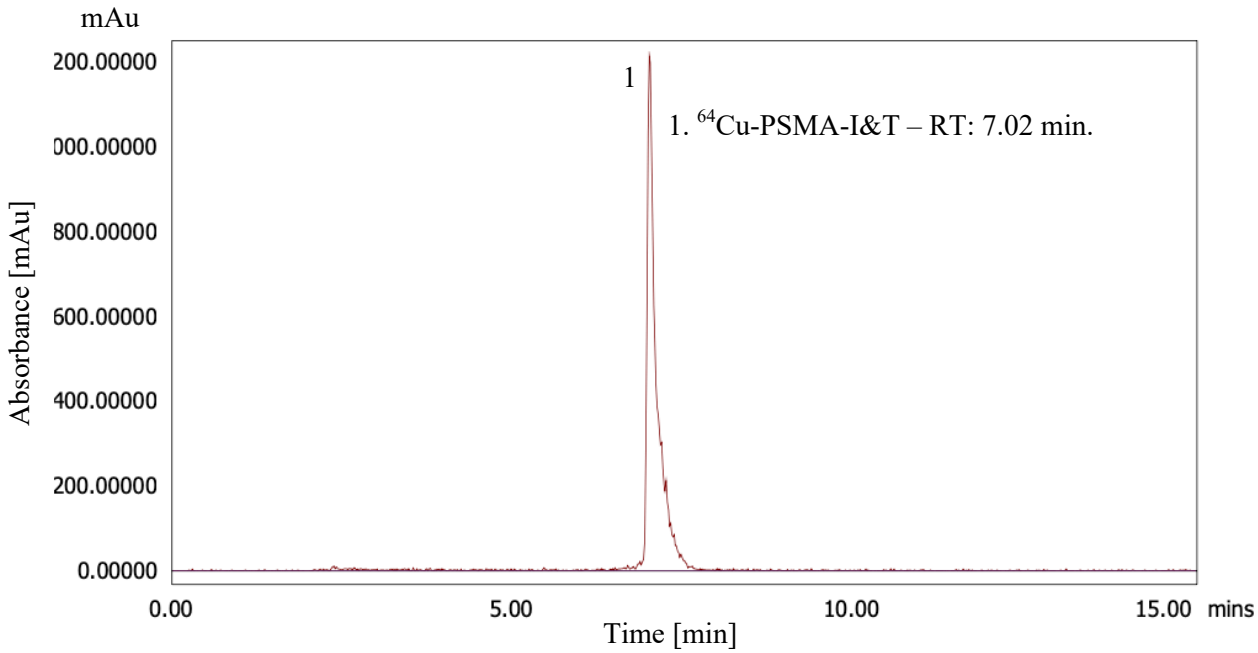

Figure 18 Chromatogram for the RCP and stability test of ^{64}Cu-PSMA-I&T at 8 hrs. Peak 1: Retention time: 7.02 min. and RCP ≥ 95%.

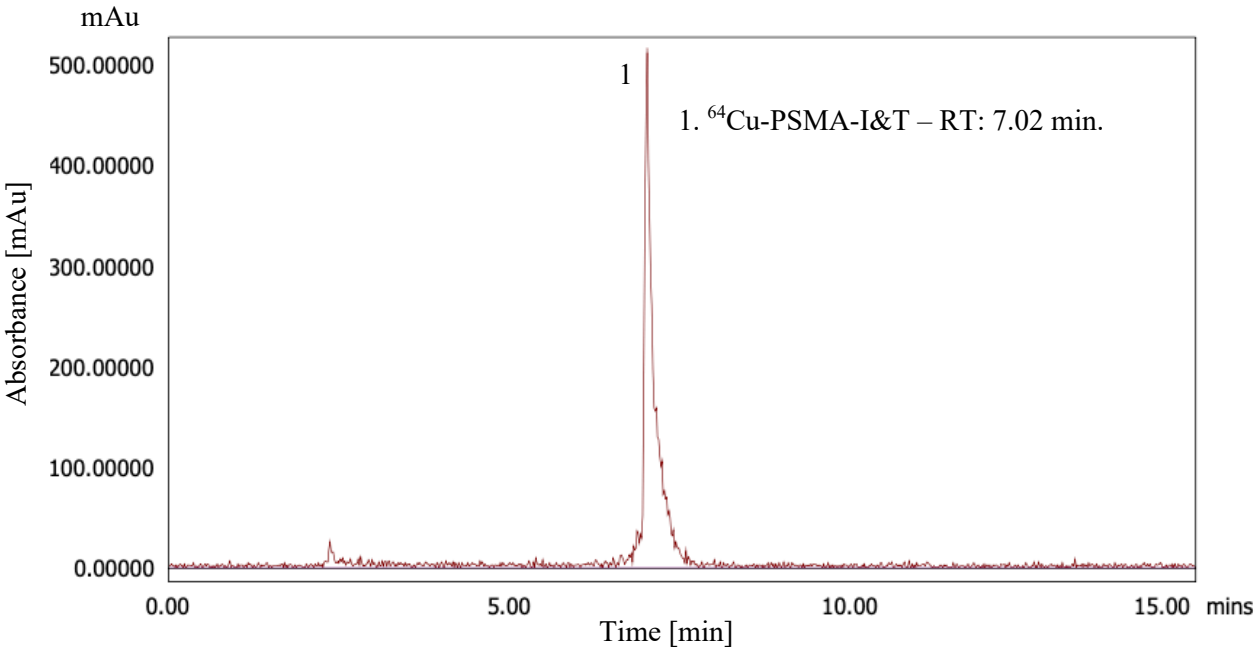

Figure 19 Chromatogram for the RCP and stability test of ^{64}Cu-PSMA-I&T at 24 hrs. Peak 1: Retention time: 7.02 min. and RCP ≥ 95%.

3.1.2 ^{68}Ga-PSMA-I&T Quality Control & Stability Test

^{68}Ga-PSMA-I&T stability was tested up to 4 hrs. only due to the short half-life of ^{68}Ga (68 min). The radiotracer was shown to be stable and intact at room temperature at the selected testing time points (0, 2, and 4 hrs.). However, as it can be seen from the radiochromatogram a second isomer (peak 2, retention time: 9.30 min) was present along with the more thermodynamically stable one (peak 1, retention time: 9.50 min). This phenomenon is attributed to the nature of PSMA inhibitors, which contain a hydrophobic part that upon complexation with (^{68}Ga) tends to form three diastereomers, RR, RS, and SS at its amine nitrogens [59]. While all these diastereomers exhibit the same binding affinity to PSMA and radiochemical stability, the RR was reported to be the more favorable and thermodynamically stable isomer [59].

Additionally, the isomers formation was reported to be dependent on concentration, pH and affected by temperature [60]. Although, ^{68}Ga-PSMA-I&T was radiolabeled at a pH of ~ 4 and heated at 95 °C, and produced under cGMP, a small fraction of the other two isomers (RS, SS) would at times be present at the final formulation along with the more favorable isomer formed (RR). Nevertheless, the presence of such small isomer fraction was demonstrated not to have any negative impact on the PSMA-binding properties or comprising the quality of the PET imaging [61-64].

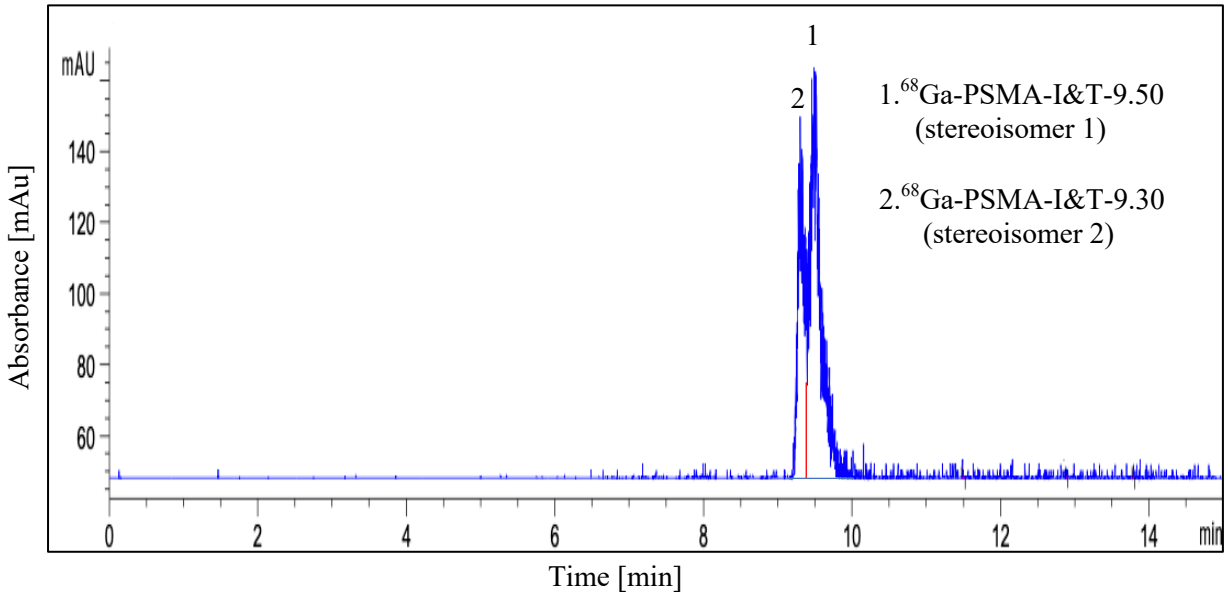

Figure 20 Chromatogram for the RCP and stability test of ^{68}Ga-PSMA-I&T at end of synthesis (EOS). 1. Peak 1: Retention time: 9.50 min. (stereoisomer 1), 2. Peak 2: Retention time: 9.30 min. (stereoisomer 2) and RCP ≥ 95%.

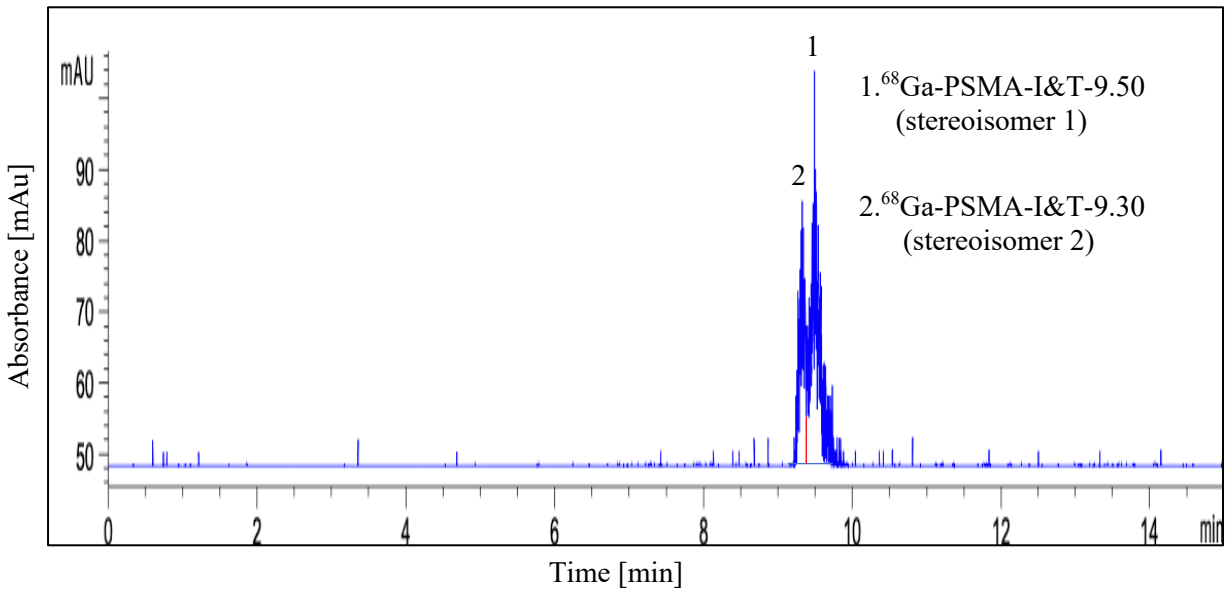

Figure 21 Chromatogram for the RCP and stability test of ^{68}Ga-PSMA-I&T at 2 hrs. 1. Peak 1: Retention time: 9.50 min. (stereoisomer 1), 2. Peak 2: Retention time: 9.30 min. (stereoisomer 2) and RCP ≥ 95%.

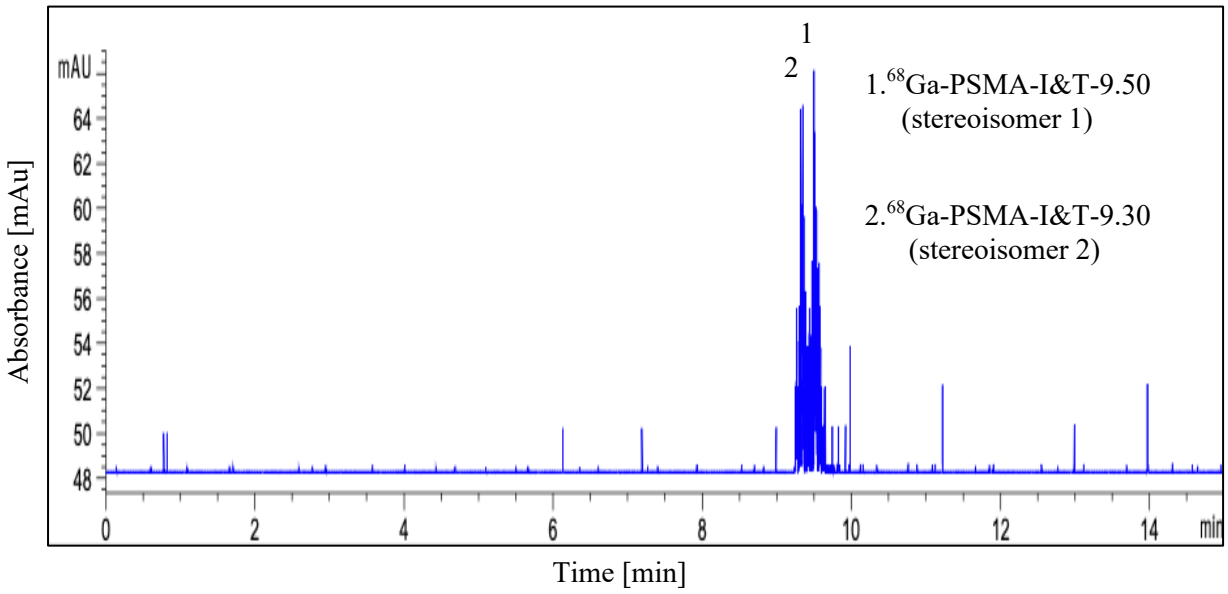

Figure 22 Chromatogram for the RCP and stability test of ^{68}Ga-PSMA-I&T at 4 hrs. 1. Peak 1: Retention time: 9.50 min. (stereoisomer 1), 2. Peak 2: Retention time: 9.30 min. (stereoisomer 2) and RCP ≥ 95%.

3.1.3 ^{68}Ga-PSMA-11 Quality Control & Stability Test

Similar to ^{68}Ga-PSMA-I&T, ^{68}Ga-PSMA-11 stability was tested up to 4 hrs. The radiotracer was shown to be stable and intact at room temperature at the selected testing time points (0, 2, 4 hrs.). In addition, the product retention time (peak 1) was at 6.20 min. followed by a second isomer (peak 2, retention time: 6.90 min). As previously explained such isomers are formed due to the hydrophobic part of PSMA-based inhibitors. However, imaging quality or binding affinity to PSMA are not hindered by the existence of small isomer fractions [61-64].

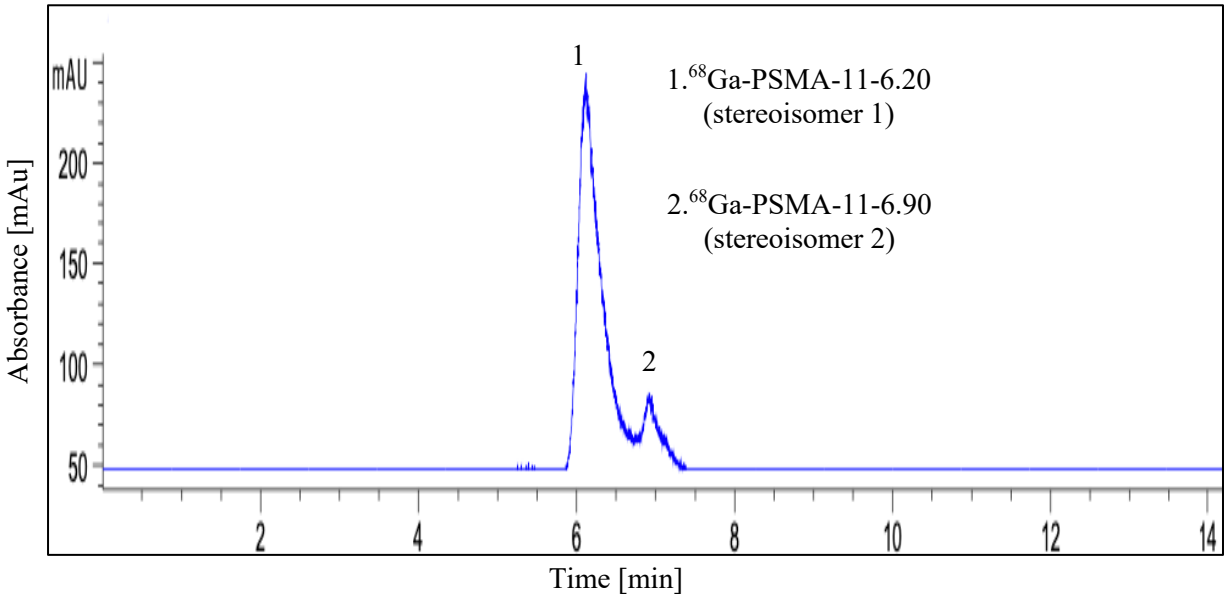

Figure 23 Chromatogram for the RCP and stability test of ^{68}Ga-PSMA-11 at end of synthesis (EOS). Peak 1: Retention time: 6.20 min. (stereoisomer 1), 2. Peak 2: Retention time: 6.90 min. (stereoisomer 2) and RCP ≥ 95%.

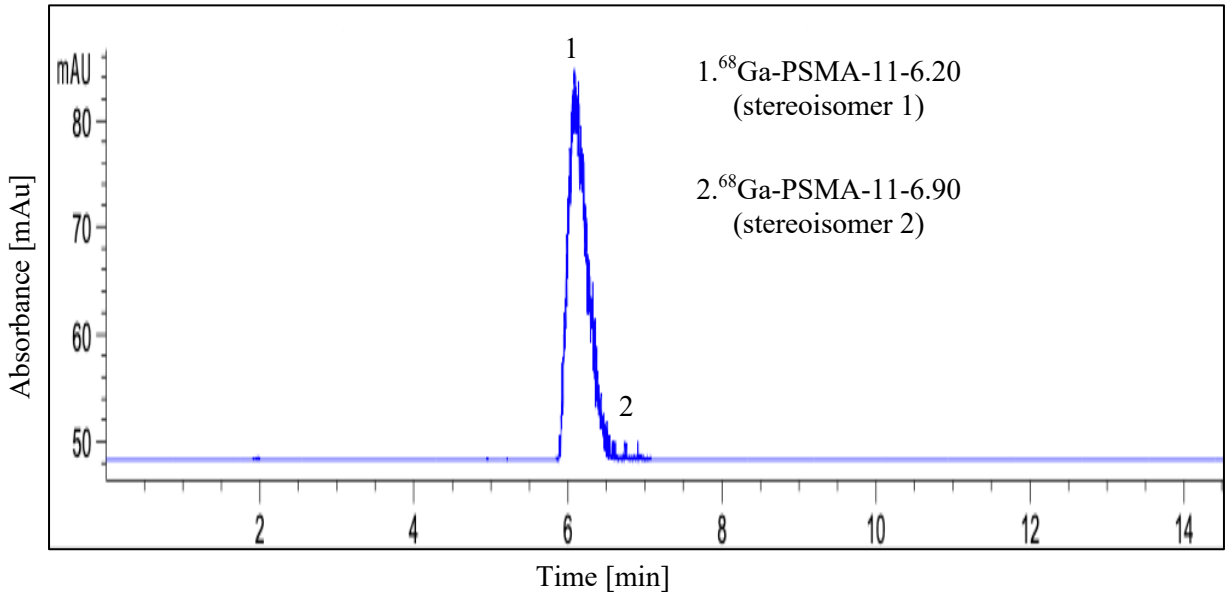

Figure 24 Chromatogram for the RCP and stability test of ^{68}Ga-PSMA-11 at 2 hrs. Peak 1: Retention time: 6.20 min. (stereoisomer 1), 2. Peak 2: Retention time: 6.90 min. (stereoisomer 2) and RCP ≥ 95%.

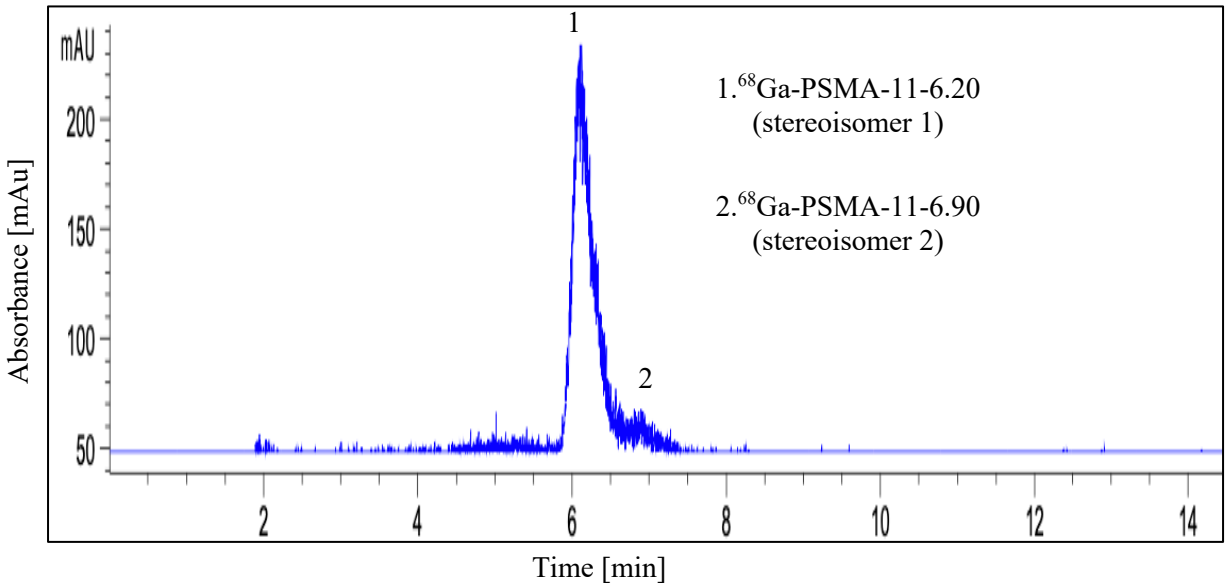

Figure 25 Chromatogram for the RCP and stability test of ^{68}Ga-PSMA-11 at 4 hrs. Peak 1: Retention time: 6.20 min. (stereoisomer 1), 2. Peak 2: Retention time: 6.90 min. (stereoisomer 2) and RCP ≥ 95%.

3.1.4 Radiolabeling Quality Control

A secondary technique that was used for a rapid testing to determine the percentage of the radiolabeling yield was using instant thin layer chromatography (ITLC). A sample of each radiotracer was scanned by the radioactivity detector, generating radiochromatograms for each one tested. The incorporation yields always exceed 95% (Fig. 26-28).

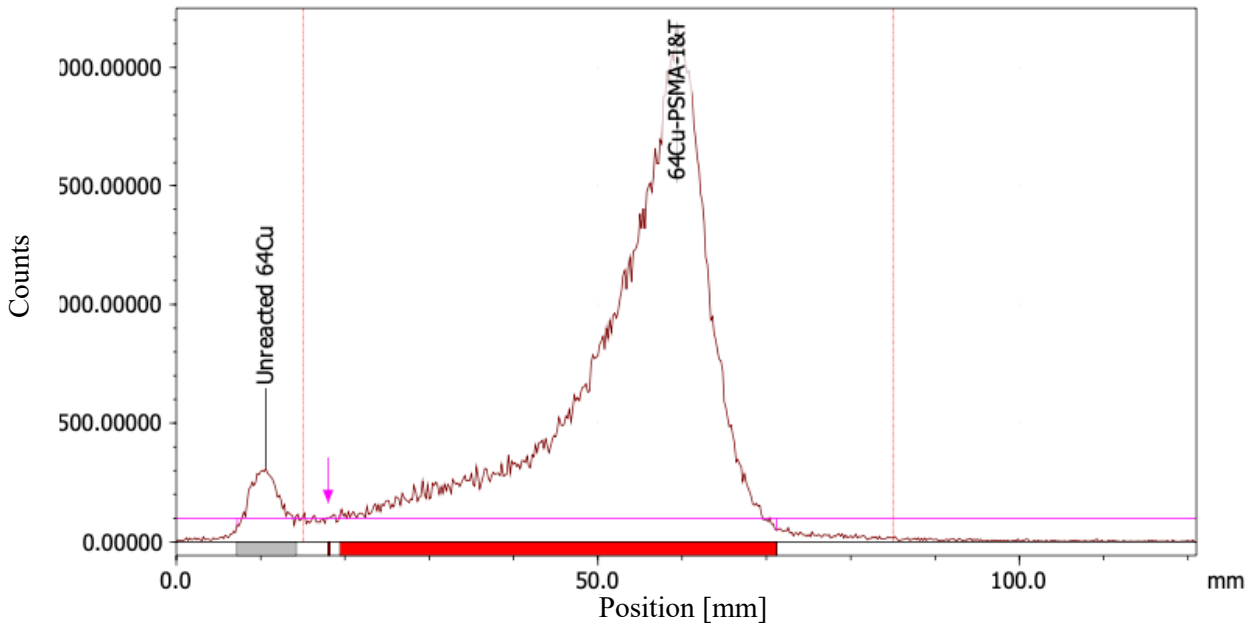

Figure 26 ITLC radiochromatogram of ^{64}Cu-PSMA-I&T radiolabeling yield > 95%.

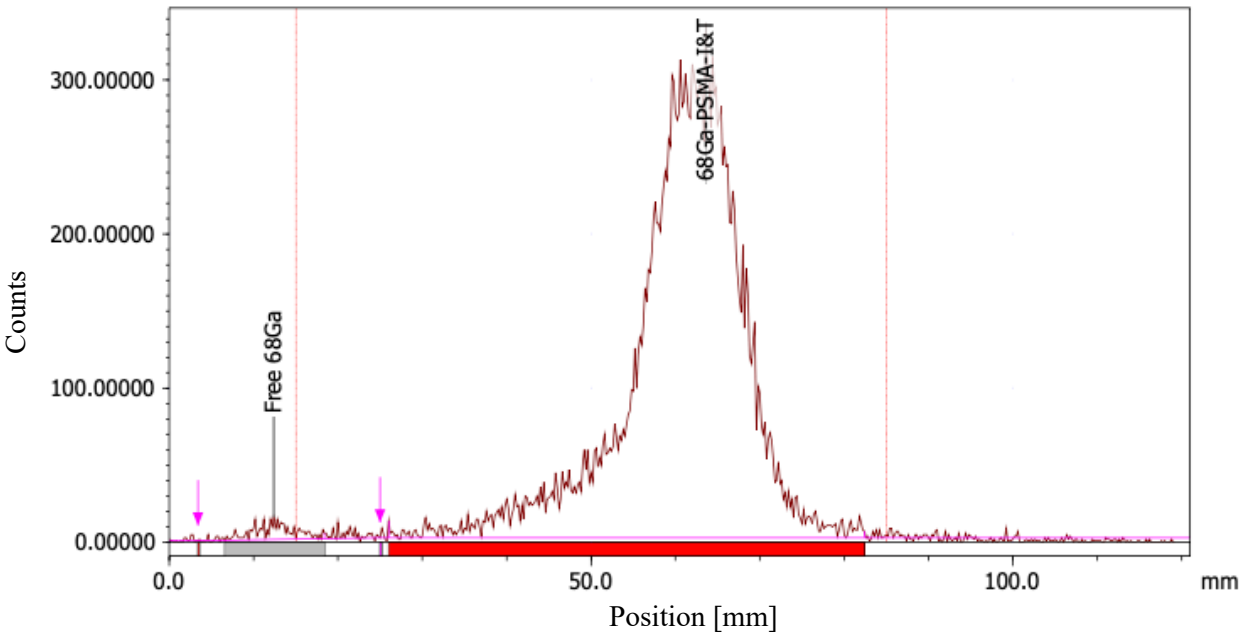

Figure 27 ITLC radiochromatogram of ^{68}Ga-PSMA-I&T, radiolabeling yield > 95%.

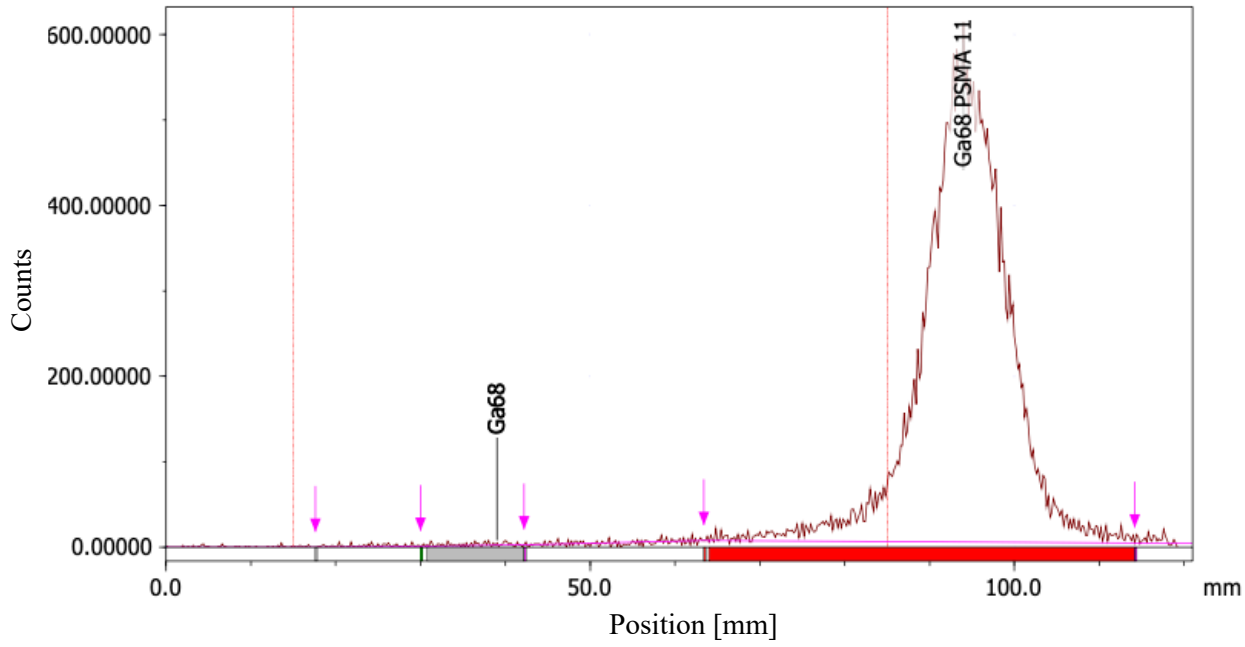

Figure 28 ITLC radiochromatogram of ^{68}Ga-PSMA-11, radiolabeling yield > 95%.

3.2 In Vitro Cell Uptake and PSMA Expression Evaluation

The expression of PSMA was evaluated by western blot in the cell lines selected for this study, LNCaP (PSMA+) and PC-3 (PSMA-). The PSMA protein expression was successfully confirmed on the LNCaP cell line by scanning the membrane containing the anti-PSMA antibody. While PC-3 had no PSMA expression as anticipated. The measured molecular weight (MW) of 100 kDa corresponds well with the expected value, as reported in the literature, and verified by the manufacture [65-69].

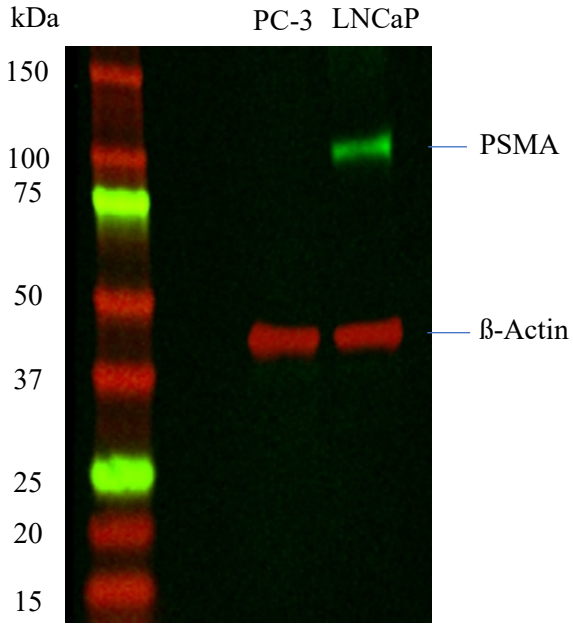

Figure 29 Confirmation of PSMA expression. The western blot analyses of LNCaP and PC3 cells. Confirming the expression of PSMA in LNCaP cells, while PC3 cells show no expression of PSMA. β-Actin was used as a loading control.

3.2.1 Radiotracers Cell Uptake Assay

Significant uptake of ^{64}Cu-PSMA-I&T was observed in the LNCaP (PSMA+) cells (5.59±0.41%ID/1x10^6 cells) vs. (0.72±0.26%ID/1x10^6 cells) in the PC-3 (PSMA-) cells, which demonstrated the targeting specificity of ^{64}Cu-PSMA-I&T in PCa cells. Although, ^{68}Ga-PSMA-11 had the best contrast in terms of uptake ratio between the PSMA+ and PSMA- cells (1:0.02). ^{64}Cu-PSMA-I&T showed promising results in comparison to its ^{68}Ga-labeled counterpart (^{68}Ga-PSMA-I&T) that only had an average uptake of (3.32± 0.34%ID/1x10^6 cells) in the LNCaP (PSMA+) cells.

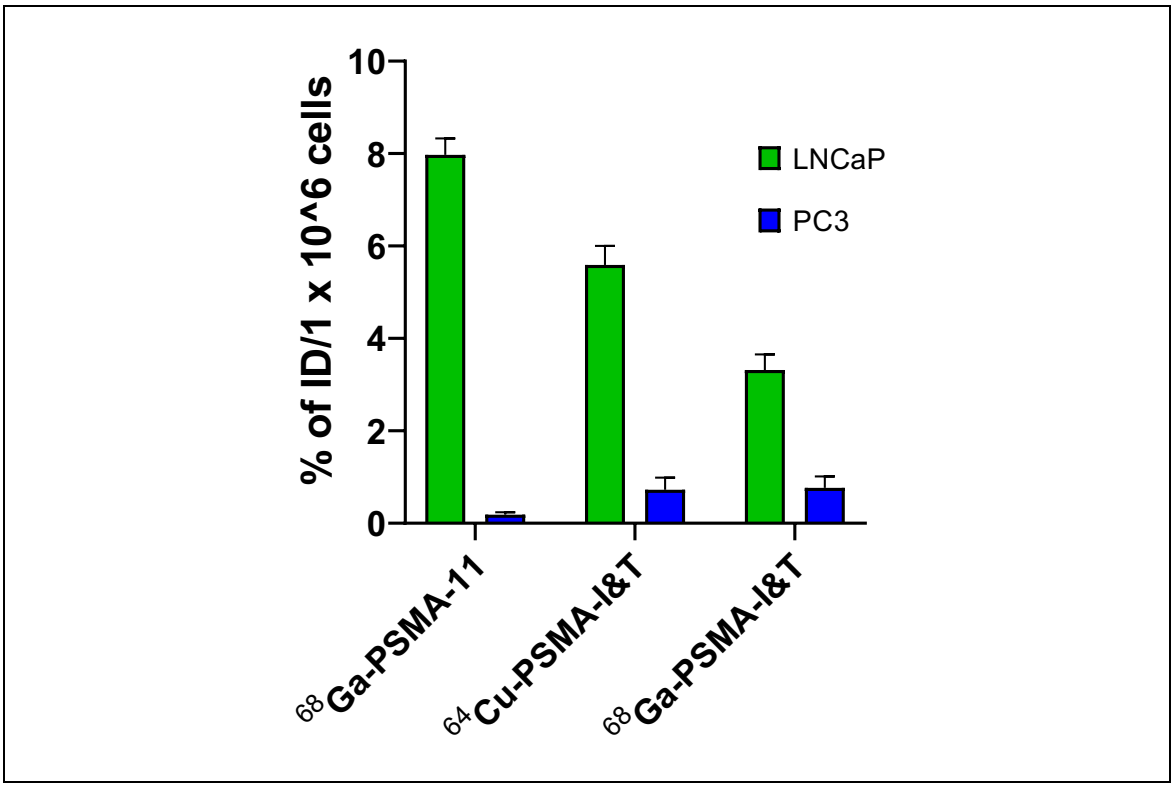

Figure 30 Comparison of *in vitro* radiotracer cell uptake (^{68}Ga-PSMA-11, ^{64}Cu-PSMA-I&T and ^{68}Ga-PSMA-I&T) in LNCaP (PSMA+) and PC-3 (PSMA-) cell lines.

Table 3 Results of the radiotracer in vitro cell uptake assay.

Radiotracer	Average Uptake LNCaP (%ID/1x10^6)	Average Uptake PC-3 (%ID/1x10^6)
^{68}Ga-PSMA-11	7.97±0.35	0.19±0.05
^{64}Cu-PSMA-I&T	5.59±0.41	0.72±0.26
^{68}Ga-PSMA-I&T	3.32 ± 0.34	0.77±0.25

3.3 Small Animal Imaging PET/CT

3.3.1 ^{64}Cu-PSMA-I&T PET/CT Imaging

PSMA-specific targeted imaging of ^{64}Cu-PSMA-I&T was evaluated *in vivo*, by injecting around (100-150 uCi) into established tumor xenograft models bearing LNCaP (PSMA+) and PC-3 (PSMA-) cells. A dynamic PET scan in list mode from (1-60 min) post injection was first acquired then a static scan at 2, 24 and 48 hrs. post injection (Fig. 31-33). The images clearly show a significantly higher specific uptake of ^{64}Cu-PSMA-I&T in the LNCaP tumor region than in the PC-3 one, demonstrating that tumors with high PSMA expression could clearly be visualized by ^{64}Cu- PSMA I&T PET/CT.

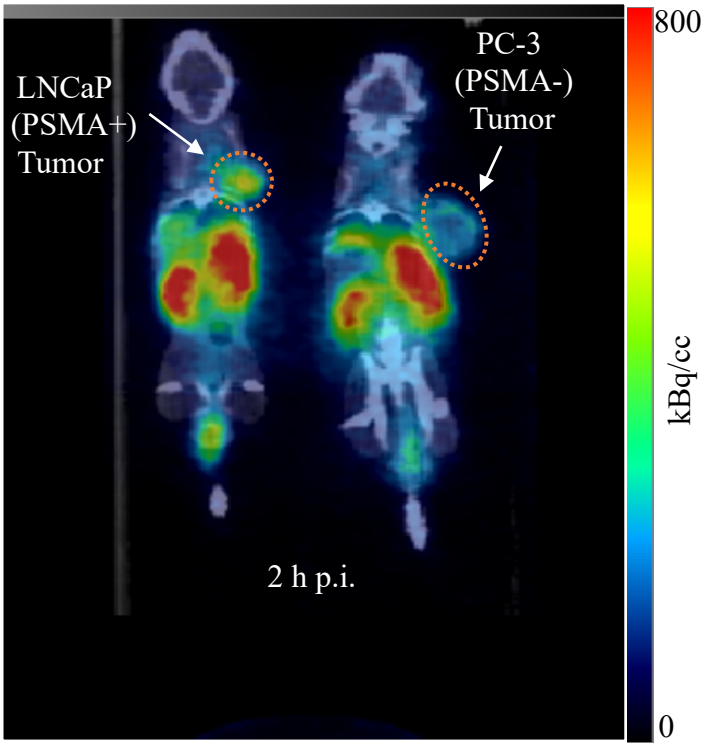

Figure 31 PET imaging 2 h p.i., ^{64}Cu-PSMA-I&T (LNCaP) vs. (PC-3) tumor uptake.

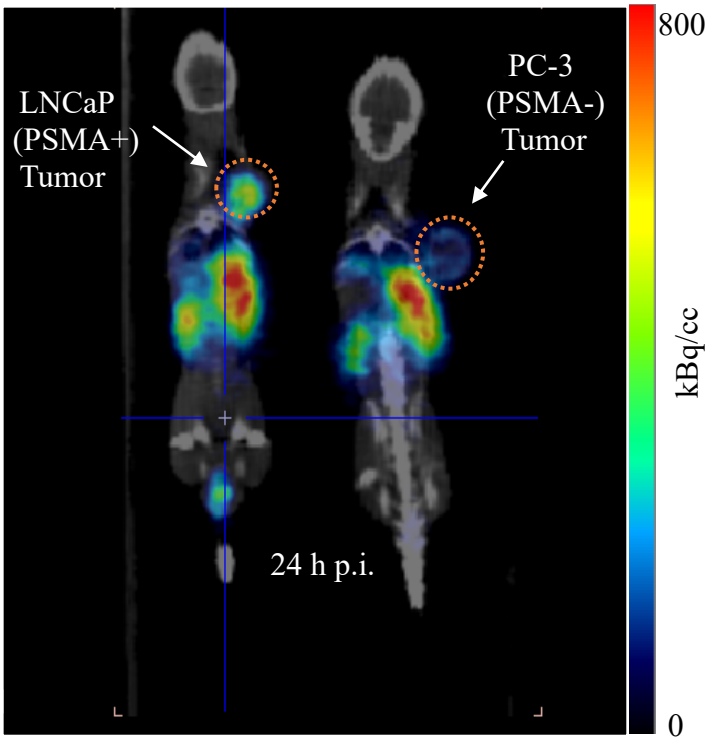

Figure 32 PET imaging 24 h p.i., ^{64}Cu-PSMA-I&T (LNCaP) vs. (PC-3) tumor uptake.

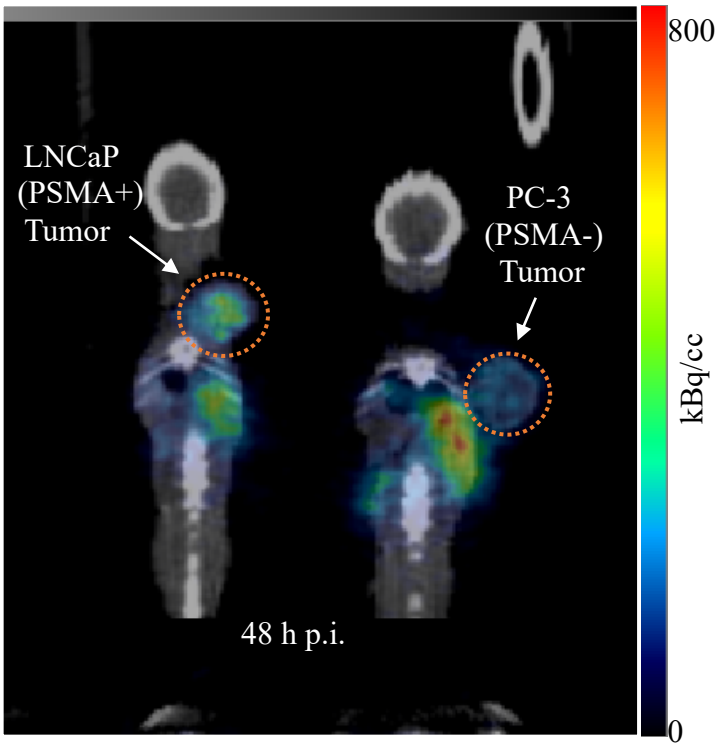

Figure 33 PET imaging 48 h p.i., ^{64}Cu-PSMA-I&T (LNCaP) vs. (PC-3) tumor uptake.

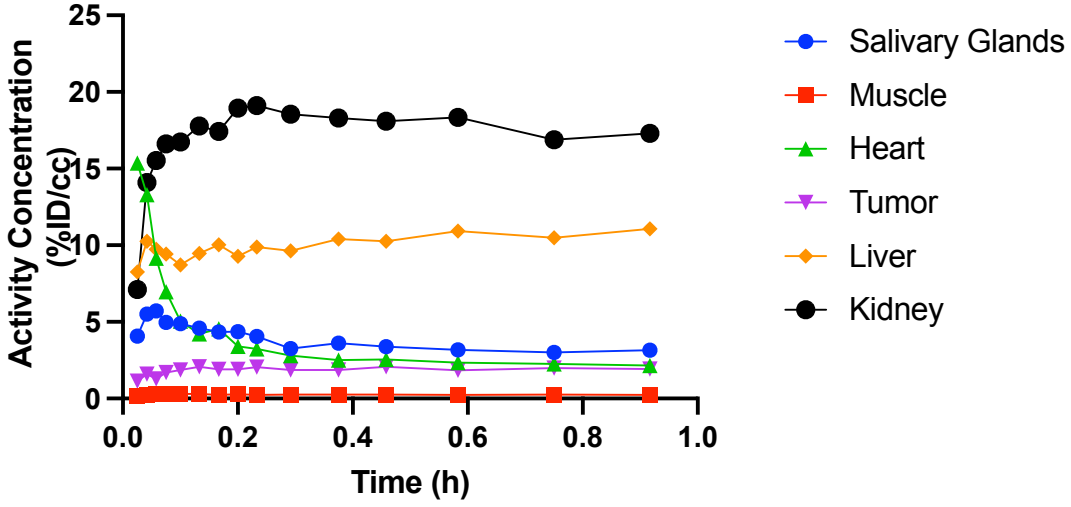

Figure 34 Time activity curves of ^{64}Cu-PSMA-I&T biodistribution of excretory organs [salivary glands; muscle; heart; tumor; liver and kidney].

3.3.1 ^{68}Ga-PSMA-I&T PET/CT Imaging

^{68}Ga-PSMA-I&T PET/CT scans were obtained by injecting around (100-150 uCi) into established tumor xenograft models bearing LNCaP (PSMA+) and PC-3 (PSMA-) cells. A dynamic PET scan in list mode from (1-60 min) post injection was first acquired then a static scan at 90 mins and 120 mins post injection (Fig. 35). The image clearly shows the radiotracer high affinity towards the LNCaP tumor region 60 mins post injection. Additionally, the time activity biodistribution of ^{68}Ga-PSMA-I&T from 0-60 min in the salivary glands, muscle, heart, tumor, liver, and kidney (Figure 36), show peak uptake (50 %ID/cc) in the kidney at around 27 min then slightly decreasing afterwards.

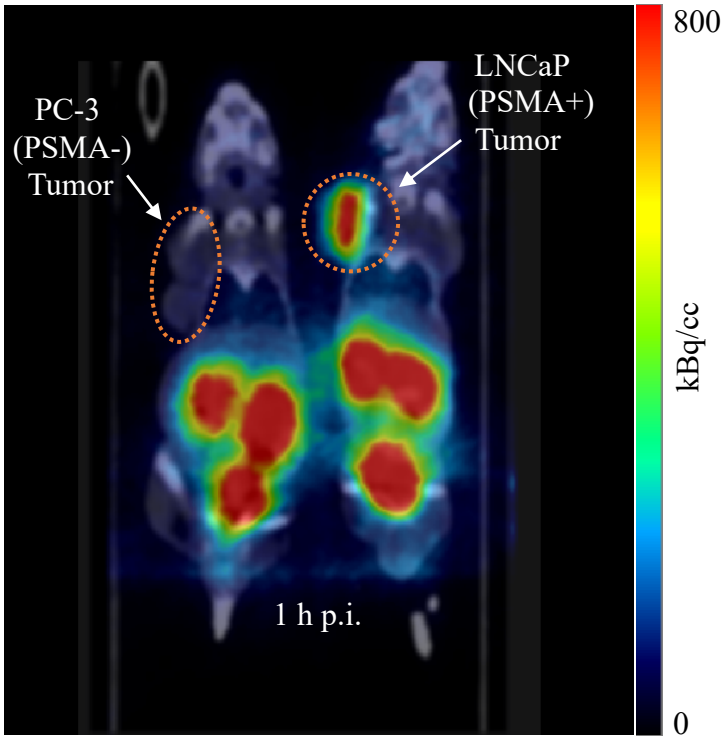

Figure 35 PET imaging 1 h p.i., ^{68}Ga-PSMA-I&T (LNCaP) vs. (PC-3) tumor uptake.

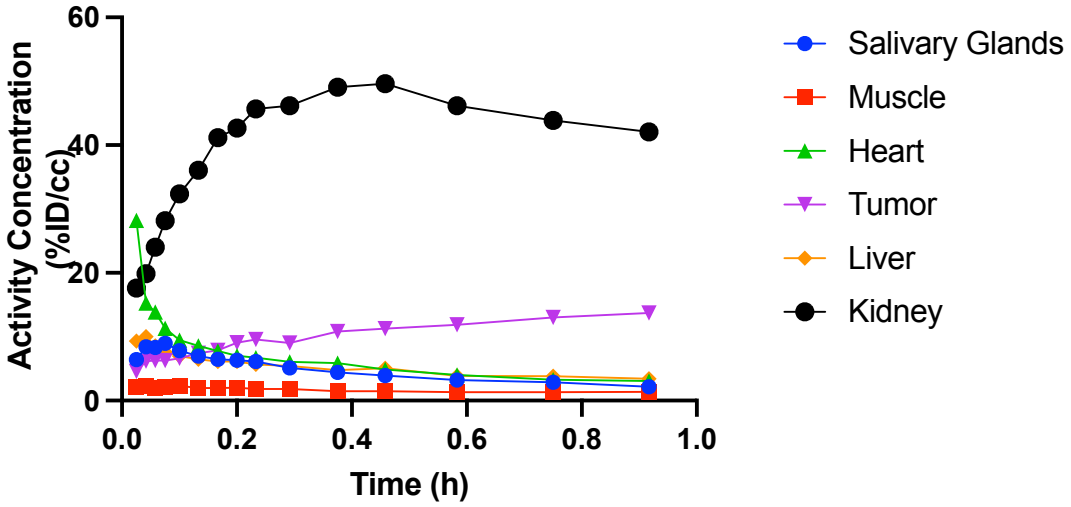

Figure 36 Time activity curves of ^{68}Ga-PSMA-I&T biodistribution of excretory organs [salivary glands; muscle; heart; tumor; liver and kidney].

3.3.1 ^{68}Ga-PSMA-11 PET/CT Imaging

PET/CT images of ^{68}Ga-PSMA-11 were acquired by injecting around (100-150 uCi) into established tumor xenograft models bearing LNCaP (PSMA+) and PC-3 (PSMA-) cells. A dynamic PET scan in list mode from (1-60 min) post injection was first acquired then a static scan at 90 mins and 120 mins post injection (Fig. 37). High binding affinity was observed in the LNCaP tumor 60 mins post injection. In addition, Figure 38 displays the time activity biodistribution of ^{68}Ga-PSMA-11 from 0-60 min in the salivary glands, muscle, heart, tumor, liver, and the kidney. A significant peak uptake (78 %ID/cc) in the kidney was observed around 55 min into imaging.

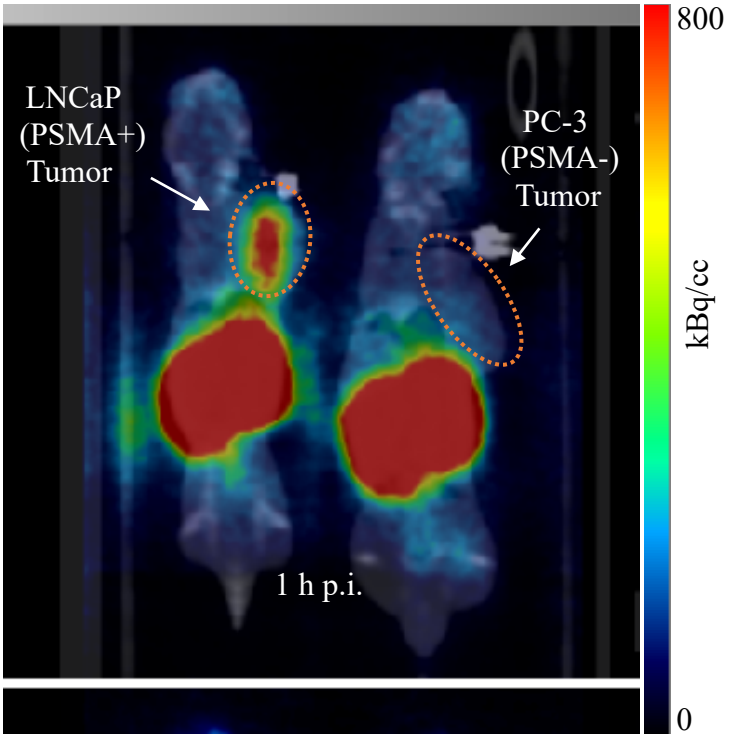

Figure 37 PET imaging 1 h p.i., ^{68}Ga-PSMA-11 (LNCaP) vs. (PC-3) tumor uptake.

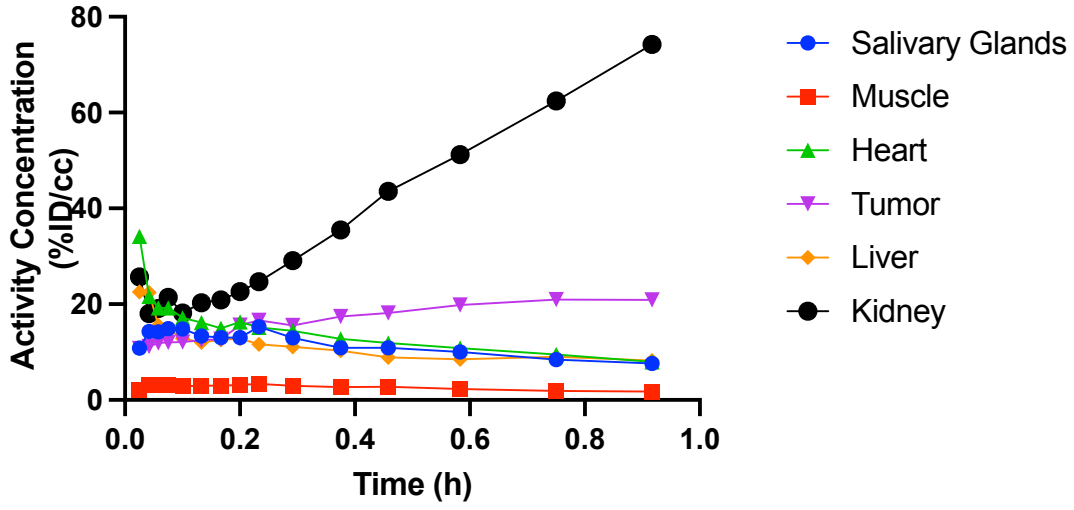

Figure 38 Time activity curves of ^{68}Ga-PSMA-11 biodistribution of excretory organs [salivary glands; muscle; heart; tumor; liver and kidney].

3.4 Biodistribution Studies

3.4.1 ^{64}Cu-PSMA-I&T Ex Vivo Biodistribution

The *in vivo* biodistribution of ^{64}Cu-PSMA-I&T in tumor-bearing mice at 2, 24 and 48 hrs. post injection (5.5 MBq) were assessed (n= 4 each time point). Table 4 below lists the measured percentage of injected dose per gram tissue (%ID/g) for each organ extracted. The highest uptake (%ID/g) was initially seen in the kidneys after 2 hrs. at (45.7 ± 7.019), however, this seemed to have sharply declined after 24 hrs. and 48 hrs. (21.2 ± 6.74) and (16.4 ± 5.54) respectively. Of great interest, ^{64}Cu-PSMA I&T (PSMA+) tumor uptake seemed to be highest at 2 hrs. (5.27 ± 0.85), then slowly decreasing over the next 24 and 48 hrs. (4.61 ± 0.94) and (3.89 ± 0.54) respectively. In addition, the liver uptake was observed to be within a similar range from 2 to 24 hrs. (12.2-10.1) and slightly decreasing at 48 hrs. (8.49 ± 1.55).

Table 4 *In vivo* biodistribution data of ^{64}Cu-PSMA I&T in LNCaP (PSMA+) tumor bearing mice (%ID/g).

Organ	2h	24h	48h
Tumor (+)	5.27 ± 0.85	4.61 ± 0.94	3.89 ± 0.54
Tumor (-)	1.99 ± 0.06	3.51 ± 0.29	2.51 ± 0.22
Brain	0.20 ± 0.02	0.35 ± 0.03	0.39 ± 0.07
Spleen	2.33 ± 0.63	1.74 ± 0.12	1.46 ± 0.33
Pancreas	1.77 ± 0.26	1.40 ± 0.22	1.34 ± 0.19
Kidneys	45.7 ± 7.019	21.2 ± 6.74	16.4 ± 5.54
Liver	12.2 ± 0.56	10.1 ± 1.74	8.49 ± 1.55
Stomach	1.87 ± 0.80	1.95 ± 0.57	1.69 ± 0.63
GI	5.79 ± 1.32	3.40 ± 0.58	3.26 ± 0.85
Muscle	0.43 ± 0.05	0.44 ± 0.05	0.40 ± 0.18

Table 4 Continued

Organ	2h	24h	48h
Bone	1.17 ± 0.29	1.18 ± 0.19	0.95 ± 0.17
Tail	2.47 ± 0.19	1.58 ± 0.23	1.23 ± 0.23
Lungs	5.36 ± 0.87	4.67 ± 0.88	3.44 ± 0.55
Heart	1.88 ± 0.10	2.33 ± 0.38	2.30 ± 0.46
Fat	0.75 ± 0.08	1.01 ± 0.29	0.93 ± 0.27
Blood	1.14 ± 0.11	1.24 ± 0.23	1.06 ± 0.13
Skin	2.14 ± 0.43	1.12 ± 0.28	1.31 ± 0.35
Testes	0.94 ± 0.04	0.90 ± 0.08	0.86 ± 0.12
Salivary Glands	3.23 ± 0.35	2.09 ± 0.35	1.84 ± 0.22
Prostate	2.55±0.31	1.38±0.52	1.28±0.22

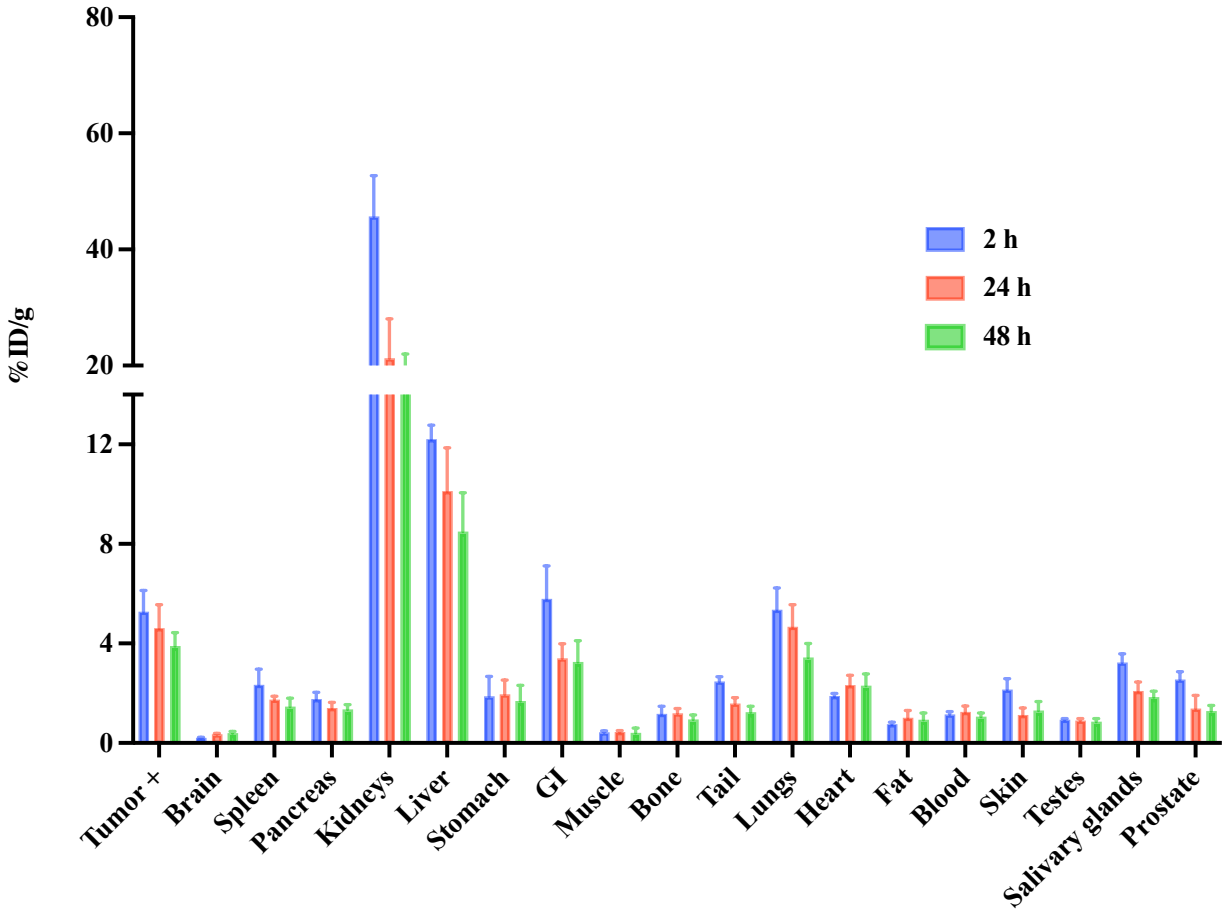

Figure 39 ^{64}Cu-PSMA-I&T biodistribution in LNCaP tumor models. Radioactivity of dissected organs were measured at 2, 24 and 48 hrs. post injection.

3.4.2 ^{68}Ga-PSMA-I&T Ex Vivo Biodistribution

Biodistribution studies of ^{68}Ga-PSMA I&T were performed for comparison with that of ^{64}Cu-PSMA-I&T. The same number of organs (19) were extracted at 1 and 2 hrs. in tumor-bearing mice (n= 4 each group). The measured (%ID/g) for each organ extracted is listed in Table 5. The highest uptake was observed in the kidneys after 1 hr. post injection (p.i.) at (76.33 ± 8.13), followed by the (PSMA+) tumor (5.68±0.54), and spleen (2.51±0.55). A similar uptake was seen at 2 hr. p.i. with slight activity decreases.

Table 5 *In vivo* biodistribution data of ^{68}Ga-PSMA I&T in LNCaP (PSMA+) tumor bearing mice (%ID/g).

Organ	1h	2h
Tumor (+)	5.68 ± 0.54	4.96 ± 0.30
Brain	0.03 ± 0.01	0.06 ± 0.04
Spleen	2.51 ± 0.55	2.43 ± 1.75
Pancreas	0.24 ± 0.02	0.26 ± 0.05
Kidneys	76.33 ± 8.13	64.40 ± 12.16
Liver	0.71 ± 0.15	0.28 ± 0.18
Stomach	0.36 ± 0.11	0.09 ± 0.04
GI	0.47 ± 0.14	0.14 ± 0.05
Muscle	0.12 ± 0.04	0.13 ± 0.07
Bone	0.22 ± 0.02	0.27 ± 0.12
Tail	0.74 ± 0.23	0.18 ± 0.02
Lungs	2.18 ± 0.54	0.50 ± 0.18
Heart	0.23 ± 0.04	0.21 ± 0.09
Fat	1.19 ± 0.90	0.83 ± 0.30
Blood	0.38 ± 0.27	0.18 ± 0.06
Skin	0.67 ± 0.63	0.28 ± 0.09
Testes	0.25 ± 0.10	0.29 ± 0.12
Salivary Glands	0.35 ± 0.06	0.32 ± 0.05
Prostate	1.99 ± 1.68	1.05 ± 0.94

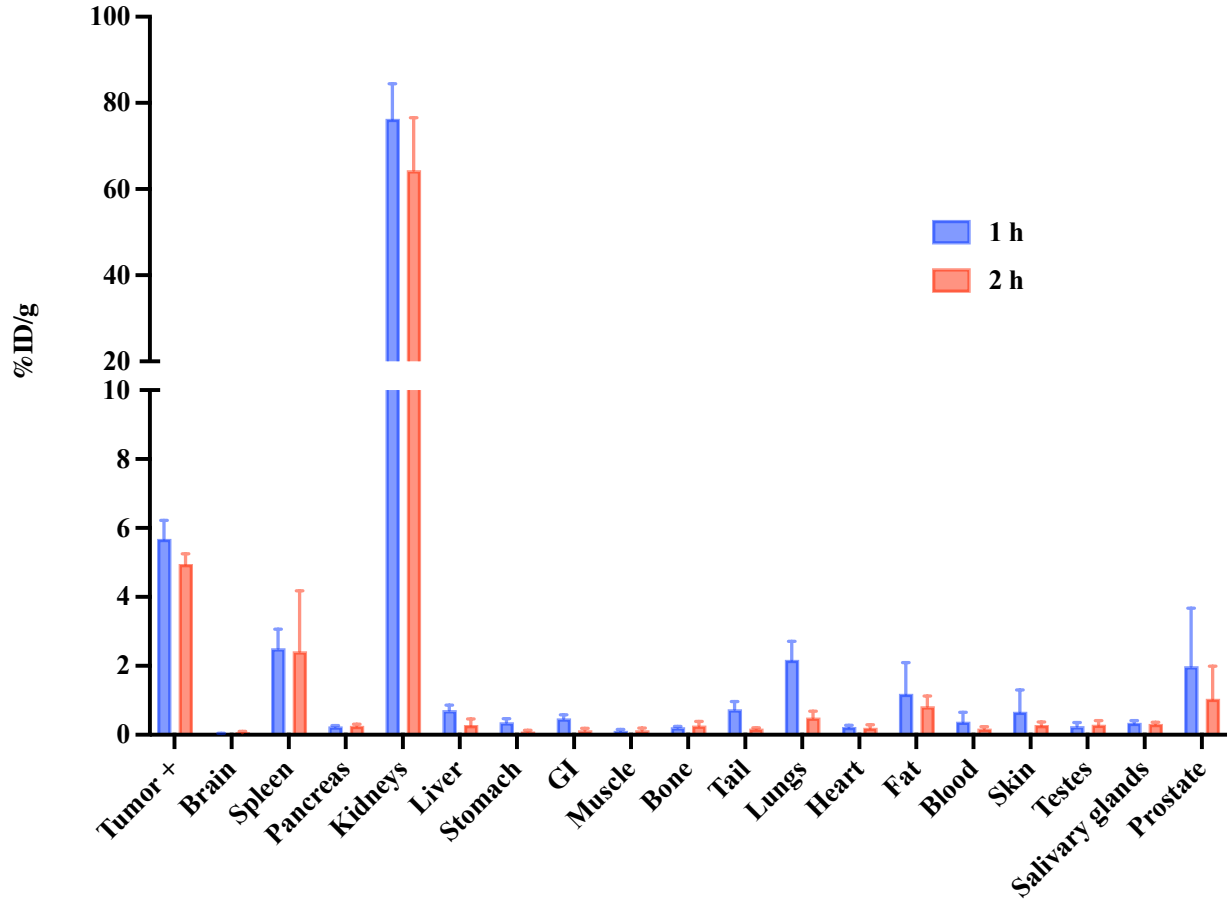

Figure 40 ^{68}Ga-PSMA-I&T biodistribution in LNCaP tumor models. Radioactivity of dissected organs were measured at 2, 24 and 48 hrs. post injection.

3.4.3 ^{68}Ga-PSMA-11 Ex Vivo Biodistribution

^{68}Ga-PSMA-11 ex vivo biodistribution was also assessed at 1 and 2 hrs. post injection in tumor-bearing mice (n= 4 each group). The measured (%ID/g) are listed in Table 6 for each the extracted organs. The highest uptake occurred in the kidneys after 1 hr. of i.v. (174.04 ± 37.84), this seemed to have then declined to (164.76 ± 30.57) after 2 hrs. Significant uptake was also noted in (PSMA+) tumor, (11.48 ± 3.39), followed by spleen (12.06 ± 2.02) at 1 hr. and 2 hr. respectively.

Table 6 *In vivo* biodistribution data of ^{68}Ga-PSMA-11 in LNCaP (PSMA+) tumor bearing mice (%ID/g).

Organ	1h	2h
Tumor (+)	11.48 ± 3.39	10.67 ± 2.50
Brain	0.20 ± 0.13	0.15 ± 0.04
Spleen	7.55 ± 1.87	12.06 ± 2.02
Pancreas	1.21 ± 0.65	1.10 ± 0.52
Kidneys	174.04 ± 37.84	164.76 ± 30.57
Liver	0.59 ± 0.38	0.76 ± 0.29
Stomach	0.36 ± 0.24	0.31 ± 0.08
GI	0.37 ± 0.17	0.48 ± 0.09
Muscle	0.83 ± 0.16	0.43 ± 0.20
Bone	0.88 ± 0.39	0.89 ± 0.74
Tail	0.78 ± 0.75	0.68 ± 0.34
Lungs	1.54 ± 0.68	2.20 ± 0.84
Heart	0.73 ± 0.28	0.87 ± 0.24
Fat	2.43 ± 1.12	1.68 ± 1.04
Blood	0.36 ± 0.15	0.58 ± 0.43
Skin	1.15 ± 0.87	1.40 ± 0.58
Testes	1.12 ± 0.44	0.85 ± 0.34
Salivary Glands	1.41 ± 0.25	2.24 ± 1.19
Prostate	3.28 ± 1.02	2.36 ± 1.17

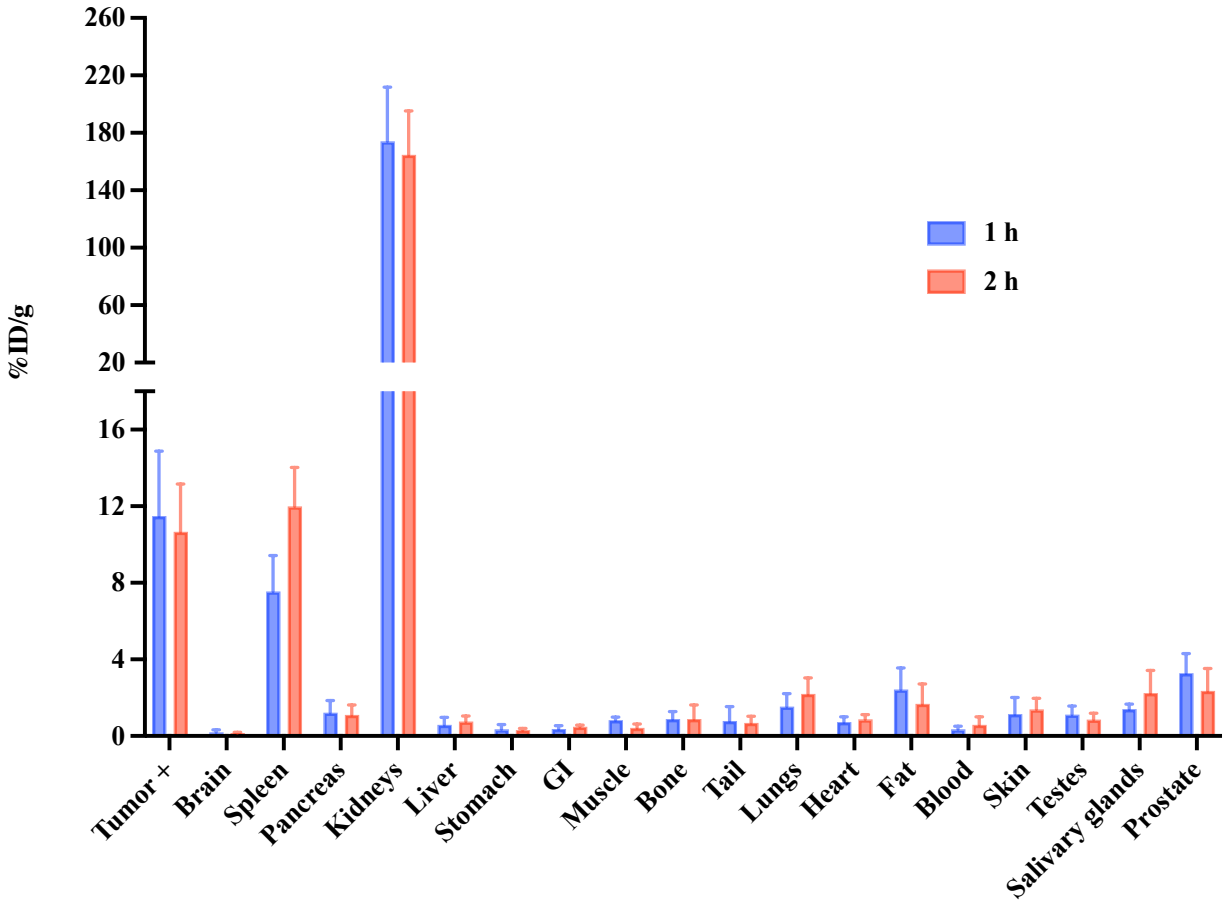

Figure 41 ^{68}Ga-PSMA-11 biodistribution in LNCaP tumor bearing mice. Radioactivity of dissected organs was measured at 1 hr. and 2 hr. post injection.

3.4.4 Comparative Biodistribution

A comparison of the biodistribution of ^{64}Cu-PSMA-I&T, ^{68}Ga-PSMA-11, and ^{68}Ga-PSMA-I&T at 2 hr. post injection (n=4 each group) is shown in Table 7. ^{68}Ga-PSMA-11 had the highest tumor uptake (10.67 ± 2.50), followed closely by both ^{64}Cu-PSMA-I&T, ^{68}Ga-PSMA-I&T at (5.27 ± 0.85) and at (4.96 ± 0.30) respectively. However, significant uptake was noted in the kidney by ^{68}Ga-PSMA-11 (164.76 ± 30.57) vs. only (45.7 ± 7.019)

by ^{64}Cu-PSMA-I&T and (64.40 ± 12.16) for ^{68}Ga-PSMA-I&T, leading to undesirable higher non-target to target (kidney to tumor) ratio.

Table 7 *In vivo* comparative biodistribution data of ^{64}Cu-PSMA-I&T, ^{68}Ga-PSMA-11 and ^{68}Ga-PSMA-I&T in LNCaP (PSMA+) tumor bearing mice (%ID/g).

Organ	^{64}Cu-PSMA-I&T	^{68}Ga-PSMA-11	^{68}Ga-PSMA-I&T
Tumor (+)	5.27 ± 0.85	10.67 ± 2.50	4.96 ± 0.30
Brain	0.20 ± 0.02	0.15 ± 0.04	0.06 ± 0.04
Spleen	2.33 ± 0.63	12.06 ± 2.02	2.43 ± 1.75
Pancreas	1.77 ± 0.26	1.10 ± 0.52	0.26 ± 0.05
Kidneys	45.7 ± 7.019	164.76 ± 30.57	64.40 ± 12.16
Liver	12.2 ± 0.56	0.76 ± 0.29	0.28 ± 0.18
Stomach	1.87 ± 0.80	0.31 ± 0.08	0.09 ± 0.04
GI	5.79 ± 1.32	0.48 ± 0.09	0.14 ± 0.05
Muscle	0.43 ± 0.05	0.43 ± 0.20	0.13 ± 0.07
Bone	1.17 ± 0.29	0.89 ± 0.74	0.27 ± 0.12
Tail	2.47 ± 0.19	0.68 ± 0.34	0.18 ± 0.02
Lungs	5.36 ± 0.87	2.20 ± 0.84	0.50 ± 0.18
Heart	1.88 ± 0.10	0.87 ± 0.24	0.21 ± 0.09
Fat	0.75 ± 0.08	1.68 ± 1.04	0.83 ± 0.30
Blood	1.14 ± 0.11	0.58 ± 0.43	0.18 ± 0.06
Skin	2.14 ± 0.43	1.40 ± 0.58	0.28 ± 0.09
Testes	0.94 ± 0.04	0.85 ± 0.34	0.29 ± 0.12
Salivary Glands	3.23 ± 0.35	2.24 ± 1.19	0.32 ± 0.05
Prostate	2.55±0.31	2.36 ± 1.17	1.05 ± 0.94

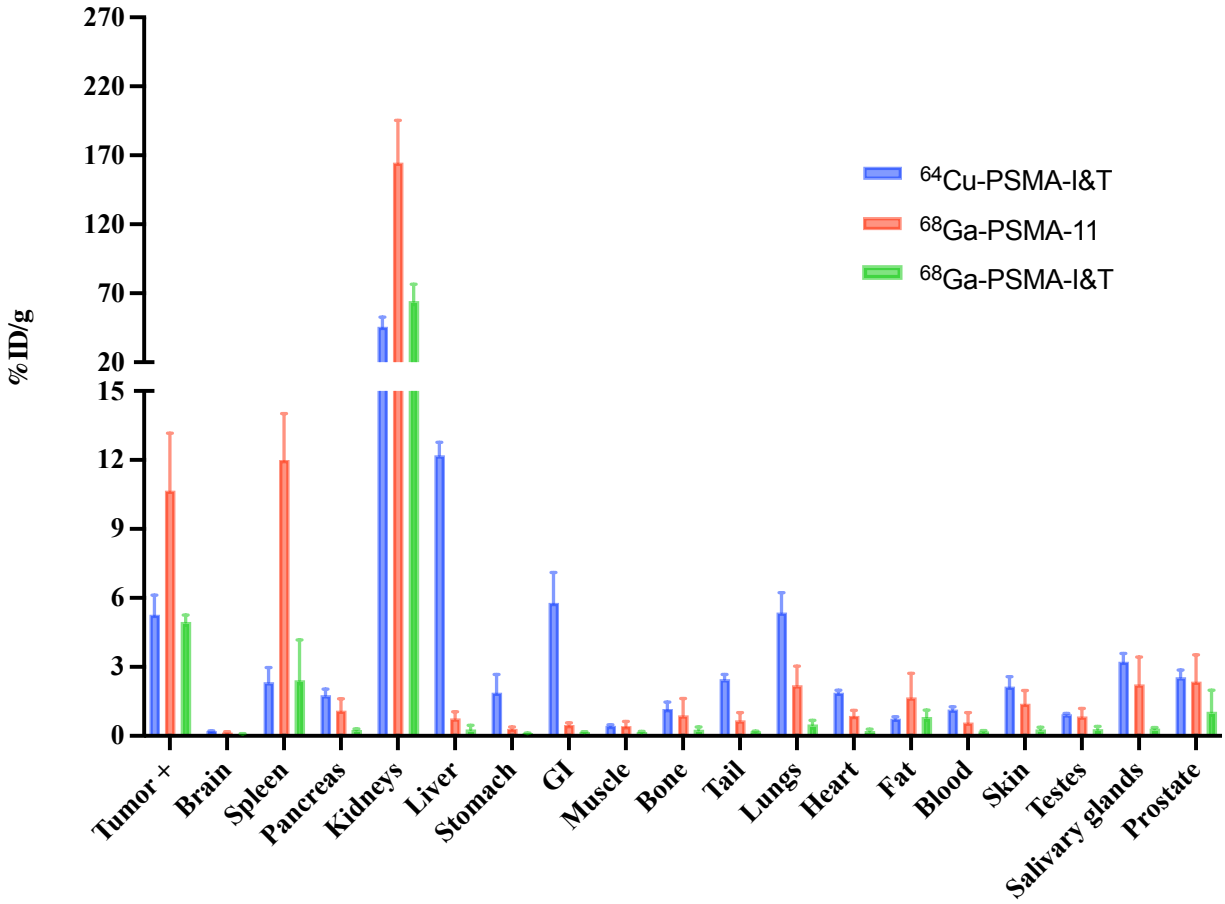

Figure 42 Comparative biodistribution of ^{64}Cu-PSMA-I&T, ^{68}Ga-PSMA-11, and ^{68}Ga-PSMA-I&T biodistribution in LNCaP tumor bearing mice. Radioactivity of dissected organs were measured at 2 hr. post injection (n=4 each group).

3.4.5 PET/CT Biodistribution Time Activity Curves

Following the injection of each radiotracer into xenografts tumor models, a 60 min dynamic PET/CT was performed. Time activity curves (TACs) of the pharmacokinetics illustrating the biodistribution of each tracer in selected organs are shown in (Fig. 43-48). These TACs were further analyzed and processed for the dosimetry measurements as explained in sections (2.3-2.4), and the following section 3.5.

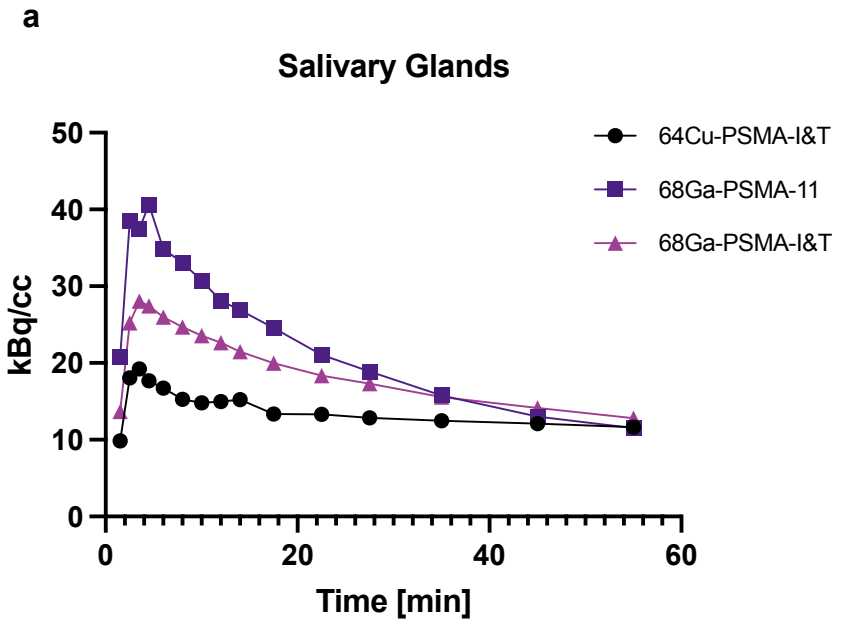

Figure 43 Dynamic PET time activity curve (60 min) of ^{64}Cu-PSMA-I&T, ^{68}Ga-PSMA-11, and ^{68}Ga-PSMA-I&T in salivary glands of xenograft mouse models (n=3).

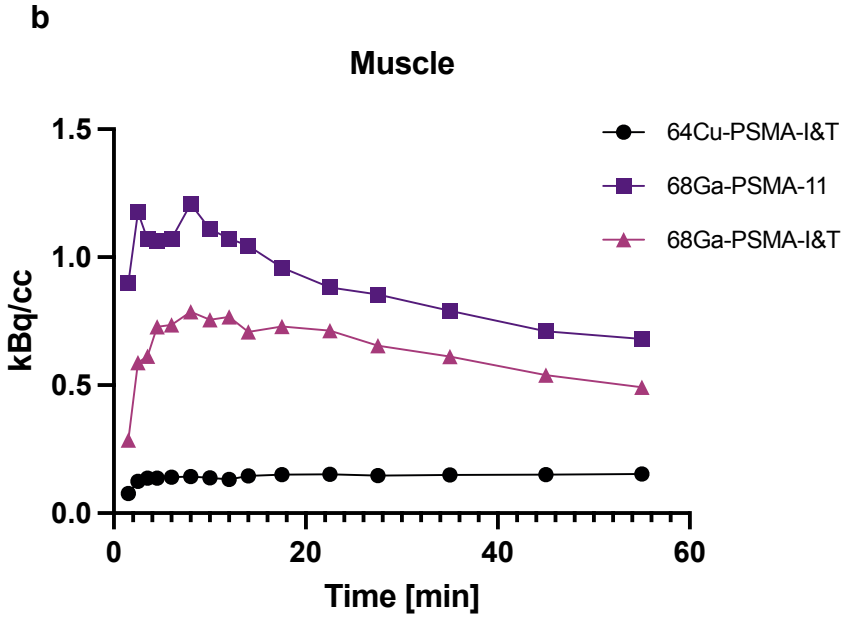

Figure 44 Dynamic PET time activity curve (60 min) of ^{64}Cu-PSMA-I&T, ^{68}Ga-PSMA-11, and ^{68}Ga-PSMA-I&T in muscle of xenograft mouse models (n=3).

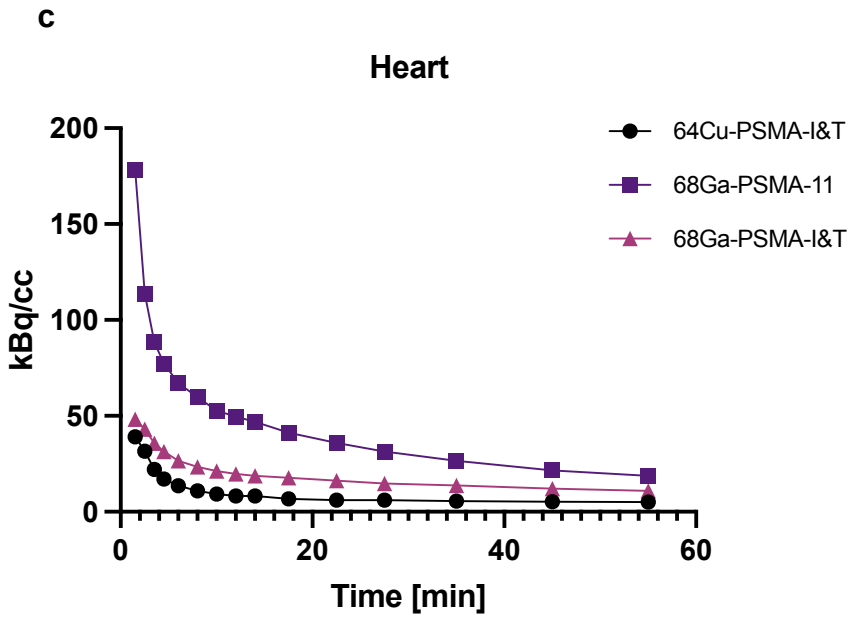

Figure 45 Dynamic PET time activity curve (60 min) of ^{64}Cu-PSMA-I&T, ^{68}Ga-PSMA-11, and ^{68}Ga-PSMA-I&T in heart of xenograft mouse models (n=3).

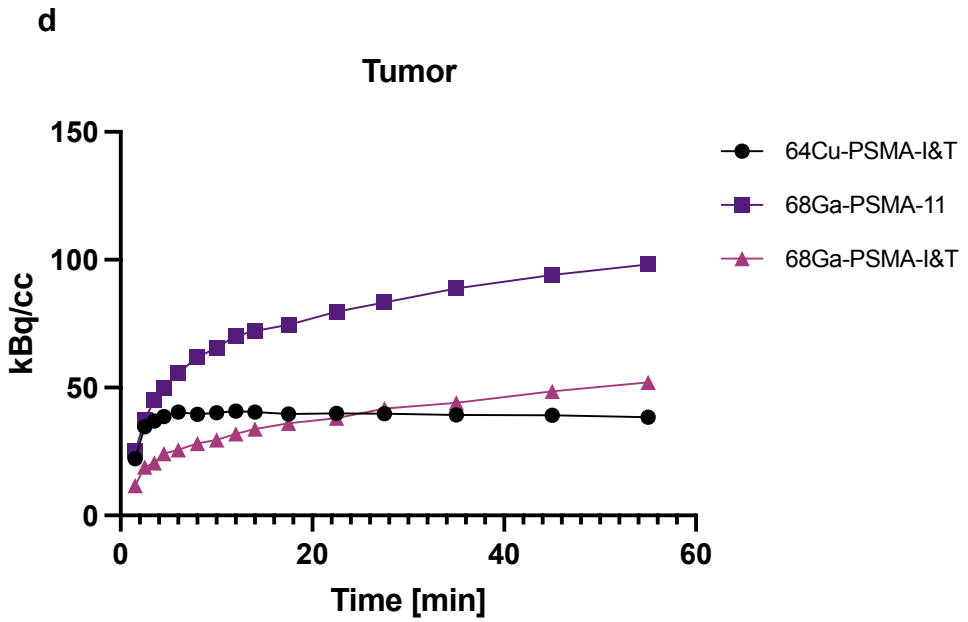

Figure 46 Dynamic PET time activity curve (60 min) of ^{64}Cu-PSMA-I&T, ^{68}Ga-PSMA-11, and ^{68}Ga-PSMA-I&T in LNCaP (PSMA+) tumor of xenograft mouse models (n=3).

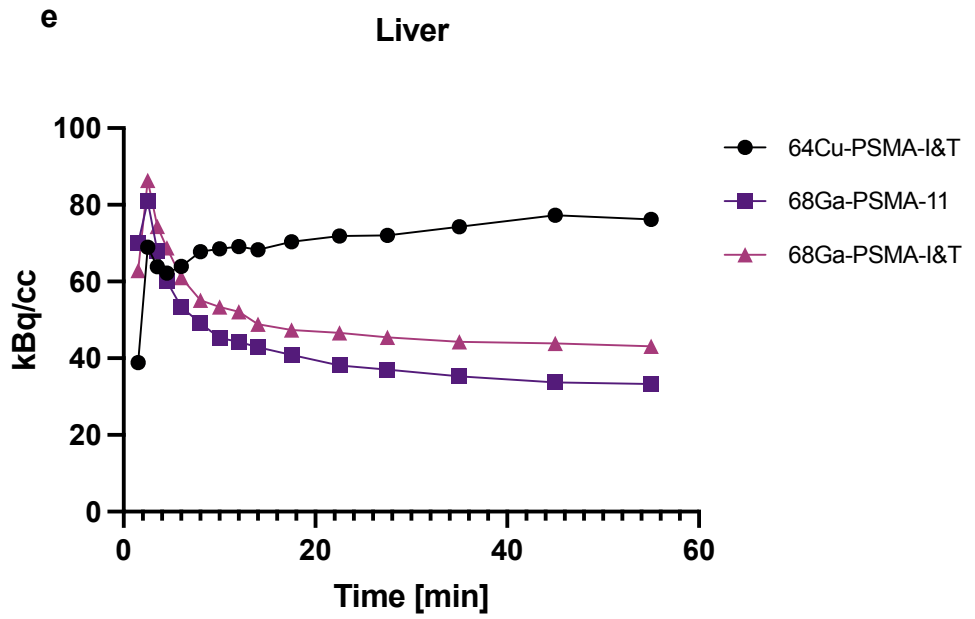

Figure 47 Dynamic PET time activity curve (60 min) of ^{64}Cu-PSMA-I&T, ^{68}Ga-PSMA-11, and ^{68}Ga-PSMA-I&T in liver of xenograft mouse models (n=3).

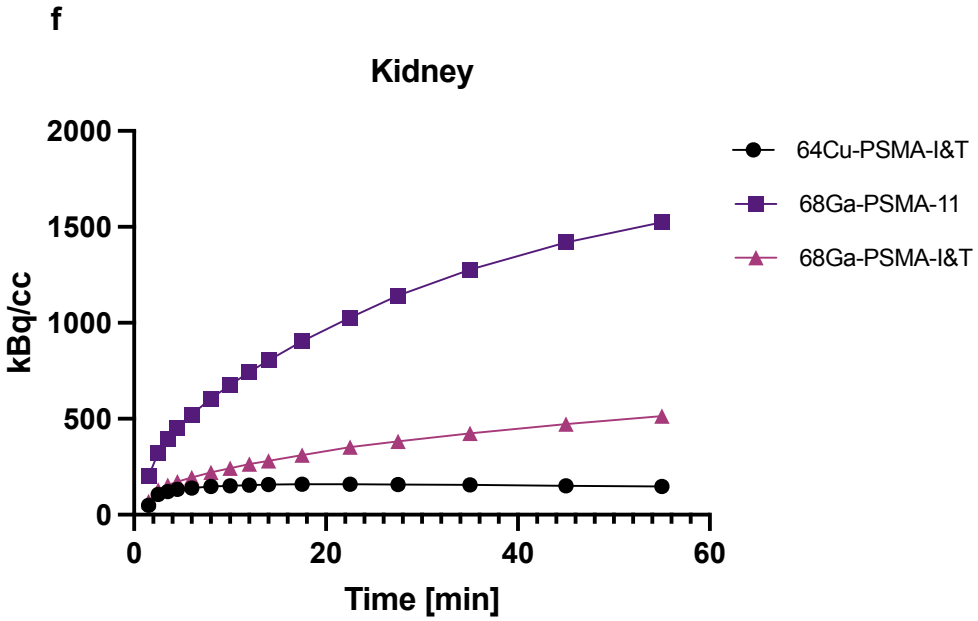

Figure 48 Dynamic PET time activity curve (60 min) of ^{64}Cu-PSMA-I&T, ^{68}Ga-PSMA-11, and ^{68}Ga-PSMA-I&T in kidneys of xenograft mouse models (n=3).

3.5 Radiation Dosimetry Measurements

^{64}Cu-PSMA-I&T radiation dosimetry was calculated in accordance with the MIRD (Medical Internal Radiation Dose committee of the Society of Nuclear Medicine) method. The aim of the measurement was to estimate the absorbed dose (energy per unit mass of tissue) in each target organ delivered by one or more source organs in the body. The PET scans of the xenograft mouse models were used to draw volumes of interest on several organs that were identified as source organs. Time-activity curves were generated for each of these organs then fitted to exponential equations. The integral of each curve gave the total number of disintegrations also known as the cumulated activity ($\tilde{A}$), which the (residence time) was derived from for each organ. Organ residence times are shown in Table 8. The same method was used to calculate the dosimetry for both ^{68}Ga-PSMA-I&T and ^{68}Ga-PSMA-11 for comparison purposes.

Table 8 Residence times (Bq x Hr/Bq administered) for xenografts models.

Source Organ	^{64}Cu-PSMA-I&T	^{68}Ga-PSMA-11	^{68}Ga-PSMA-I&T
Salivary glands	1.68E-02	6.20E-03	4.65E-03
Muscle	7.41E-04	2.15E-04	2.09E-03
Heart	1.17E-02	8.07E-03	4.41E-03
Tumor	8.40E-02	3.83E-02	9.95E-02
Liver	1.20E-01	1.33E-01	1.91E-02
Kidney	1.80E-01	8.41E-01	3.60E-01
Reminder body	1.75E-02	6.40E-03	6.74E-03

These organ residence times were then used as inputs to a dosimetry program (OLINDA) to calculate the organ doses (Table 9). The same method was used to calculate the dosimetry for both ^{68}Ga-PSMA-I&T and ^{68}Ga-PSMA-11 for comparison purposes.

Table 9 Absorbed mouse organ doses in (mSv/MBq) for ^{64}Cu-PSMA I&T, ^{68}Ga-PSMA-11, and ^{68}Ga-PSMA-I&T.

Target Organ	^{64}Cu-PSMA-I&T	^{68}Ga-PSMA-11	^{68}Ga-PSMA-I&T
Brain	5.24E-02	1.71E-01	1.28E-01
Large Int	2.33E-01	1.43E+01	3.75E+00
Small Intestine	1.52E-01	4.56E+00	1.27E+00
Stomach Wall	5.19E-01	6.75E+00	2.00E+00
Heart	3.11E+00	1.37E+01	5.62E+00
Kidneys	3.21E+01	2.74E+02	1.21E+02
Liver	4.02E+00	7.30E+00	2.77E+00
Lungs	5.15E-01	2.20E+00	1.01E+00
Pancreas	7.03E-01	3.81E+01	9.91E+00
Skeleton	1.12E-01	9.77E-01	3.83E-01
Spleen	2.93E-01	2.55E+01	6.60E+00
Testes	5.43E-02	2.28E-01	1.42E-01
Thyroid	5.87E-02	1.97E-01	1.37E-01
Urinary Bladder	6.24E-02	3.38E-01	1.72E-01
Total Body	8.28E-01	1.06E+01	2.88E+00

4. DISCUSSION

4.1 ^{64}Cu-PSMA-I&T: A Potential PSMA-Targeted Radiopharmaceutical

The aim of this research work was to preclinically evaluate ^{64}Cu-labeled PSMA I&T as a promising PSMA-targeted PET imaging agent for routine clinical applications. PSMA is a well-defined prostate cancer biomarker and is overexpressed at different stages of prostatic cancer by 100-1000-fold in 95% of PCa cells [10,20]. While PSMA-I&T is a highly potential PSMA-binding-inhibitor and is considered one of the first theranostic tracers, due to its ability to be radiolabeled with various radiometals for imaging or radiotherapy applications [35]. In this study, ^{64}Cu was selected as the radioisotope of choice to be coupled with PSMA-I&T for PSMA-based PET imaging. ^{64}Cu decays by (β+: 17.9% [0.653 MeV]) with a positron range of 1mm, and a half-life of ($t_{1/2}$: 12.7 h) making it ideal for imaging, and its relatively long half-life allows it to be produced in large batches by a medial cyclotron facilitating production and commercial distribution.

^{64}Cu-PSMA I&T was successfully synthesized, and its radiochemical purity and stability was tested and confirmed by radio-HPLC. The radiotracer met all quality control criteria and did not contain any free ^{64}Cu and was safely administered into tumor bearing mice. The HPLC analysis of the finished product consistently reported a radiochemical purity of greater than 95%. Additionally, the final product was determined to be sterile, colorless, and remained radiochemically pure and stable (≥ 95%) up to 24 hrs. after radiosynthesis at room temperature. These results confirmed that the compound was stable and did not experience any decomposition due to radiolysis, preventing any unnecessary radiation exposure or compromising the outcome of the study.

In vitro cell uptake assays were performed using the human prostate carcinoma LNCaP (PSMA+) and PC-3 (PSMA-) cell lines. Prior to the experiment, PSMA expression in the cell lines used was verified by western blot. The PSMA protein expression was successfully confirmed in the LNCaP cell line by scanning the membrane containing the anti-PSMA antibody with a measured molecular weight (MW) of 100 kDa (Figure 29), and no expression in the PC-3 cell line. Next, PSMA specific targeting of the radiotracer was assessed and validated by the *in vitro* cell uptake assay where significant uptake of ^{64}Cu-PSMA-I&T was observed in the LNCaP (PSMA+) cells (5.59±0.41%ID/1x10^6 cells) vs. (0.72±0.26%ID/1x10^6 cells) in the PC-3 (PSMA-) cells (Table 3), which demonstrated the targeting specificity of ^{64}Cu-PSMA-I&T to PCa cells expressing PSMA.

Small animal imaging was conducted upon administration of ^{64}Cu-PSMA-I&T into tumor xenograft mice models bearing LNCaP (PSMA+) and PC-3 (PSMA-) tumors. The micro-PET images clearly showed the tumors, and the radiotracer accumulation over time. Contrast images were acquired at 2, 24 and 48 hrs., where higher specific uptake of ^{64}Cu-PSMA-I&T was observed in the LNCaP (PSMA+) tumor compared to the PC-3 (PSMA-) tumor. In addition, considerable uptake was also noticed in the kidneys and the liver. The decreased PC-3 tumor uptake further confirmed the specific binding of ^{64}Cu-PSMA-I&T to the PSMA+) tumor.

Biodistribution studies were performed in LNCaP and PC-3 xenografts animal models. ^{64}Cu-PSMA-I&T showed elevated uptake in LNCaP (PSMA+) tumor, with a peak concentration of (5.27 ± 0.85 %ID/g) measured at 2 hr. post injection, followed by (4.61 ± 0.94 %ID/g) and (3.89 ± 0.55 %ID/g) at 24 and 48 hr. respectively (Table 4). These results

further confirmed the high affinity of ^{64}Cu-PSMA-I&T towards the (PSMA+) tumor, demonstrating its capability as a PSMA PET imaging agent.

Additionally, substantial accumulation of ^{64}Cu-PSMA-I&T was also observed in the kidney due to receptor expression but seemed to be decreasing with time. A similar pattern of radiotracer clearance over time from the other non-target organs was noticed, except the liver that exhibited a slow clearance rate with radioactivity of (12.2 ± 0.56 %ID/g to 10.12 ± 1.74 %ID/g) over the course of 2 hrs. to 24 hrs., and then slightly decreasing to (8.49 ± 1.55 %ID/g) after 48 hrs. This is attributed to ^{64}Cu uptake and excretion with respect to the hepatic metabolism by the liver [70-71]. As PSMA is reported to be also expressed in non-specific tissue or organs [72], medium uptake of ^{64}Cu-PSMA-I&T was observed in the salivary glands, prostate and gastrointestinal. While in other non-specific organs such as the muscle, there was low level of uptake, displaying a high contrast ratio of tumor to muscle.

Moreover, the xenograft mice models bearing the PC-3 tumor (PSMA-) were noted to have measurable ^{64}Cu-PSMA-I&T uptake of (1.99 ± 0.06 %ID/g, 3.51 ± 0.29 %ID/g and 2.51 ± 0.22 %ID/g) at 2, 24 and 48 hrs. respectively. PC-3 are typical solid tumors with abundant neovasculature, and PSMA expression has been reported in neovasculature of solid tumors [73-74], which PC-3 tumors may have expressed explaining the uptake of ^{64}Cu-PSMA-I&T. Similar findings were also found to be reported in the literature, by Han et al. observing ^{64}Cu-PSMA-617 uptake in PC-3 tumor xenograft models (3.47 – 0.48%ID/g) at 24 hr. [75].

Time-integrated activity coefficients (also known as residence times) of segmented organs were estimated for the LNCaP bearing tumor mice injected with ^{64}Cu-PSMA-I&T, using the MIRD method to estimate the radiation dosimetry of the radiotracer. The time-

integrated activity coefficients of the following organs (salivary glands, kidney, liver, muscle, heart, and tumor) were calculated then multiplied by dose factors using the OLINDA software that computed the absorbed dose in target organs per disintegration in source organs. The highest number of disintegrations per organ occurred in the kidneys and liver, with an average time-integrated activity coefficient of (0.18 MBq-h/MBq) and (0.12 MBq-h/MBq) respectively. The highest absorbed dose per unit activity was observed in the tumor (0.042 Gy/MBq) followed by the kidneys (0.032 Gy/MBq), the liver (0.0042 Gy/MBq), and the heart (0.0031 Gy/MBq) (Table 9).

To further evaluate the potential of ^{64}Cu-PSMA-I&T as a PSMA imaging agent, its biodistribution and dosimetry were compared to that of ^{68}Ga-PSMA-I&T and ^{68}Ga-PSMA-11. All radiotracers seemed to have a significant uptake in the LNCaP (PSMA+) tumor, as seen by the micro-PET images as well as showing similar uptake patterns, which could be attributed to their common (Glu-urea-Lys) PSMA structure. In addition, the pharmacokinetics of these radiotracers were noted to be comparable, as displayed by the time activity curves of selected organs measured at 60 min post injection with varying radioactivity accumulation (Figure 43-48). However, ^{68}Ga-PSMA-11 constantly had a considerable uptake in the kidneys amongst all three radiotracers. In terms of the radiation dosimetry, the highest absorbed dose per unit activity for ^{68}Ga-PSMA-I&T was observed in the kidneys (0.121 Gy/MBq) followed by the pancreas (0.0099 Gy/MBq), the spleen (0.0066 Gy/MBq), the heart (0.0056 Gy/MBq), and liver (0.00277 Gy/MBq) (Table 9). While the highest absorbed dose per unit activity for ^{68}Ga-PSMA-11 was observed in the kidneys (0.274 Gy/MBq) followed by the pancreas (0.038 Gy/MBq), the spleen (0.0255 Gy/MBq),

the heart (0.0137 Gy/MBq), and the liver (0.0073 Gy/MBq) (Table 9). These results agree with reports published in the literature [76].

Both ^{68}Ga-PSMA-I&T and ^{68}Ga-PSMA-11 seem to have substantial absorbed dose to kidney at (0.121 Gy/MBq) and (0.274 Gy/MBq) respectively, when compared to only (0.032 Gy/MBq kidney by ^{64}Cu-PSMA-I&T.

In the biodistribution studies, it was observed that ^{68}Ga-PSMA-11 had the highest (PSMA+) tumor uptake at a peak concentration of (10.67 ± 2.50 %ID/g) 2 hr. post injection, followed by ^{64}Cu-PSMA-I&T (5.27 ± 0.85 %ID/g), and ^{68}Ga-PSMA-I&T (4.96 ± 0.30 %ID/g). The high tumor uptake exhibited by ^{68}Ga-PSMA-11 may be attributed to the (HBED-CC) chelator of the PSMA-11 precursor, which contains a benzene moiety that favors interaction with the hydrophobic accessory pocket of PSMA [61]. However, the HBED-CC chelator is not suitable for radiolabeling with other radiometals due to the Ga-specific acyclic chelator. Hence, other DOTA-conjugated PSMA inhibitors such as PSMA-I&T with specific targeting towards PSMA as demonstrated in this work, were introduced to expand the potential applications with other radiometals for imaging or therapy of PCa [61,77]. It was also noted that there ^{64}Cu-PSMA-I&T had the lowest kidney uptake compared to ^{68}Ga-PSMA-11 (164.76 ± 30.57 %ID/g) and ^{68}Ga-PSMA-I&T (64.40 ± 12.16 %ID/g). Similarly, to ^{64}Cu-PSMA-I&T the radiotracer clearance of ^{68}Ga-PSMA-11 and ^{68}Ga-PSMA-I&T from non-target organs was noted over time. Both ^{68}Ga-PSMA-11 and ^{68}Ga-PSMA-I&T are well-established imaging agents that are routinely and safely administrated into human patients. As such the mean effective dose of ^{68}Ga-PSMA-11 is reported to be (0.023 mSv/MBq) [78], and (0.020 mSv/MBq) for ^{68}Ga-PSMA-I&T [79].

While ^{64}Cu-PSMA-I&T has demonstrated promising results, and comparable capabilities to be considered for clinical trials, and potentially become a routine PSMA PET imaging agent.

4.2 Significance

Prostate cancer continues to be the most cancer type amongst men, thus, early detection and accurate diagnosis is of prime importance for patient management and treatment outcome. Molecular imaging targeting PSMA (prostate-specific membrane antigen) by PET has proven to be a vital and effective tool to identify lesions of prostate cancer at different stages. ^{68}Ga-PSMA-11 has undoubtedly revolutionized the diagnosis of PCa, since it was first injected in humans in 2011 hence, its current name (traditionally known as ^{68}Ga-HBED-PSMA), and it has equally inspired further research and developments into PSMA inhibitors with promising targeting properties. Even though, the commercial availability of a ^{68}Ge/^{68}Ga-generator has been advantageous to obtain ^{68}Ga for PSMA-inhibitors radiolabeling without needing a cyclotron on site, the activity of ^{68}Ga obtained per day is limited. Moreover, extended lead times (several months) continue to be experienced with the limited supply of ^{68}Ge-^{68}Ga-geneartors, increasing the cost of the generators substantially, as they are required to be replaced every year due to their shelf life [80]. This in turn, has become a burden and limited clinics to provide imaging services to patients. Hence, it is essential to continually research and evaluate alternative PSMA-targeted radiopharmaceuticals to help meet the increasing demand. As such ^{64}Cu-PSMA-I&T possess high potential for PSMA-based PET imaging. The relatively long half-life of ^{64}Cu is optimal for centralized radioisotope production at regional or national cyclotron facilities to be distributed to local or remote nuclear medicine departments, enabling ^{64}Cu-

PSMA-I&T to be supplied as an on-demand dose. This would ultimately, eliminate the need for high-cost generators, and allowing wider availability and accessibility to radiopharmaceuticals. Furthermore, a ^{64}Cu-based PSMA imaging radiotracer could potentially add higher clinical values by having a matched therapeutic surrogate radiometal pair (e.g., ^{67}Cu) for β-therapy (β–: 100%, t1/2: 2.58 d), where both radiotracers would have similar pharmacokinetics and biodistribution profiles. Additionally, due to the short positron range of ^{64}Cu (1mm) this could lead to higher PET imaging resolution improving detection. In fact, in a comparative PET/CT study of ^{64}Cu-DOTATATE and ^{68}Ga-DOTATOC of patients with neuroendocrine tumors, the investigators were able to demonstrate that ^{64}Cu-DOTATATE had detected more lesions than ^{68}Ga-DOTATOC as shown in Figures 49-50.

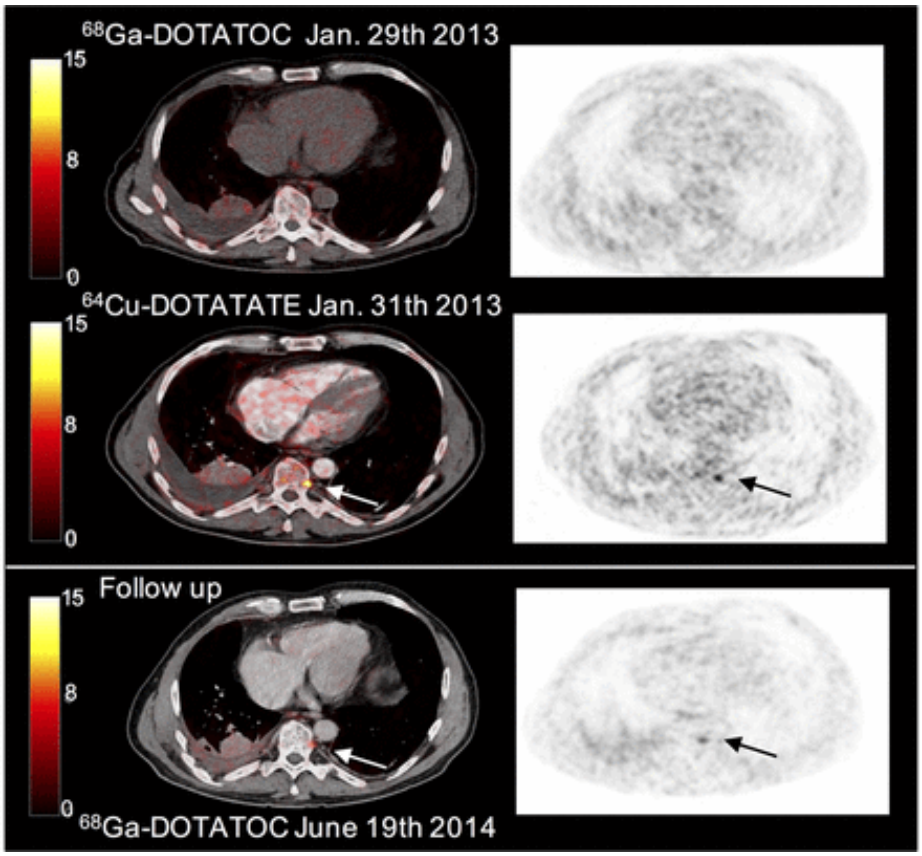

Figure 49 Initial PET/CT (left) and PET (right) scans show an additional bone lesion (arrow) with ^{64}Cu-DOTATATE. Reprinted with permission from [81].

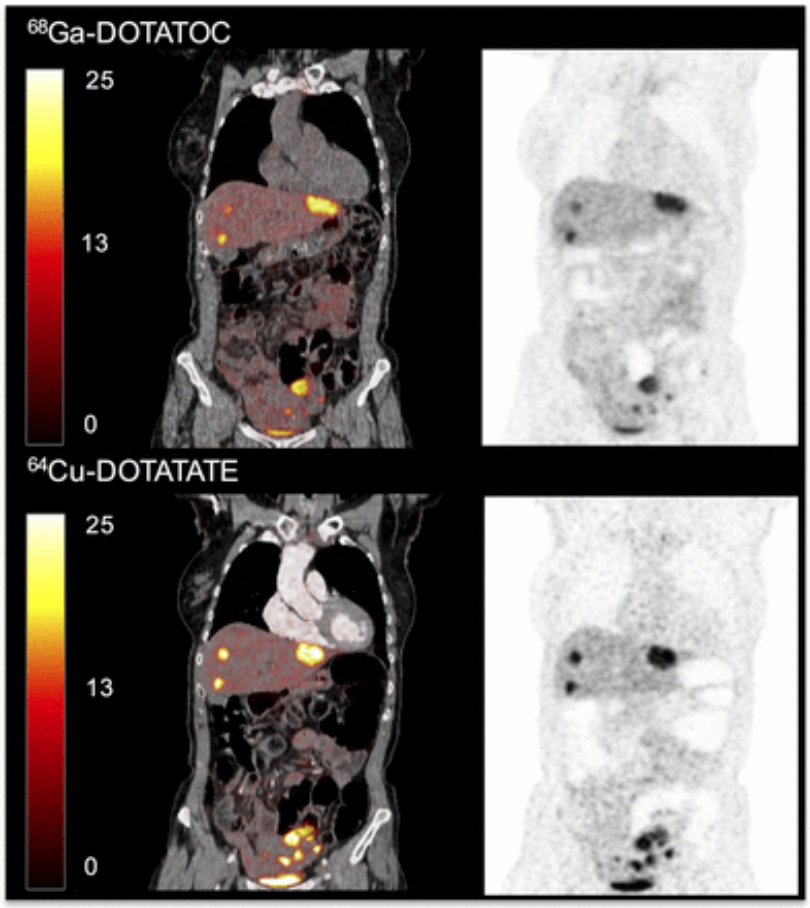

Figure 50 PET/CT (left) and PET (right) scans of patient with intestinal NET and multiple metastases. More lesions are seen in intestinal region with ^{64}Cu-DOTATATE than with ^{68}Ga-DOTATOC. Reprinted with permission from [81].

4.3 Future work

A highly promising future research route is to investigate the feasibility of developing a matched theranostic pair (^{64}Cu-PSMA-I&T) for imaging, and (^{67}Cu-PSMA-I&T) for β-therapy. More importantly, dog prostate cancer (DPC-1) models for example should be considered for preclinical studies to narrow the gap between small animal and lack of correlation with human subjects. This would also help better estimating the human radiation dosimetry of ^{64}Cu-PSMA-I&T and ^{67}Cu-PSMA-I&T, which would be of great interest to generate valuable data for potential clinical trials

5. CONCLUSIONS

The aim of this research was to preclinically evaluate ^{64}Cu-PSAM-I&T as a potential PSMA-based PET imaging for routine clinical applications. ^{64}Cu-PSAM-I&T displayed specific binding uptake to the LNCaP (PSMA+) tumor in the *in vitro* cell uptake assay and in the *in vivo* biological evaluations in xenografts tumor models. In addition, the radiotracer seemed to be stable up to 24 hr. post synthesis at room temperature. After direct comparison in the animal models, ^{64}Cu-PSMA-I&T exhibited similar biodistribution patterns to that of ^{68}Ga-PSMA-I&T and ^{68}Ga-PSMA-11 but with a significantly lower kidney uptake, which is favorable with respect to its dosimetry. Unlike ^{68}Ga-PSMA-I&T and ^{68}Ga-PSMA-11 imaging with ^{64}Cu-PSMA-I&T was possible up to 48 hrs. post synthesis, owing to the relatively long half-life of ^{64}Cu (12.7 h). This is advantageous for facilitating the production and commercial distribution of radiopharmaceuticals. In summary, ^{64}Cu-PSMA-I&T was demonstrated to be a specific PSMA-targeted imaging agent that warrants further investigation to be considered for routine clinical applications.

REFERENCES

1. Society of Nuclear Medicine and Molecular Imaging, 2021. Available at: http://www.snmmi.org/AboutSNMMI/Content.aspx?ItemNumber=4175 Accessed 01 May 2021.

2. Advancing Nuclear Medicine Through Innovation. Available at: https://www.ncbi.nlm.nih.gov/books/NBK11471/ Accessed 01 May 2021.

3. American Cancer Society, 2021. Available at: https://www.cancer.org/cancer/prostate-cancer/about/key-statistics.html Accessed 05 May 2021.

4. International Agency for Research on Cancer, 2020. Available at: https://gco.iarc.fr/today/online-analysis-multi-bars Accessed 1 June 2021.

5. Rawla, P., *Epidemiology of Prostate Cancer*. World J Oncol., 2019. 10(2): 63-89.

6. Balk, S.P., Y.J. Ko, and G.J. Bubley, *Biology of Prostate Specific Antigen*. J Clin Oncol., 2003. 21:383-391.

7. Bostwick, D.G., *Prostate-specific antigen. Current role in diagnostic pathology of prostate cancer*. Am J Clin Pathol., 1994. 102 (4 Suppl 1): S31-7.

8. Silver, D.A., I. Pellicer, W.R. Fair, et al., *Prostate- specific membrane antigen expression in normal and malignant human tissues*. Clin Cancer Res., 1997. 3:81-85.

9. Maurer, T., M. Eiber, M. Schwaiger, J.E. Gschwend, *Current use of PSMA–PET in prostate cancer management* Nat. Rev. Urol., 2016.13, 226–235.

10. Ghosh, A., W. Xinning, E. Klein, W.D.W. Heston. *Novel Role of Prostate-Specific Membrane Antigen in Suppressing Prostate Cancer Invasiveness*. Cancer Res., 2005. 65(3): 727-31.

11. Luthi-Carter, R., A.K. Barczak, H. Speno, and J.T. Coyle, *Molecular Characterization of Human Brain N-Acetylated α-Linked Acidic Dipeptidase (NAALADase)*. Journal of Pharmacology and Experimental Therapeutics, 1998. 286 (2) 1020-1025.

12. Pinto, J. T., B.P. Suffoletto, T.M. Berzin, et al., *Prostate-specific membrane antigen: a novel folate hydrolase in human prostatic carcinoma cells*. Clin Cancer Res.*,*1996. 2:1445-1451.

13. Chang, S.S.*, Overview of Prostate-Specific Membrane Antigen*. Reviews in Urology, 2004. Vol. 6 Suppl. 10.

14. Rajasekaran, S.A., G. Anilkumar, E. Oshima, et al., *A novel cytoplasmic tail MXXXL motif mediates the internalization of prostate-specific membrane antigen*. Mol Biol Cell., 2003.14: 4835 – 4845.

15. Wright Jr, G.L., B.M. Grob, C. Haley, et al., *Upregulation of prostate-specific membrane antigen after androgen-deprivation therapy*. Urology, 1996. 48: 326-334.

16. Ceci, F., S. Fanti. *PSMA-PET/CT imaging in prostate cancer: why and when*. Clinical and Translational Imaging, 2019. 7:377–379.

17. Taneja*, S. S., Imaging in the Diagnosis and Management of Prostate Cancer*. Rev Urol., 2004. 6 (3): 101-113.

18. American Urology Association, 2020. Available at: https://www.urologyhealth.org/urologic-conditions/prostate-cancer Accessed 11 April 2021.

19. Wallitt, K.L., S.R. Khan, S. Dubash, et al., *Clinical PET Imaging in Prostate Cancer.* RadioGraphics., 2017. 37:1512–1536.

20. Lenzo, N.P., D. Meyrick, J.H. Turner, *Review of Gallium-68 PSMA PET/CT Imaging in the Management of Prostate Cancer.* Diagnostics (Basel), 2018. 8(1): 16.

21. Mease, R.C., C.A. Foss, and M.G. Pomper. *PET Imaging in Prostate Cancer: Focus on Prostate-Specific Membrane Antigen*. Curr Top Med Chem., 2013. 13(8): 951–962.

22. Eder, M., M. Schäfer, M, U. Bauder-Wust, et al., *^{68}Ga-complex lipophilicity and the targeting property of a urea-based PSMA inhibitor for PET imaging.* Bioconjugate Chem., 2012. 23:688-697.

23. Afshar-Oromieh, A., U. Haberkorn, M. Eder, et al., *[^{68}Ga] Galliumlabelled PSMA ligand as superior PET tracer for the diagnosis of prostate cancer: Comparison with ^{18}F-FECH.* Eur J Nucl Med Mol Imaging, 2012. 39:1085-1086.

24. Afshar-Oromieh, A., A. Malcher, M. Eder M, et al., *PET imaging with a [^{68}Ga] gallium-labelled PSMA ligand for the diagnosis of prostate cancer*: *Biodistribution in humans and first evaluation of tumor lesions*. Eur J Nucl Med Mol Imaging, 2013. 40:486-495.

25. Afshar-Oromieh, A., C. M. Zechmann, A. Malcher, et al., *Comparison of PET imaging with a ^{68}Ga-labelled PSMA ligand and ^{18}F-choline based PET/CT for the diagnosis of recurrent prostate cancer*. Eur J Nucl Med Mol Imaging, 2014. 41:11-20.

26. Eiber, M., T. Maurer, M. Souvatzoglou, et al., *Evaluation of hybrid ^{68}Ga-PSMA ligand PET/CT in 248 patients with biochemical recurrence after radical prostatectomy*. J Nucl Med., 2015. 56:668-674.

27. Caroli, P., I. Sandler, F. Matteucci, et al., *^{68}Ga-PSMA PET/CT in patients with recurrent prostate cancer after radical treatment: prospective results in 314 patients.* Eur J Nucl Med Mol Imaging, 2018. (12):2035-2044.

28. Perera, M., N. Papa, D. Christidis et al., *Sensitivity, Specificity, and Predictors of Positive ^{68}Ga-Prostate-specific Membrane Antigen Positron Emission Tomography in Advanced Prostate Cancer: A Systematic Review and Meta-analysis.* Eur Urol, 2016. 70(6): p. 926-937.

29. Han, S., S. Woo, Y. J. Kim, C. H. Suh, *Impact of ^{68}Ga-PSMA PET on the Management of Patients with Prostate Cancer: A Systematic Review and Meta-analysis.* Eur Urol., 2018. 74(2);179-190.

30. Eissa, A., A. Elsherbiny, R.F. Coelho, J. Rassweiler, et al., *The role of ^{68}Ga-PSMA PET/CT scan in biochemical recurrence after primary treatment for prostate cancer: a systematic review of literature.* Minerva Urol Nefrol., 2018. 70(5):462-478.

31. Corfield, J., M. Perera, D. Bolton, N. Lawrentschuk, *^{68}Ga-prostate specific membrane antigen (PSMA) positron emission tomography (PET) for primary staging of high-risk prostate cancer: a systematic review.* World J Urol, 2018. 36(4): p. 519-527.

32. von Eyben, F. E., M. Picchio, R. von Eyben, H. Rhee, G. Bauman, *^{68}Ga-Labeled Prostate-specific Membrane Antigen Ligand Positron Emission Tomography/Computed Tomography for Prostate Cancer: A Systematic Review and Meta-analysis.* Eur Urol. Focus, 2018. 689-693.

33. Carlucci, G., R. Ippisch, R. Slavik, A. Mishoe, J. Blecha, S. Zhu, *^{68}Ga-PSMA-11 NDA Approval: A Novel and Successful Academic Partnership*. J Nucl Med., 2021. 62:149–155.

34. Weineisen, M., M. Schottelius, J. Simecek, R.P. Baum, A. Yildiz, S. Beykan, et al., *^{68}Ga- and ^{177}Lu-Labeled PSMA I&T: Optimization of a PSMA-Targeted Theranostic Concept and First Proof-of-Concept Human Studies*. J Nucl Med., 2020. 61:70–79.

35. Wester, H.J., M. Schottelius. *PSMA-Targeted Radiopharmaceuticals for Imaging and Therapy*. Seminars in Nucl Med., 2019. 49 (4), p. 302-312.

36. Baum, R.P., H.R. Kulkarni, C. Schuchardt, et al., *^{177}Lu-labeled prostate-specific membrane antigen radioligand therapy of metastatic castration-resistant prostate cancer: Safety and efficacy*. Nucl Med., 2016. 57:1006-1013.

37. Heck, M.M., R. Tauber, S. Schwaiger, et al., *Treatment outcome, toxicity, and predictive factors for radioligand therapy with ^{177}Lu-PSMA-I&T in metastatic castration-resistant prostate cancer*. Eur Urol., 2018. 75(6):920-926.

38. Heck, M.M., M. Retz, C. D'Alessandria, I. Rauscher, K. Scheidhauer, T. Maurer, E. Storz, et al., *Systemic radioligand therapy with ^{177}Lu labeled prostate specific membrane antigen ligand for imaging and therapy in patients with metastatic castration resistant prostate cancer*. J. Urol., 2016. 196 (2), pp. 382-391.

39. Lütje, S., R. Slavik, W. Fendler, K. Herrmann, M. Eiber, *PSMA ligands in prostate cancer – Probe optimization and theranostic applications*. Methods, 2017. 130: p. 42-50.

40. Cullinane, C., M.C. Jeffery, D. P. Roselt, E. M. van Dam, S. Jackson, et al., *Peptide Receptor Radionuclide Therapy with ^{67}Cu-CuSarTATE Is Highly Efficacious Against a Somatostatin-Positive Neuroendocrine Tumor Model*. J Nucl Med., 2020. 61(12): p. 1800-1805.

41. Champion, C., M. A. Quinto, C. Morgat, P. Zanotti-Fregonara, E. Hindié, *Comparison between Three Promising ß-emitting Radionuclides, ^{67}Cu, ^{47}Sc and ^{161}Tb, with Emphasis on Doses Delivered to Minimal Residual Disease.* Theranostics, 2016. 6(10): 1611-1618.

42. Keinänen, Q., K. Fung, J. M. Brennan, N. Zia, M. Harris, et al., *Harnessing $^{64}Cu/^{67}Cu$ for a theranostic approach to pretargeted radioimmunotherapy*. PSNA, 2020. 117 (45) 28316-28327.

43. Hao, G., T. Mastren, W. Silvers, G. Hassan, O.K. Öz, X. Sun, *Copper-67 radioimmunotheranostics for simultaneous immunotherapy and immuno-SPECT*. Scientific Reports, 2021. 11:3622.

44. Merrick, M.J., D.A. Rotsch, A. Tiwari, J. Nolen J, T. Brossard, et al., *Imaging and dosimetric characteristics of ^{67}Cu*. Phys. Med. Biol., 2021. 66-035002.

45. Carlos dos Santos, J., B. Beijer, U. Bauder-Wüst, M. Schäfer, K. Leotta, et al., *Development of Novel PSMA Ligands for Imaging and Therapy with Copper Isotopes.* J Nucl Med., 2020. 61:70–79.

46. Sevcenco, S., H.C. Klingler, K. Eredics, A. Friedl, J. Schneeweiss, P. Knoll, et al., *Application of Cu-64 NODAGA-PSMA PET in Prostate Cancer*. Adv Ther., 2018. 35:779–784.

47. Carolyn J. Anderson, Riccardo Ferdani, *Copper-64 Radiopharmaceuticals for PET Imaging of Cancer: Advances in Preclinical and Clinical Research*. Cancer Biotherapy and Radiopharmacuticals, 2009. 24;4.

48. Bonvin, V., F. Bochud, J. Damet, C. Theis, H. Vincke, R. Geyer, *Detailed study of the distribution of activation inside the magnet coils of a compact PET cyclotron*. Applied Radiation and Isotopes, 2021. 168:109446.

49. Ashhar, Z., N.A. Yusof, F.F. Ahmad Saad, S.M. Mohd Nor, F. Mohammad, et al., *Preparation, Characterization, and Radiolabeling of [^{68}Ga]Ga-NODAGA-Pamidronic Acid: A Potential PET Bone Imaging Agent*. Molecules, 2020. 25, 2668.

50. Brandt, M., J. Cardinale, M.L. Aulsebrook, G. Gasser, T.L. Mindt, *An Overview of PET Radiochemistry, Part 2: Radiometals*. J Nucl Med, 2018. 59:1500–1506.

51. Velikyan, I., *^{68}Ga-Based Radiopharmaceuticals: Production and Application Relationship*. Molecules. 2015. 20, 12913-12943.

52. Velikyan, I., *Prospective of ^{68}Ga-radiopharmaceutical development*. Theranostics, 2014. 4, 47–80.

53. Velikyan, I., *Radionuclides for Imaging and Therapy in Oncology*; *In Cancer Theranostics*; Chen, X., Wong, S., Eds.; Elsevier: Amsterdam, The Netherlands, 2014. pp. 285–325.

54. Velikyan, I., *Positron emitting [^{68}Ga] Ga-based imaging agents*: Chemistry and diversity. Med. Chem., 2011. 7, 338–372.

55. Velikyan, I., *The diversity of ^{68}Ga-based imaging agents*. Recent Results Cancer Res., 2013. 194, 101–131.

56. Velikyan, I., *Continued rapid growth in Ga applications*: *Update 2013 to June 2014*. J. Label. Compd. Radiopharm., 2015. 99–121.

57. Bloch, W. E., K.F. Eckerman, G. Sgouros, S. R. Thomas. *MIRD Pamphlet No. 21: A Generalized Schema for Radiopharmaceutical Dosimetry Standardization of Nomenclature*. J Nucl Med., 2009. 50:477–484.

58. Chapter <823> Radiopharmaceuticals for positron emission tomography—compounding. In: *United States Pharmacopeia 32/National Formulary 27*. Rockville, MD: United States Pharmacopeial Convention, 2009. 365-369.

59. Schuhmacher, J., G. Klivényi, W.E. Hull, R. Matys, H. Hauser, et al., *A bifunctional HBED- derivative for labeling of antibodies with ^{67}Ga, ^{111}In and ^{59}Fe. Comparative biodistribution with ^{111}In-DPTA and ^{131}I-labeled antibodies in mice bearing antibody internalizing and non-internalizing tumors*. Int J Rad Appl Instrum B., 1992. 19:809-824.

60. Schuhmacher, J., G. Klivenyi, R. Matys, M. Stadler, T. Regiert, et al., *Multistep tumor targeting in nude mice using bispecific antibodies and a gallium chelate suitable for immunoscintigraphy with positron emission tomography*. Cancer Res., 1995. 55, 115–123.

61. Eder, M., O. Neels, M. Müller, U. Bauder-Wüst U, Y. Remde, et al., *Novel preclinical and radiopharmaceutical aspects of [^{68}Ga] Ga-PSMA-HBED-CC: A New PET tracer for imaging of prostate cancer*. Pharmaceuticals, 2014. 7, 779−796.

62. Eder, M., M. Schafer, U. Bauder-Wüst, et al., *^{68}Ga-Complex Lipophilicity and the Targeting Property of a Urea-Based PSMA Inhibitor for PET Imaging*. Bioconjugate Chem., 2012. 23, 688−697.

63. Migliari, S., A. Sammartano, M. Scarlattei, G. Serreli, C. Ghetti et al., *Development and Validation of a High-Pressure Liquid Chromatography Method for the Determination of Chemical Purity and Radiochemical Purity of a [^{68}Ga]-Labeled Glu-Urea-Lys (Ahx)-HBED-CC (Positron Emission Tomography) Tracer*. ACS Omega, 2017. 2, 7120−7126.

64. Bois, F., C. Noirot, S. Dietemann, I.C. Mainta, T. Zilli, et al., *[^{68}Ga] Ga-PSMA-11 in prostate cancer: a comprehensive review.* Am J Nucl Med Mol Imaging, 2020. 10 (6): 349-374.

65. Sounak, R., H.D. Axelrod, K.C. Valkenburg, S. Amend S, K.J. Pienta, *Optimization of prostate cancer cell detection using multiplex tyramide signal amplification*. J Cell Biochem., 2019. 120, 4804–4812.

66. Martin, K. B., I. Derecichei, Y. Li, R.M. Ferraiuolo, M. Dunning, et. al., *Neuroendocrine differentiation of prostate cancer leads to PSMA suppression*. Endocrine-Related Cancer, 2019. 26:131–146.

67. Nimmagadda, S., M. Pullambhatla, Y. Chen, P. Parsana, A. Lisok, et. al., *Low-Level Endogenous PSMA Expression in Nonprostatic Tumor Xenografts Is Sufficient for In Vivo Tumor Targeting and Imaging*. J Nucl Med., 2018. 59:486–493.

68. Stock, K., K. Steinestel, R. Wiesch, J.H. Mikesch, A. Hansmeier et. al., *Neovascular Prostate-Specific Membrane Antigen Expression Is Associated with Improved Overall Survival under Palliative Chemotherapy in Patients with Pancreatic Ductal Adenocarcinoma*. Biomed Res Int., 2017. 2017: 2847303.

69. Prostate Specific Membrane Antigen (D4S1F) Rabbit mAb #12702. Available at: https://www.cellsignal.com/products/primary-antibodies/prostate-specific-membrane-antigen-d4s1f-rabbit-mab/12702 Accessed 10 August 2021.

70. Chervu, L.R., I. Sternlieb, *Dosimetry of copper radionuclides*. J Nucl Med., 1974. 15:1011.

71. Andreozzi, E.M., J.B. Torres, K. Sunassee, et al*., Studies of copper trafficking in a mouse model of Alzheimer's disease by positron emission tomography: Comparison of ^{64}Cu acetate and ^{64}CuGTSM.* Metallomics., 2017. 9:1622.

72. Banerjee, S.R., Z. Chen, M. Pullambhatla, A. Lisok, J. Chen, R.C. Mease, M.G. Pomper, *Preclinical Comparative Study of ^{68}Ga-Labeled DOTA, NOTA, and HBED-CC Chelated Radiotracers for Targeting PSMA*. Bioconjug Chem., 2016. 27:1447–1455.

73. Pandit-Taskar, N., J.A. O'Donoghue, C.R. Divgi, E.A. Wills, L. Schwartz, Gonen M, et al., *Indium 111-labeled J591 anti-PSMA antibody for vascular targeted imaging in progressive solid tumors*. EJNMMI Res., 2015. 5:28.

74. Calabria, F., *Fifty shades of Meningioma: Challenges and Perspectives of Different PET Molecular Probes*. Clin Transl Imaging, 2017. 5:403.

75. Han, X.D., C. Liu, F. Liu, Q.H. Xie, T.L. Liu, et al., *^{64}Cu-PSMA-617: A novel PSMA-targeted radiotracer for PET imaging in gastric adenocarcinoma xenografted mice model*. Oncotarget, 2017. 8:74159.

76. Kim, S. B., I.H. Song, Y.S. Song, B.C. Lee, A. Gupta et al., *Biodistribution and internal radiation dosimetry of a companion diagnostic radiopharmaceutical, [^{68}Ga] PSMA-11, in subcutaneous prostate cancer xenograft model mice.* Scientific Reports, 2021. 11:15263.

77. Chatalic, K.L.S., S. Heskamp, M. Konijnenberg, J.D.M. Molkenboer-Kuenen, G.M. Franssen GM, et al., *Towards Personalized Treatment of Prostate Cancer: PSMA I&T, a Promising Prostate-Specific Membrane Antigen-Targeted Theranostic Agent*. Theranostics, 2016.6:849–61.

78. Hartmann, H., K. Zophel, R. Freudenberg, L. Oehme, M. Andreeff, G. Wunderlich, et al., *Radiation exposure of patients during ^{68}Ga-DOTATOC PET/CT examinations*. Nuklearmedizin (Nuclear medicine), 2009. 48:201–7.

79. Walker, R.C., G.T. Smith, E. Liu, B. Moore, J. Clanton, M. Stabin, *Measured human dosimetry of ^{68}Ga-DOTATATE*. J Nucl Med., 2013. 54:855–60.

80. Krishan Kumar. *The Current Status of the Production and Supply of Gallium-68*. Cancer Biotherapy and Radiopharmaceuticals, 2020. 35(3):163-166.

81. Johnbeck, C.B., U. Knigge, A. Loft, A.K. Berthelsen, J. Mortensen, et al., *Head-to-Head Comparison of ^{64}Cu-DOTATATE and ^{68}Ga-DOTATOC PET/CT: A Prospective Study of 59 Patients with Neuroendocrine Tumors*. J Nucl Med., 2017. 58:451–457.

APPENDIX A

^{64}Ni TARGET ELECTROLATING

^{64}Ni Target Preparation

Enriched ^{64}Ni metal in the amount of (60-120 mg) was transferred to a tared weighing paper and the weight was recorded. Next, the Nickel powder was poured into a 50 mL beaker, and the weighing paper was rinsed quantitatively with Milli-Q water. The plating cell, graphite rod, and platinum target holder were obtained to prepare for electroplating. The PTFE/Silicone plating spacer was washed with Milli-Q water, then dried it in the oven. Also, the surface of the graphite rod was wiped with a Milli-Q moistened Kimwipe, followed by a dry Kimwipe to ensure all loose graphite particles were removed. Lastly, the platinum disc of the target holder was cleaned with heated 50% nitric acid (HNO_3) for five minutes. The platinum disc was then rinsed with Milli-Q water and then dried in the oven. Once dry, the target holder was left to cool and then placed on the balance to record its weight. Next, the plating cell and PTFE/Silicone spacer were assembled and fastened to the plating mount as displayed in (Figure 51 AB). The assembled cell was also inspected for any leaks.

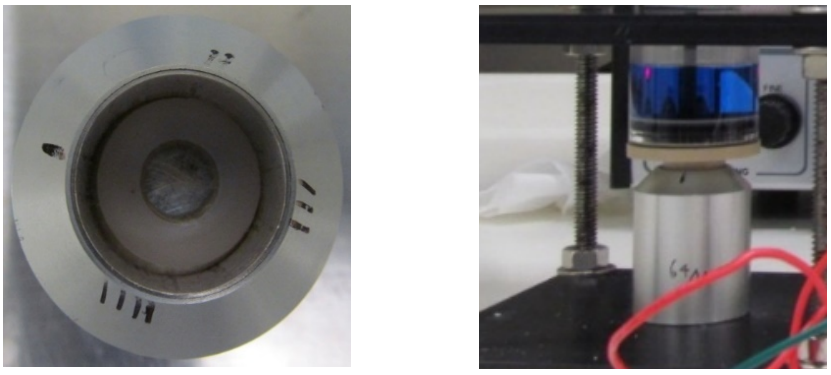

(a) **(b)**

Figure 51 Top view of the target holder (a) PTFE/Silicone spacer, (b) Target holder attached to the plating mount assembly.

^{64}Ni Electroplating Solution Preparation

The electroplating solution of ^{64}Ni was prepared by adding 10 mL of concentrated nitric acid, (HNO_3) solution to a 50 ml beaker, and allowed it to stir and placed on a hot plate with the following settings: heating temp. - 120°C; stir rate - 350 rpm. The solution was left to heat and evaporate to a green film. Once evaporated, another 10 mL of concentrated nitric acid solution was added to the beaker and placed on the hot plate and allowed to evaporate to a green film. This step was repeated twice. Next, 10 mL of Milli-Q water was added to the beaker and evaporated to a green film. The beaker was then left to cool, before adding 0.2 mL of sulfuric acid (H_2SO_4) to the beaker and slowly adding another 10 mL of Milli-Q water, and the solution was evaporated to near dryness. Once dry, the beaker was removed from the hot plate and allowed to cool, then 7 mL Milli-Q water was added to the beaker and placed on the hot plate at (heat: 100°C; stir rate: 350 rpm). After the solution appearance changed to cloudy green, 3.5 mL of ammonium hydroxide (NH_4OH) was added to the ^{64}Ni solution, and its color changed from light green to royal blue with a pH range between 9-10. Lastly, 0.15-0.2 g of ammonium sulfate $(NH_4)_2SO_4$ was added to the solution, which was then transferred to the plating cell.

^{64}Ni Target Electroplating

Once the target materials and the ^{64}Ni solution were prepared and assembled as shown in (Figure 52), the electroplating of the target was ready to commence. The voltmeter power supply was set at 2.2 mA with a voltage limitation of 4.0 V. Then, electroplating was allowed to proceed for 48-60 hours. The progress of the electroplating was checked observing the color of the solution, as it transitioned from royal blue to light blue. In addition, 0.5 mL of NH_4OH was periodically added to maintain the solution pH of 9-10. Once electroplating was completed, the solution was transferred from the plating cell into a waste bottle. Next, the PTFE/Silicone plating spacer was removed, and the target holder was rinsed thoroughly with Milli-Q water. The target was then placed in the oven to dry. After 20 minutes, the target holder was removed from the oven and allowed to cool to record its weight.

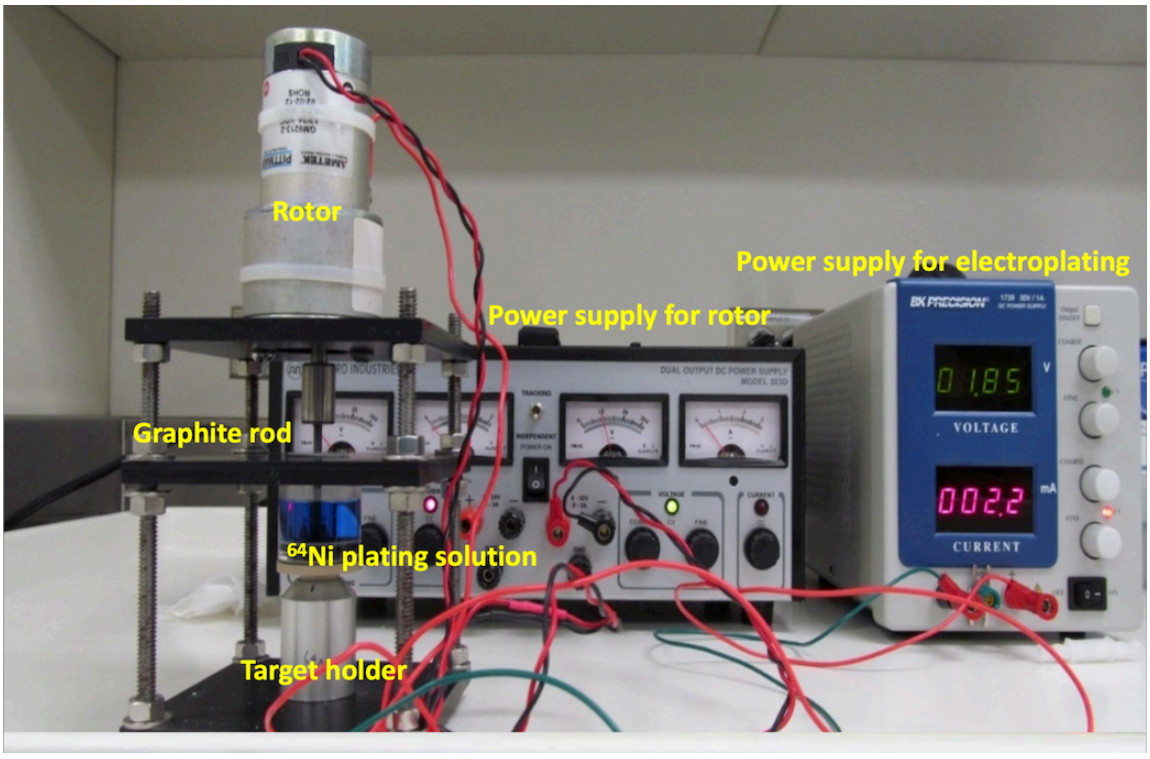

Figure 52 Electroplating Assembly of the ^{64}Ni target for ^{64}Cu production.

Cyclotron and the Solid Target System

The enriched ^{64}Ni solid target (enrichment: 99+%, 80-100 mg) that had been electroplated on a platinum plate, was irradiated with protons at 11.4 MeV energy, and beam current of 45 μA via the ^{64}Ni (p, n) ^{64}Cu nuclear reaction. The target was irritated by the PETtrace cyclotron housed at CRF (GE Healthcare, Chicago, IL), which is equipped with a solid target station to produce the radiometals of interest.

The ALCEO solid target processing system (Comecer, Castel Bolognese, Italy) installed on the cyclotron consists of an irradiation unit and cooling system (PTS), an electrodeposition, dissolution, storage, and transfer unit (EDS), and one purification module (PRF). The PTS unit is directly linked to the cyclotron ensuring that the target is correctly positioned in the direction of the beam port. In addition, a water and helium cooling system are connected to the irradiation unit.

While the EDS unit is housed inside a hot cell and is connected to the cyclotron via the target transfer tube (Figure 53). It is a controllable pneumatic system that performs the following functions: electrochemical deposition of the enriched metal isotope, automatic shuttle transfer between the hot cell and the cyclotron, dissolution of the irradiated isotope and storage of target shuttles.

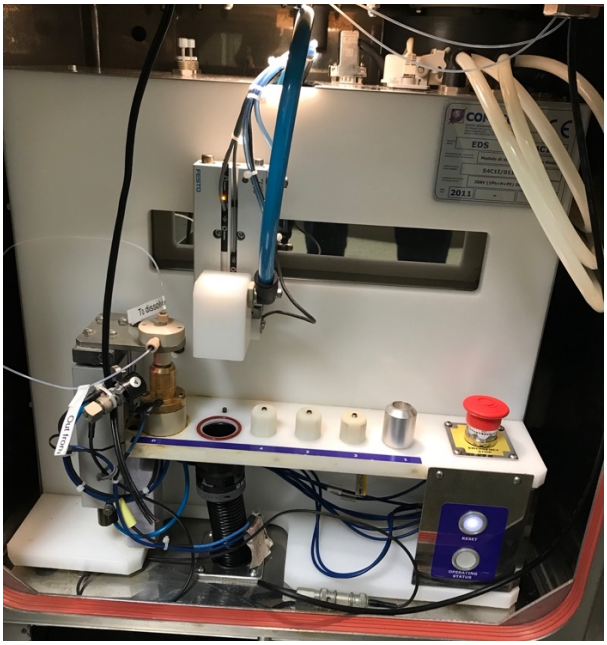

Figure 53 The EDS unit placed inside a hot cell for target processing.

Lastly, the PRF unit is typically placed in a hot cell above the EDS module and is connected to it via capillary lines (Figure 54). It is main function is to purify produced isotope (^{64}Cu) by Ion Chromatography through a series of programmed procedure that was developed internally.

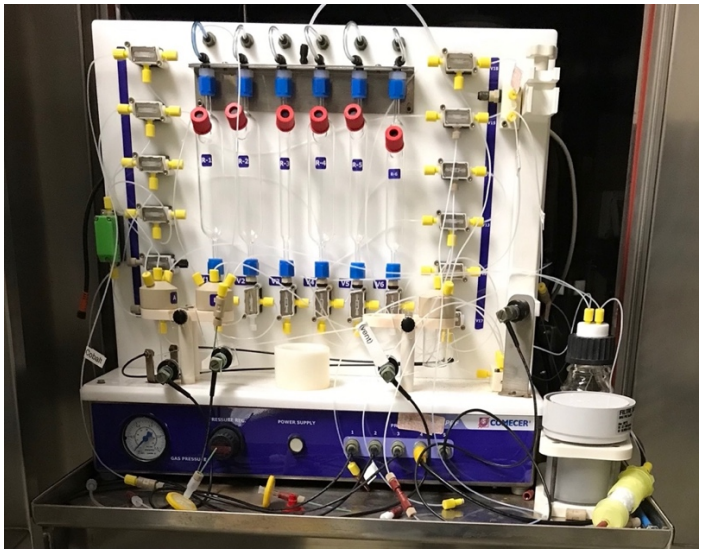

Figure 54 The PRF unit used for purification of the produced isotope.

^{64}Ni Target Irradiation

The software interfaces to control the PTS, EDS and PRF modules were opened (Figure 55). First, the valves of the PRF unit were checked by clicking the “Manual” mode via the MAN/AUT switch, all valves were then reset back to their default condition (Figure 56).

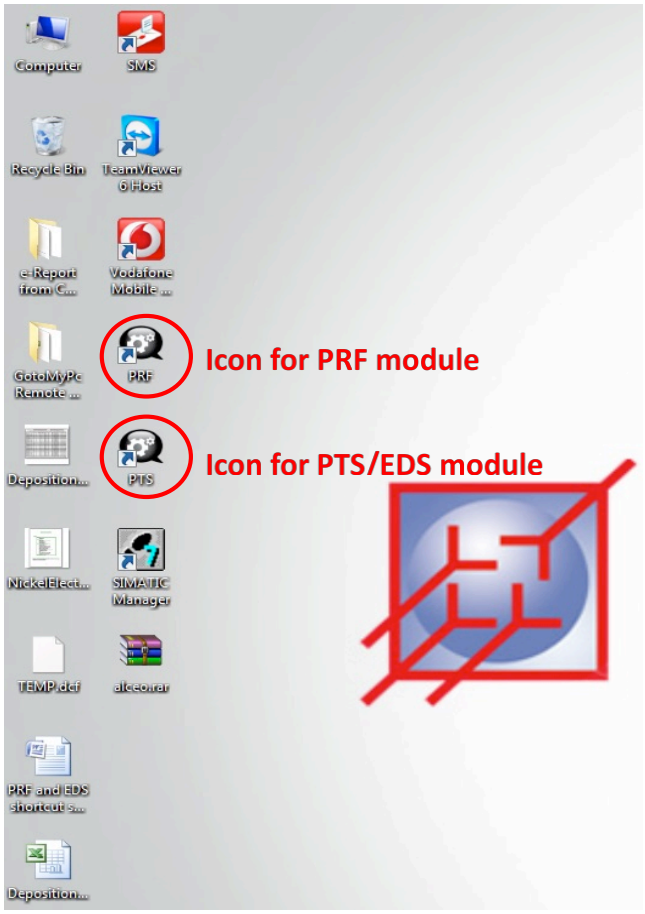

Figure 55 Icons for starting PRF and PTS/EDS Software Interfaces.

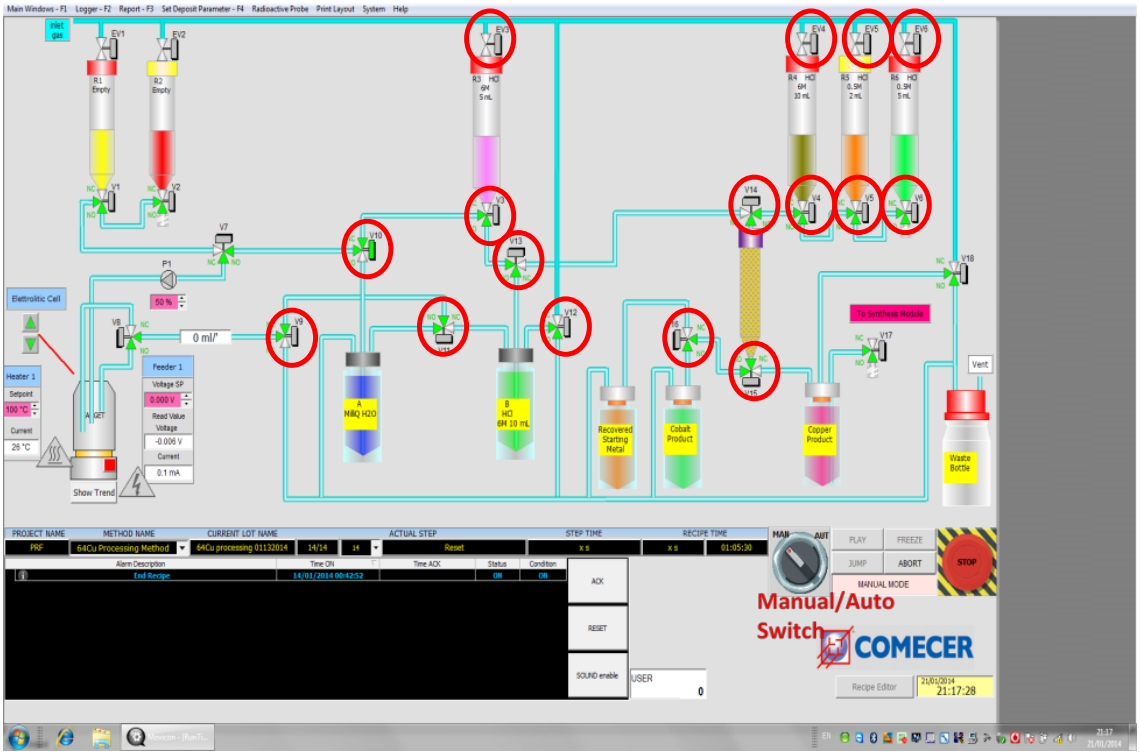

Figure 56 The software interface of PRF module. O indicates the valves to be checked prior to operation.

Next, a leak test was performed on the PRF and EDS modules. Once done, the ^{64}Ni-plated target holder was placed in the designated position on the EDS module (Figure 57).

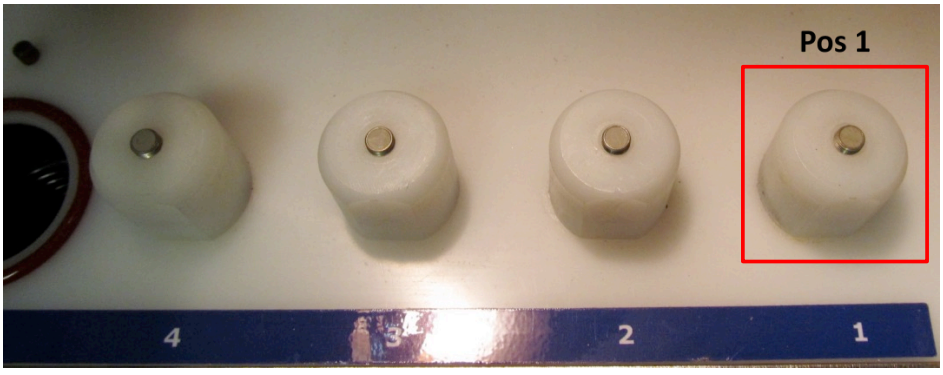

Figure 57 Target storage seats of the EDS module. Position 1 is as indicated.

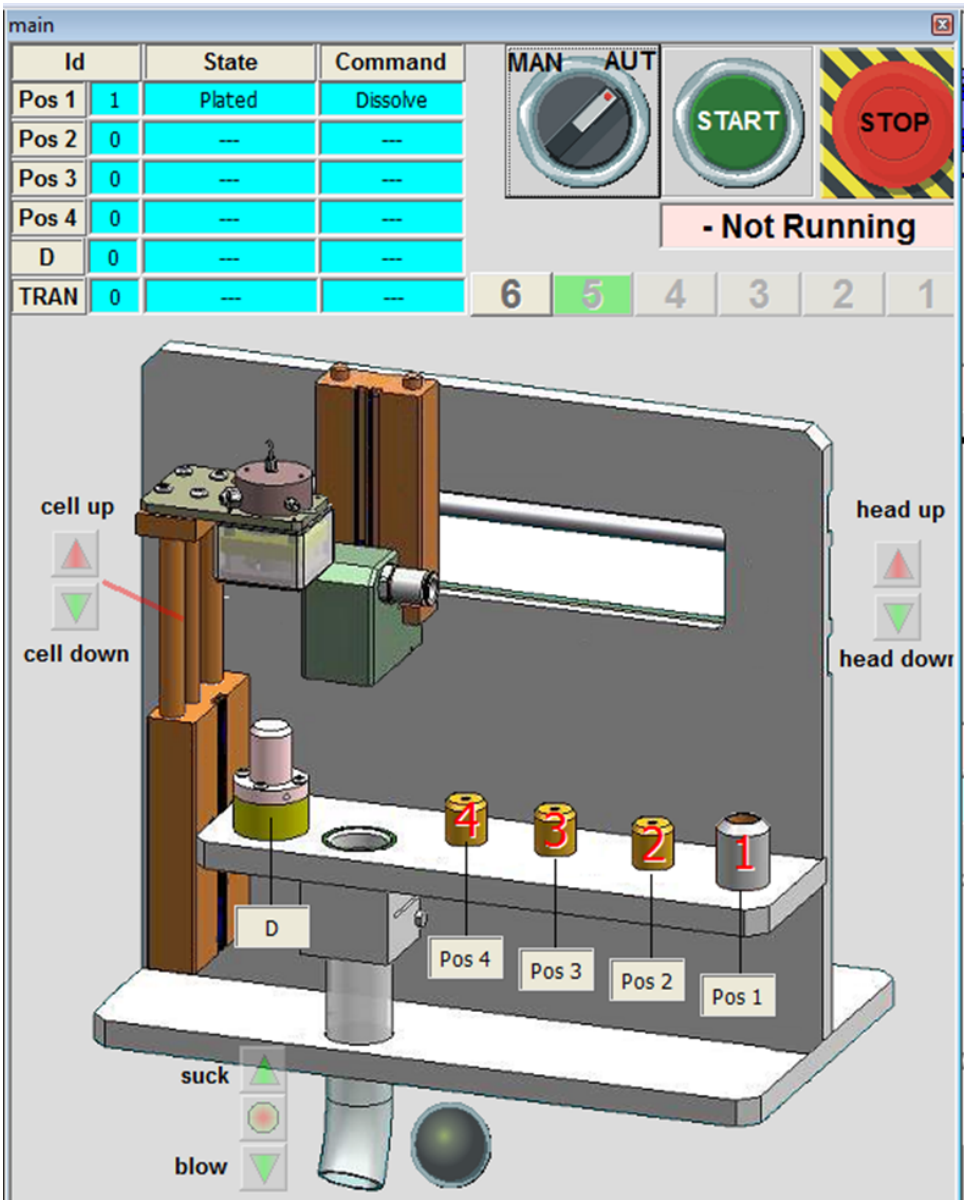

Figure 58 The software interface of the EDS module.

After clicking the start button the module automatically transported the target holder to the PTS module by the cyclotron to be irradiated (Figure 59).

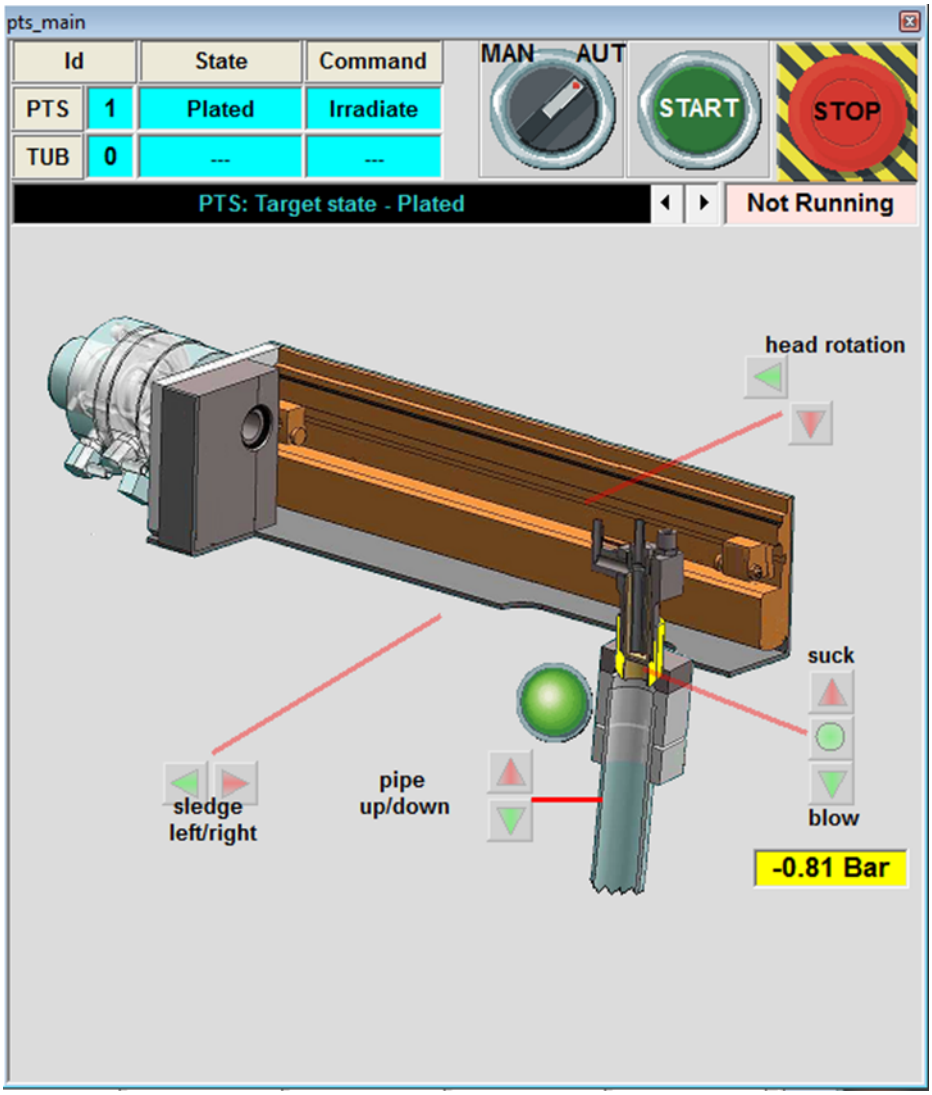

Figure 59 The software interface of the PTS module.

Once the irradiation was completed and confirmed by the cyclotron operator, the irradiated target was retrieved. The target was then dissolved and further purified by the PRF module as described in section 2.1.2.

APPENDIX B

^{68}Ge/^{68}Ga-GENERATOR RADIONUCLIDE PURITY

^{68}Ge Breakthrough Test

An important criterion of the clinical application of the ^{68}Ge/^{68}Ga generator is to determine the presence of the Ge-68 breakthrough from the generator on a weekly basis. The breakthrough is defined as the activity of ^{68}Ge in the eluate in proportion to the activity present on the column within the generator. An elution from the ^{68}Ge/^{68}Ga- generator was obtained using 5 mL of 0.1 M ultrapure hydrochloric acid solution into a collecting vial. Then, 5.0 μL of the eluted test solution was transferred to an Eppendorf tube and 1 mL of Milli-Q water was added. The tube was sealed with parafilm and labelled Sample_X1. Next, the gamma counter program was setup to run a 1-minute scan of each sample in the following order: Position 1 – Background, Position 2 – Cesium-137 and Position Ci – Sample_X1. Upon completion, the data was saved, and the Total Initial Counts were determined. The Sample_X1 was stored in a secure area and left for 48 hours after the initial reading, to allow all the short half-life isotopes to decay to a negligible amount. After 48 hours, the same samples (Background, Cesium-137 and Sample_X1) were scanned for 1 minute using the same sequence. The gamma counter readings were recorded to determine the Ge-68 Final Counts. Finally, the Ge-68 breakthrough was calculated as: Breakthrough % = (Ge-68 Final Counts / Total Initial Counts) × 100. The ^{68}Ge breakthrough of the eluent should not exceed 0.001%.

APPENDIX C

WESTERN BLOT: PSMA EXPRESSION QUANTIFICATION

Protein Purification and Quantification

Pellets of LNCaP and PC-3 cell lines were processed for protein quantification. Briefly, pellets were dissolved in radioimmunoprecipitation assay buffer (RIPA buffer) containing proteinase and phosphatases inhibitors (Bio-Rad, Hercules, CA). Fours cycles of 15 seconds in boiling water and 5 min. on ice were performed. Next, the total proteins extracts were centrifuged at 13000 rpm for 20 min., then the soluble fraction was recovered and placed in a new 1.5 mL Eppendorf tube. Protein concentration was measured using the Pierce BCA Protein Assay Kit and read by the microplate reader (ThermoFisher scientific, Waltham, MA). Samples were then processed for WB running in 4X protein loading buffer (10% of beta-mercaptoethanol).

Protein Separation and Transfer

For electrophoretic separation 40 ug of total protein were run in a precast (4-15%) protein gels by SDS-PAGE (Sodium dodecyl-sulfate polyacrylamide gel electrophoresis) for 2 hrs. at 75V (Figure 30). Proteins were transferred to the nitrocellulose membrane over night at 25V.

Membrane Processing Phase 1

Once the transfer was complete, the membrane was recovered and washed with distilled water to discard salt and was left to dry, it was then rehydrated with PBS and blocked using Li-Cor blocking buffer (LI-COR, Lincoln, NE) at room temperature for 1 hr. Next, the primary antibody: rabbit monoclonal IgG human anti-PSMA (Cell Signaling Technology #12815, Danvers, MA), was diluted in a ratio of 1:1000 in Li-Cor antibody diluent buffer. The antibody was then added to the target protein on the membrane and incubated overnight at 4^{o} C. Expected MW 100 kDa.

Membrane Processing Phase 2

Membrane was washed 3 times for 5 min. each with PBS-Tween (0.2%). The Primary antibody: mouse monoclonal IgG human B-actin (Cell Signaling Technology #3700, Danvers, MA) was diluted 1:10000 in Li-Cor antibody diluent buffer and incubated for 1 hr. at room temperature. Expected MW 45 kDa. The membrane was then washed 3 times for 5 min. each with PBS-Tween (0.2%). Secondary antibodies: anti-rabbit plus anti-mouse (LI-COR) IRD-linked, diluted 1:20000 in Li-Cor antibody diluent buffer were add and incubated at room temperature for 1 hr. The membrane was then washed 3 times for 5 min. each with PBS-Tween (0.2%). Next, the membrane was scanned by the odyssey imaging system (LI-COR Biosciences, USA) at room temperature for signal quantification to confirm the protein expression using the anti-PSMA antibody.

APPENDIX D

PET/CT BIODISTRIBUTON DATA: ^{64}Cu-PSMA-I&T

VOIs [string]	Time [seconds]	Averaged [kBq/cc]
Salivary Glands+	5	0.017650115
Salivary Glands+	15	3.25E-04
Salivary Glands+	25	0.015443816
Salivary Glands+	35	0.020617284
Salivary Glands+	45	0.00438543
Salivary Glands+	55	0.064271747
Salivary Glands+	90	74.15453944
Salivary Glands+	150	131.5281332
Salivary Glands+	210	129.6355759
Salivary Glands+	270	125.8336231
Salivary Glands+	360	117.9617708
Salivary Glands+	480	110.3346271
Salivary Glands+	600	105.8050907
Salivary Glands+	720	101.5578346
Salivary Glands+	840	95.40574272
Salivary Glands+	1050	92.4629849
Salivary Glands+	1350	89.39249383
Salivary Glands+	1650	87.164083
Salivary Glands+	2100	83.66471452

Salivary Glands+	2700	82.53936891
Salivary Glands+	3300.0188	79.85834539
Muscle+	5	0.003753305
Muscle+	1.50E+01	1.69E-04
Muscle+	25	1.31E-04
Muscle+	35	6.80E-08
Muscle+	45	5.70E-06
Muscle+	55	5.94E-04
Muscle+	90	22.25402861
Muscle+	150	40.9763557
Muscle+	210	41.55433948
Muscle+	270	35.89663797
Muscle+	360	40.747053
Muscle+	480	38.68774296
Muscle+	600	37.73384537
Muscle+	720	36.66287858
Muscle+	840	33.81099946
Muscle+	1050	32.88827644
Muscle+	1350	31.64542011
Muscle+	1650	30.41929933
Muscle+	2100	29.80170615
Muscle+	2700	28.65326541

Muscle+	3300.0188	25.88847794
Tumor+	5	0.019270603
Tumor+	15	0.044294861
Tumor+	25	0.057186704
Tumor+	35	0.016112141
Tumor+	45	0.006114152
Tumor+	55	0.115266826
Tumor+	90	43.11337846
Tumor+	150	55.52660207
Tumor+	210	62.11293388
Tumor+	270	58.15683518
Tumor+	360	65.39306072
Tumor+	480	64.34125612
Tumor+	600	67.40969615
Tumor+	720	71.70521286
Tumor+	840	75.91303696
Tumor+	1050	74.7807954
Tumor+	1350	71.57121288
Tumor+	1650	74.67598194
Tumor+	2100	77.59691707
Tumor+	2700	77.24007851
Tumor+	3300.0188	78.61796086

Liver+	5	0.00179805
Liver+	15	0.022294792
Liver+	25	0.026440083
Liver+	35	0.004698952
Liver+	45	0.035607535
Liver+	55	0.020468706
Liver+	90	170.9635079
Liver+	150	249.4641812
Liver+	210	230.1389704
Liver+	270	220.354311
Liver+	360	224.9783451
Liver+	480	237.9498735
Liver+	600	239.2996744
Liver+	720	242.9310242
Liver+	840	243.1307915
Liver+	1050	247.897952
Liver+	1350	247.358422
Liver+	1650	249.4706899
Liver+	2100	252.2673372
Liver+	2700	253.7259292
Liver+	3300.0188	258.1830422
Kidney+	5	0.053136215

Kidney+	15	0.084232474
Kidney+	25	0.014715265
Kidney+	35	0.012980053
Kidney+	45	0.007667582
Kidney+	55	0.0019198
Kidney+	90	157.9202721
Kidney+	150	292.0447166
Kidney+	210	333.5142066
Kidney+	270	372.5558991
Kidney+	360	406.4666497
Kidney+	480	425.8028968
Kidney+	600	447.396148
Kidney+	720	461.8908006
Kidney+	840	467.5064822
Kidney+	1050	482.5979166
Kidney+	1350	496.1569868
Kidney+	1650	509.1018913
Kidney+	2100	519.3358999
Kidney+	2700	527.3612178
Kidney+	3300.0188	527.5838297
Heart+	5	0.005362853
Heart+	15	0.090764946

Heart+	25	0.011977866
Heart+	35	0.032706372
Heart+	45	0.008141757
Heart+	55	0.003342797
Heart+	90	479.2196938
Heart+	150	306.5984545
Heart+	210	219.264735
Heart+	270	179.8972407
Heart+	360	145.0338477
Heart+	480	114.5928518
Heart+	600	98.21385019
Heart+	720	91.92106197
Heart+	840	85.23304384
Heart+	1050	76.55379626
Heart+	1350	70.35091266
Heart+	1650	65.39846773
Heart+	2100	60.57355634
Heart+	2700	58.67697684
Heart+	3300.0188	56.74116285

VOIs [string]	Time [seconds]	Averaged [kBq/cc]
Salivary Glands-	5	0.000149
Salivary Glands-	15	0.000426
Salivary Glands-	25	0
Salivary Glands-	35	0.002889622
Salivary Glands-	45	0.001202578
Salivary Glands-	55	0.046888722
Salivary Glands-	90	238.4899616
Salivary Glands-	150	485.5368128
Salivary Glands-	210	471.9132232
Salivary Glands-	270	450.9805805
Salivary Glands-	360	428.5292607
Salivary Glands-	480	397.2636353
Salivary Glands-	600	400.9814334
Salivary Glands-	720	386.0805721
Salivary Glands-	840	375.9482128
Salivary Glands-	1050	370.0189145
Salivary Glands-	1350	354.1345348
Salivary Glands-	1650	340.5277014
Salivary Glands-	2100	334.6778923
Salivary Glands-	2700	316.374734
Salivary Glands-	3300.0188	301.9504123

Muscle-	5	0
Muscle-	1.50E+01	0.004857312
Muscle-	25	0
Muscle-	35	0
Muscle-	45	0
Muscle-	55	0
Muscle-	90	27.6307961
Muscle-	150	48.02451767
Muscle-	210	57.19110543
Muscle-	270	57.49559226
Muscle-	360	61.50074866
Muscle-	480	54.89080737
Muscle-	600	55.39545901
Muscle-	720	54.01925514
Muscle-	840	53.28432744
Muscle-	1050	49.53955898
Muscle-	1350	47.93030947
Muscle-	1650	43.88458438
Muscle-	2100	41.43819726
Muscle-	2700	39.81209539
Muscle-	3300.0188	39.31222887
Tumor-	5	4.27E-12

Tumor-	15	0.001015323
Tumor-	25	0
Tumor-	35	0
Tumor-	45	0
Tumor-	55	0.002827367
Tumor-	90	47.5582395
Tumor-	150	79.99627126
Tumor-	210	86.119358
Tumor-	270	90.52783417
Tumor-	360	95.27419651
Tumor-	480	92.96672456
Tumor-	600	94.60507128
Tumor-	720	96.25747471
Tumor-	840	95.11216086
Tumor-	1050	93.02968153
Tumor-	1350	93.74883275
Tumor-	1650	93.52132157
Tumor-	2100	92.15136458
Tumor-	2700	91.80835755
Tumor-	3300.0188	90.01874376
Liver-	5	0.002483448
Liver-	15	3.68E-10

Liver-	25	0.00036
Liver-	35	0.00059
Liver-	45	0.000267
Liver-	55	0.0000357
Liver-	90	387.1504729
Liver-	150	819.61956
Liver-	210	816.6298403
Liver-	270	848.9082213
Liver-	360	920.2503331
Liver-	480	991.7194276
Liver-	600	1041.582699
Liver-	720	1077.769654
Liver-	840	1084.101748
Liver-	1050	1128.354667
Liver-	1350	1150.782071
Liver-	1650	1170.417855
Liver-	2100	1183.160857
Liver-	2700	1195.613788
Liver-	3300.0188	1198.041926
Kidney-	5	0
Kidney-	15	0
Kidney-	25	0

Kidney-	35	0.001592567
Kidney-	45	0.012340584
Kidney-	55	0.000518
Kidney-	90	422.1387076
Kidney-	150	787.7711581
Kidney-	210	901.4541545
Kidney-	270	976.7379871
Kidney-	360	1045.661791
Kidney-	480	1091.736108
Kidney-	600	1146.162567
Kidney-	720	1166.98829
Kidney-	840	1199.758853
Kidney-	1050	1229.101292
Kidney-	1350	1249.703035
Kidney-	1650	1274.866177
Kidney-	2100	1277.132539
Kidney-	2700	1293.309555
Kidney-	3300.0188	1306.964467
Heart-	5	0.009672907
Heart-	15	0.003646786
Heart-	25	0
Heart-	35	0

Heart-	45	0
Heart-	55	0.003803925
Heart-	90	1537.061812
Heart-	150	1038.787001
Heart-	210	752.8677816
Heart-	270	623.2187545
Heart-	360	505.5656708
Heart-	480	457.0522456
Heart-	600	408.6068371
Heart-	720	387.355214
Heart-	840	386.8377896
Heart-	1050	356.25234
Heart-	1350	339.7730692
Heart-	1650	333.6845042
Heart-	2100	328.0544135
Heart-	2700	329.3599994
Heart-	3300.0188	334.2858787

APPENDIX E

PET/CT BIODISTRIBUTON DATA: ^{68}Ga-PSMA-11

VOIs [string]	Time [seconds]	Averaged [kBq/cc]
Salivary Glands+	5	0.13624095
Salivary Glands+	15	0.10702618
Salivary Glands+	25	0.131337596
Salivary Glands+	35	0.052562848
Salivary Glands+	45	0.023959089
Salivary Glands+	55	0.015718206
Salivary Glands+	90	502.3525932
Salivary Glands+	150	811.835077
Salivary Glands+	210	958.7649717
Salivary Glands+	270	1099.037343
Salivary Glands+	360	964.6039982
Salivary Glands+	480	1087.609211
Salivary Glands+	600	1313.818131
Salivary Glands+	720	1271.654681
Salivary Glands+	840	1459.624263
Salivary Glands+	1050	2094.614017
Salivary Glands+	1350	2070.25508
Salivary Glands+	1650	2555.747543
Salivary Glands+	2100	2901.537016

Salivary Glands+	2700	3352.417006
Salivary Glands+	3300.0188	3616.158865
Muscle+	5	0.007512895
Muscle+	1.50E+01	3.23693E-07
Muscle+	25	2.83643E-07
Muscle+	35	0.002073953
Muscle+	45	7.06602E-06
Muscle+	55	0.485492097
Muscle+	90	39.29622901
Muscle+	150	71.43532308
Muscle+	210	73.55355079
Muscle+	270	72.17419766
Muscle+	360	61.19059577
Muscle+	480	53.46416749
Muscle+	600	51.32931441
Muscle+	720	42.1116605
Muscle+	840	45.7269107
Muscle+	1050	51.2800435
Muscle+	1350	40.98259714
Muscle+	1650	42.61447235
Muscle+	2100	39.71774829
Muscle+	2700	33.23828461

Muscle+	3300.0188	30.74662728
Tumor+	5	0.043359752
Tumor+	15	0.003446926
Tumor+	25	0.037804158
Tumor+	35	0.070311996
Tumor+	45	0.0037784
Tumor+	55	0.023632108
Tumor+	90	140.3545193
Tumor+	150	224.5894379
Tumor+	210	260.1803522
Tumor+	270	293.9708493
Tumor+	360	252.9230793
Tumor+	480	275.2953504
Tumor+	600	317.6939557
Tumor+	720	296.6696538
Tumor+	840	327.4290796
Tumor+	1050	439.3312874
Tumor+	1350	404.0323553
Tumor+	1650	472.9495411
Tumor+	2100	506.9678094
Tumor+	2700	562.0145648
Tumor+	3300.0188	594.782246

Liver+	5	0.010388183
Liver+	15	0.025749771
Liver+	25	0.154819352
Liver+	35	0.003345801
Liver+	45	0.009241023
Liver+	55	0.005845655
Liver+	90	249.9407702
Liver+	150	320.2197668
Liver+	210	283.6835157
Liver+	270	263.3641152
Liver+	360	191.9878243
Liver+	480	171.8882542
Liver+	600	178.3167284
Liver+	720	151.7112871
Liver+	840	154.7522743
Liver+	1050	191.5571459
Liver+	1350	158.2401399
Liver+	1650	173.4660919
Liver+	2100	166.218787
Liver+	2700	169.9424043
Liver+	3300.0188	168.3013461
Kidney+	5	0

Kidney+	15	0.009178111
Kidney+	25	0.000576946
Kidney+	35	0.006013879
Kidney+	45	0.00037129
Kidney+	55	0.000210405
Kidney+	90	297.8948035
Kidney+	150	452.8362846
Kidney+	210	476.7081634
Kidney+	270	437.9999857
Kidney+	360	311.6660391
Kidney+	480	292.9538861
Kidney+	600	292.9093285
Kidney+	720	238.4770882
Kidney+	840	240.3966589
Kidney+	1050	278.2066681
Kidney+	1350	211.0362667
Kidney+	1650	211.5137399
Kidney+	2100	183.7954477
Kidney+	2700	162.1196794
Kidney+	3300.0188	140.1135078
Heart+	5	8.14673E-06
Heart+	15	7.7353E-06

Heart+	25	0.001377542
Heart+	35	0.006530238
Heart+	45	0.016861751
Heart+	55	0.00316293
Heart+	90	1295.657069
Heart+	150	794.0227638
Heart+	210	632.7138227
Heart+	270	546.2147861
Heart+	360	365.3009304
Heart+	480	310.2959226
Heart+	600	307.9236863
Heart+	720	247.8638594
Heart+	840	248.9757587
Heart+	1050	278.0412117
Heart+	1350	209.1457962
Heart+	1650	211.602395
Heart+	2100	175.1249255
Heart+	2700	151.9766616
Heart+	3300.0188	133.8213971

VOIs [string]	Time [seconds]	Averaged [kBq/cc]
Salivary Glands-	5	0.001538094
Salivary Glands-	15	0.081000493
Salivary Glands-	25	0.006548575
Salivary Glands-	35	0.002980446
Salivary Glands-	45	6.46E-05
Salivary Glands-	55	1.66E-04
Salivary Glands-	90	237.8278785
Salivary Glands-	150	307.244597
Salivary Glands-	210	338.8676181
Salivary Glands-	270	363.8981304
Salivary Glands-	360	392.4255679
Salivary Glands-	480	430.2370687
Salivary Glands-	600	470.8112584
Salivary Glands-	720	501.7887546
Salivary Glands-	840	5.26E+02
Salivary Glands-	1050	5.63E+02
Salivary Glands-	1350	6.00E+02
Salivary Glands-	1650	6.12E+02
Salivary Glands-	2100	6.21E+02
Salivary Glands-	2700	6.27E+02
Salivary Glands-	3300.0188	636.4698196

Muscle-	5	4.27E-05
Muscle-	1.50E+01	0
Muscle-	25	0
Muscle-	35	8.97E-04
Muscle-	45	4.17E-07
Muscle-	55	0
Muscle-	90	14.72186961
Muscle-	150	35.70189463
Muscle-	210	45.70220309
Muscle-	270	47.97779142
Muscle-	360	52.57940261
Muscle-	480	53.10314136
Muscle-	600	50.28960827
Muscle-	720	50.04138581
Muscle-	840	4.87E+01
Muscle-	1050	44.00533668
Muscle-	1350	38.92334172
Muscle-	1650	3.33E+01
Muscle-	2100	3.00E+01
Muscle-	2700	28.33290553
Muscle-	3300.0188	26.62632714
Tumor-	5	1.20E-04

Tumor-	15	0
Tumor-	25	3.26E-23
Tumor-	35	4.54E-08
Tumor-	45	2.59E-04
Tumor-	55	0
Tumor-	90	60.71123576
Tumor-	150	93.88785451
Tumor-	210	112.1309388
Tumor-	270	116.4247266
Tumor-	360	128.7272893
Tumor-	480	131.654021
Tumor-	600	130.5750852
Tumor-	720	130.9182613
Tumor-	840	1.29E+02
Tumor-	1050	121.3399863
Tumor-	1350	1.08E+02
Tumor-	1650	9.77E+01
Tumor-	2100	8.14E+01
Tumor-	2700	66.98236171
Tumor-	3300.0188	55.3520404
Liver-	5	2.77E-06
Liver-	15	0

Liver-	25	3.18E-07
Liver-	35	1.43E-05
Liver-	45	2.54E-05
Liver-	55	3.28E-14
Liver-	90	416.1329526
Liver-	150	471.1482982
Liver-	210	391.942049
Liver-	270	343.7427336
Liver-	360	327.874993
Liver-	480	304.3550568
Liver-	600	287.3715599
Liver-	720	277.643241
Liver-	840	2.65E+02
Liver-	1050	252.4173535
Liver-	1350	2.31E+02
Liver-	1650	2.17E+02
Liver-	2100	1.91E+02
Liver-	2700	1.71E+02
Liver-	3300.0188	154.7875962
Kidney-	5	6.02E-05
Kidney-	15	2.43E-05
Kidney-	25	3.24E-05

Kidney-	35	6.34E-06
Kidney-	45	0
Kidney-	55	6.45E-06
Kidney-	90	180.4237009
Kidney-	150	302.7996623
Kidney-	210	313.208918
Kidney-	270	304.5646587
Kidney-	360	279.461057
Kidney-	480	274.6937075
Kidney-	600	255.1946739
Kidney-	720	234.2615545
Kidney-	840	2.18E+02
Kidney-	1050	1.97E+02
Kidney-	1350	1.64E+02
Kidney-	1650	1.39E+02
Kidney-	2100	113.3647172
Kidney-	2700	8.15E+01
Kidney-	3300.0188	68.06973201
Heart-	5	0
Heart-	15	2.76E-28
Heart-	25	0
Heart-	35	2.04E-05

Heart-	45	1.03E-05
Heart-	55	0
Heart-	90	874.671474
Heart-	150	720.7321169
Heart-	210	595.4708842
Heart-	270	518.028807
Heart-	360	465.7156283
Heart-	480	399.6790767
Heart-	600	377.9526291
Heart-	720	346.6261349
Heart-	840	325.2188453
Heart-	1050	2.87E+02
Heart-	1350	252.9524482
Heart-	1650	2.20E+02
Heart-	2100	1.84E+02
Heart-	2700	148.9937249
Heart-	3300.0188	124.8004531

APPENDIX F

PET/CT BIODISTRIBUTON DATA: ^{68}Ga-PSMA-I&T

VOIs [string]	Time [seconds]	Averaged [kBq/cc]
Salivary Glands+	5	0.002223867
Salivary Glands+	15	0
Salivary Glands+	25	0.00E+00
Salivary Glands+	35	0.010261113
Salivary Glands+	45	0.005363816
Salivary Glands+	55	4.38E-12
Salivary Glands+	90	533.7335104
Salivary Glands+	150	792.5430123
Salivary Glands+	210	989.8494361
Salivary Glands+	270	1153.78827
Salivary Glands+	360	1371.874361
Salivary Glands+	480	1586.976828
Salivary Glands+	600	1756.371351
Salivary Glands+	720	1875.878734
Salivary Glands+	840	1933.254732
Salivary Glands+	1050	1997.435531
Salivary Glands+	1350	2047.552548
Salivary Glands+	1650	2031.526474
Salivary Glands+	2100	1964.197481

Salivary Glands+	2700	1859.322295
Salivary Glands+	3300.0188	1765.124118
Muscle+	5	1.01E-05
Muscle+	1.50E+01	0.00E+00
Muscle+	25	3.49E-09
Muscle+	35	0
Muscle+	45	0
Muscle+	55	0.00E+00
Muscle+	90	6.18E+01
Muscle+	150	75.43903325
Muscle+	210	70.91545376
Muscle+	270	73.68018081
Muscle+	360	79.01736414
Muscle+	480	70.213035
Muscle+	600	68.15948963
Muscle+	720	68.71351715
Muscle+	840	68.07828804
Muscle+	1050	60.79677897
Muscle+	1350	54.31160868
Muscle+	1650	51.91021248
Muscle+	2100	48.55413389
Muscle+	2700	45.6131057

Muscle+	3300.0188	45.2688632
Tumor+	5	7.59E-06
Tumor+	15	4.06E-04
Tumor+	25	1.37E-05
Tumor+	35	3.55E-05
Tumor+	45	0.051389494
Tumor+	55	0.002109552
Tumor+	90	81.71361153
Tumor+	150	1.55E+02
Tumor+	210	1.84E+02
Tumor+	270	2.04E+02
Tumor+	360	2.30E+02
Tumor+	480	244.1446701
Tumor+	600	261.2035452
Tumor+	720	275.3837774
Tumor+	840	285.1951165
Tumor+	1050	299.3880781
Tumor+	1350	322.3728512
Tumor+	1650	343.1520995
Tumor+	2100	365.3927
Tumor+	2700	390.3158151
Tumor+	3300.0188	409.0090275

Liver+	5	4.73E-05
Liver+	15	0
Liver+	25	1.47E-05
Liver+	35	1.00E-10
Liver+	45	6.80E-07
Liver+	55	7.46E-05
Liver+	90	275.0492014
Liver+	150	341.396207
Liver+	210	295.7618983
Liver+	270	254.8356828
Liver+	360	2.48E+02
Liver+	480	2.29E+02
Liver+	600	219.0284027
Liver+	720	2.05E+02
Liver+	840	1.96E+02
Liver+	1050	186.3445591
Liver+	1350	167.5828574
Liver+	1650	152.2363541
Liver+	2100	137.2066875
Liver+	2700	119.7891836
Liver+	3300.0188	106.0866498
Kidney+	5	8.17E-05

Kidney+	15	0
Kidney+	25	3.10E-06
Kidney+	35	0
Kidney+	45	2.09E-04
Kidney+	55	0
Kidney+	90	216.7503102
Kidney+	150	339.3003236
Kidney+	210	321.4142444
Kidney+	270	310.571759
Kidney+	360	292.6063893
Kidney+	480	267.7999927
Kidney+	600	254.4593528
Kidney+	720	233.6113562
Kidney+	840	2.28E+02
Kidney+	1050	205.3474625
Kidney+	1350	1.80E+02
Kidney+	1650	1.59E+02
Kidney+	2100	1.37E+02
Kidney+	2700	107.3051495
Kidney+	3300.0188	87.93645982
Heart+	5	1.91E-05
Heart+	15	1.33E-04

Heart+	25	0
Heart+	35	2.32E-05
Heart+	45	0.007168224
Heart+	55	9.79E-05
Heart+	90	1083.161124
Heart+	150	601.7184387
Heart+	210	482.9203053
Heart+	270	402.4598099
Heart+	360	367.3452105
Heart+	480	338.0159566
Heart+	600	308.8692564
Heart+	720	286.8832183
Heart+	840	261.8371292
Heart+	1050	242.848006
Heart+	1350	218.2569885
Heart+	1650	194.3027013
Heart+	2100	168.9971097
Heart+	2700	1.34E+02
Heart+	3300.0188	116.2179458

VOIs [string]	Time [seconds]	Averaged [kBq/cc]
Salivary Glands-	5	0.0058525
Salivary Glands-	15	0
Salivary Glands-	25	1.81E-05
Salivary Glands-	35	9.58E-07
Salivary Glands-	45	1.36E-04
Salivary Glands-	55	0
Salivary Glands-	90	528.7200165
Salivary Glands-	150	8.58E+02
Salivary Glands-	210	1.03E+03
Salivary Glands-	270	1.18E+03
Salivary Glands-	360	1280.751005
Salivary Glands-	480	1375.699968
Salivary Glands-	600	1445.34068
Salivary Glands-	720	1494.225461
Salivary Glands-	840	1502.862609
Salivary Glands-	1050	1555.456948
Salivary Glands-	1350	1608.065976
Salivary Glands-	1650	1607.203429
Salivary Glands-	2100	1581.240933
Salivary Glands-	2700	1526.196382
Salivary Glands-	3300.0188	1453.391385

Muscle-	5	0
Muscle-	1.50E+01	2.71E-06
Muscle-	25	3.31E-06
Muscle-	35	8.03E-04
Muscle-	45	1.18E-05
Muscle-	55	2.10E-06
Muscle-	90	2.55E+01
Muscle-	150	3.52E+01
Muscle-	210	4.05E+01
Muscle-	270	4.19E+01
Muscle-	360	4.93E+01
Muscle-	480	51.02880491
Muscle-	600	49.82309955
Muscle-	720	49.57533654
Muscle-	840	49.99777326
Muscle-	1050	46.72880855
Muscle-	1350	47.0958741
Muscle-	1650	47.69656508
Muscle-	2100	47.4289444
Muscle-	2700	52.00605222
Muscle-	3300.0188	56.12877836
Tumor-	5	4.40E-05

Tumor-	15	2.83E-05
Tumor-	25	0.002020721
Tumor-	35	0.002346964
Tumor-	45	0
Tumor-	55	1.27E-04
Tumor-	90	1.05E+02
Tumor-	150	127.9381184
Tumor-	210	132.3915228
Tumor-	270	134.9030003
Tumor-	360	1.37E+02
Tumor-	480	136.9742272
Tumor-	600	132.0399126
Tumor-	720	130.1276815
Tumor-	840	120.6346843
Tumor-	1050	112.4046929
Tumor-	1350	101.8418083
Tumor-	1650	91.3224012
Tumor-	2100	76.816769
Tumor-	2700	61.526088
Tumor-	3300.0188	50.39519294
Liver-	5	9.32E-08
Liver-	15	0

Liver-	25	4.25E-04
Liver-	35	6.98E-06
Liver-	45	1.54E-07
Liver-	55	8.19E-05
Liver-	90	381.9961418
Liver-	150	4.27E+02
Liver-	210	3.57E+02
Liver-	270	3.26E+02
Liver-	360	2.95E+02
Liver-	480	265.5471417
Liver-	600	253.3757359
Liver-	720	240.5733756
Liver-	840	222.7806596
Liver-	1050	207.317816
Liver-	1350	186.3078921
Liver-	1650	166.8035062
Liver-	2100	149.7877621
Liver-	2700	126.8626227
Liver-	3300.0188	111.2432765
Kidney-	5	1.05E-08
Kidney-	15	5.72E-08
Kidney-	25	9.05E-07

Kidney-	35	2.64E-04
Kidney-	45	8.84E-07
Kidney-	55	0.00E+00
Kidney-	90	2.06E+02
Kidney-	150	2.93E+02
Kidney-	210	3.03E+02
Kidney-	270	2.86E+02
Kidney-	360	277.5169936
Kidney-	480	247.972288
Kidney-	600	229.3871115
Kidney-	720	222.6293959
Kidney-	840	203.4794049
Kidney-	1050	186.0393421
Kidney-	1350	160.548849
Kidney-	1650	137.9270876
Kidney-	2100	111.0551697
Kidney-	2700	88.51862452
Kidney-	3300.0188	68.77366896
Heart-	5	2.92E-12
Heart-	15	3.83E-04
Heart-	25	5.22E-04
Heart-	35	9.12E-26

Heart-	45	3.00E-05
Heart-	55	0.00E+00
Heart-	90	9.39E+02
Heart-	150	6.17E+02
Heart-	210	4.89E+02
Heart-	270	4.21E+02
Heart-	360	363.841922
Heart-	480	319.6727695
Heart-	600	294.9533089
Heart-	720	267.7354571
Heart-	840	249.5429255
Heart-	1050	229.1970332
Heart-	1350	193.3197623
Heart-	1650	167.1952185
Heart-	2100	139.1226697
Heart-	2700	108.1740689
Heart-	3300.0188	88.94648495